

UNIVERSITY OF CALIFORNIA

Los Angeles

Multiscale Modeling and Control of Microstructural Defects and Surface
Morphology in Thin Film Deposition

A dissertation submitted in partial satisfaction of the
requirements for the degree Doctor of Philosophy
in Chemical Engineering

by

Xinyu Zhang

2011

This page is intended blank and should not be used in the submission of the thesis.

It has the purpose of making the next page, the signature page, page ii.

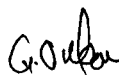
The dissertation of Xinyu Zhang is approved.



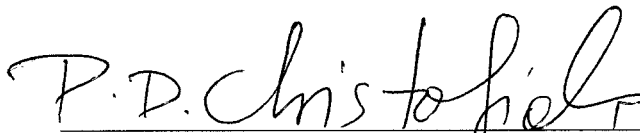
Tsu-Chin Tsao



James F. Davis



Gerassimos Orkoulas, Committee Co-Chair



Panagiotis D. Christofides, Committee Co-Chair

University of California, Los Angeles

2011

Contents

1	Introduction	1
1.1	Motivation	1
1.2	Control of thin film microstructure	6
1.3	Modeling of thin film deposition processes	9
1.4	Dissertation objectives and structure	11
2	Control of Film Thickness, Surface Roughness and Porosity in a Multiscale Thin Film Growth Process	16
2.1	Introduction	16
2.2	Preliminaries	18
2.2.1	Gas-phase model	19
2.2.2	On-lattice kinetic Monte Carlo model of thin film growth . . .	21
2.2.3	Definitions of surface height profile and film site occupancy ratio	23
2.3	Closed-form dynamic model construction	26

2.3.1	Edwards–Wilkinson-type equation of surface height	26
2.3.2	Dynamic model of film site occupancy ratio	31
2.4	Model predictive controller design	35
2.4.1	Reduced-order model for surface roughness	35
2.4.2	MPC formulation	37
2.5	Closed-loop simulations	42
2.5.1	Regulation of film surface roughness and thickness	43
2.5.2	Regulation of film porosity	44
2.5.3	Simultaneous regulation of film surface roughness, porosity and thickness	47
2.5.4	Regulation of roughness with constraint on film thickness . . .	51
2.6	Porosity estimation-based model predictive control	53
2.7	Conclusions	59
3	Control of Surface Roughness and Slope with 1D kMC Model	60
3.1	Introduction	60
3.2	Thin film deposition process	61
3.2.1	On-lattice kinetic Monte Carlo model	61
3.2.2	Definition of variables	65
3.3	Closed-form dynamic model construction	68

3.3.1	Model parameter estimation and dependence on substrate temperature	69
3.4	Model predictive controller design	73
3.4.1	MPC formulation	74
3.4.2	MPC formulation based on finite-dimensional approximations	76
3.5	Closed-loop simulations	78
3.5.1	Separate regulation of surface slope and roughness	80
3.5.2	Simultaneous regulation of surface slope and roughness for light trapping efficiency	85
3.6	Conclusions	92
4	Control of Surface Roughness and Slope with 2D SPDE Model	93
4.1	Introduction	93
4.2	Preliminaries	94
4.2.1	2D Edwards–Wilkinson equation for surface height dynamics	94
4.2.2	Film surface roughness and rms slope	99
4.3	Model predictive controller design	100
4.4	Closed–loop simulations	103
4.4.1	Control of Film Surface Roughness	104
4.4.2	Control of Film Surface rms Slope	104

4.4.3	Simultaneous control of roughness and rms slope	106
4.4.4	Application to light trapping efficiency	108
4.5	Conclusions	110
5	Control of Aggregate Surface Morphology Using a Patterned Deposition Rate Profile	112
5.1	Introduction	112
5.2	Aggregate surface morphology	113
5.2.1	Process description and modeling	113
5.2.2	Aggregate surface roughness and slope	115
5.2.3	Light reflection on a rough surface	117
5.2.4	Patterned deposition rate profile	118
5.2.5	Edwards-Wilkinson equation for surface height dynamics . . .	121
5.2.6	Determination of model parameters	127
5.3	Model predictive controller design	134
5.4	Closed-loop simulations	136
5.4.1	Control of film surface roughness	136
5.4.2	Control of film surface slope	137
5.4.3	Simultaneous control of roughness and slope	138
5.4.4	Application to light trapping efficiency	139

5.5	Conclusions	141
6	Conclusions	143
	Bibliography	146

List of Figures

1.1	Typical structure of a p-i-n thin-film solar cell with front transparent conducting oxide (TCO) layer and back contact.	3
1.2	Reflectance of thin film surface as a function of r for different m	5
1.3	Light scattering at a rough interface	6
2.1	Schematic of thin film growth process in an LPCVD reactor.	18
2.2	Thin film growth process on a triangular lattice.	22
2.3	Definition of surface height profile	25
2.4	Illustration of the definition of film SOR of eq (2.9).	26
2.5	Profiles of the expected values of surface roughness square (solid line, left y -axis) and of film thickness (dash-dotted line, right y -axis) under closed-loop operation using the MPC formulation of eq (2.34) with $q_{r^2,i} = 0.1$, $q_{h,i} = 1$ and $q_{\rho,i} = 0$	45

2.6 Profiles of the expected values of surface roughness square (solid line, left y -axis) and of film thickness (dash-dotted line, right y -axis) under closed-loop operation using the MPC formulation of eq (2.34) with $q_{r^2,i} = 1$, $q_{h,i} = 0$ and $q_{\rho,i} = 0$ 45

2.7 Profiles of expected inlet silane concentrations under closed-loop operation using the MPC formulation of eq (2.34) with $q_{r^2,i} = 0.1$, $q_{h,i} = 1$ and $q_{\rho,i} = 0$ and the MPC formulation of eq (2.34) with $q_{r^2,i} = 1$, $q_{h,i} = 0$ and $q_{\rho,i} = 0$ (dashed line). 46

2.8 Histogram of closed-loop film thickness at the end of simulation ($t = 3000$ s) using the MPC formulation of eq (2.34) with $q_{r^2,i} = 0.1$, $q_{h,i} = 1$ and $q_{\rho,i} = 0$ 46

2.9 Histogram of closed-loop surface roughness square at the end of simulation ($t = 3000$ s) using the MPC formulation of eq (2.34) with $q_{r^2,i} = 0.1$, $q_{h,i} = 1$ and $q_{\rho,i} = 0$ 47

2.10 Profiles of the expected values of film SOR (solid line, left y -axis) and of inlet silane concentration (dash-dotted line, right y -axis) under closed-loop operation using the MPC formulation of eq (2.34) with $q_{r^2,i} = 0$, $q_{h,i} = 0$ and $q_{\rho,i} = 1$ 48

2.11 Histogram of closed-loop SOR at the end of simulation ($t = 3000$ s) using the MPC formulation of eq (2.34) with $q_{r^2,i} = 0$, $q_{h,i} = 0$ and $q_{\rho,i} = 1$ 48

2.12	Profiles of the expected values of surface roughness square (solid line, left y -axis) and of film thickness (dash-dotted line, right y -axis) under closed-loop operation using the MPC formulation of eq (2.34) with $q_{r^2,i} = 1$, $q_{h,i} = 1$ and $q_{\rho,i} = 1$	49
2.13	Profiles of the expected values of film SOR (solid line, left y -axis) and of inlet silane concentration (dash-dotted line, right y -axis) under closed-loop operation using the MPC formulation of eq (2.34) with $q_{r^2,i} = 1$, $q_{h,i} = 1$ and $q_{\rho,i} = 1$	50
2.14	Histogram of closed-loop SOR at the end of simulation ($t = 3000$ s) using the MPC formulation of eq (2.34) with $q_{r^2,i} = 1$, $q_{h,i} = 1$ and $q_{\rho,i} = 1$	50
2.15	Profiles of the expected values of surface roughness square (solid line, left y -axis) and of film thickness (dash-dotted line, right y -axis) under closed-loop operation using the MPC formulation of eq (2.35) with $q_{r^2,i} = 0.1$, $q_{h,i} = 0$ and $q_{\rho,i} = 0$	52
2.16	Histogram of closed-loop film thickness at the end of simulation ($t = 3000$ s) using the MPC formulation of eq (2.35) with $q_{r^2,i} = 0.1$, $q_{h,i} = 0$ and $q_{\rho,i} = 0$	52
2.17	Histogram of closed-loop surface roughness square at the end of simulation ($t = 3000$ s) using the MPC formulation of eq (2.35) with $q_{r^2,i} = 0.1$, $q_{h,i} = 0$ and $q_{\rho,i} = 0$	53

2.18	Profiles of SOR estimated via eq (2.36) (solid line) and computed directly from the multiscale process model (dash-dotted line).	55
2.19	Profiles of the expected value of film SOR (solid line, left y -axis) and of inlet silane concentration (dash-dotted line, right y -axis) under closed-loop operation using the MPC formulation of eq (2.34) with $q_{r^2,i} = 0$, $q_{h,i} = 0$ and $q_{\rho} = 1$ and porosity estimation.	56
2.20	Histogram of closed-loop SOR at the end of simulation (t=3000 s) using the MPC formulation of eq (2.34) with $q_{r^2,i} = 0$, $q_{h,i} = 0$ and $q_{\rho} = 1$ and porosity estimation.	56
2.21	Profiles of the expected values of film SOR (solid line, left y -axis) and of inlet silane concentration (dash-dotted line, right y -axis) under closed-loop operation using the MPC formulation of eq (2.34) with $q_{r^2,i} = 1$, $q_{h,i} = 1$ and $q_{\rho} = 1$ and porosity estimation.	57
2.22	Profiles of the expected values of film SOR (solid line, left y -axis) and of inlet silane concentration (dash-dotted line, right y -axis) under closed-loop operation using the MPC formulation of eq (2.34) with $q_{r^2,i} = 1$, $q_{h,i} = 1$ and $q_{\rho} = 1$ and porosity estimation.	58
2.23	Histogram of closed-loop SOR at the end of simulation (t=3000 s) using the MPC formulation of eq (2.34) with $q_{r^2,i} = 1$, $q_{h,i} = 1$ and $q_{\rho} = 1$ and porosity estimation.	58

3.1	Thin film growth process on a triangular lattice	62
3.2	The definition of the surface height profile and surface slope profile	67
3.3	Steady-state values of the expected mean slope square computed from the EW equation and from the kMC simulations at different substrate temperatures; $W = 1$ layer/s	71
3.4	Dependence of $\ln(\nu)$ and σ^2 on substrate temperature; $W = 1$ layer/s.	72
3.5	Comparison of EW-model prediction and kMC simulation results for $\langle m^2 \rangle$; $T = 500\text{K}$ and $W = 1$ layer/s.	72
3.6	Comparison of EW-model prediction and kMC simulation results for $\langle m^2 \rangle$; $T = 600\text{K}$ and $W = 1$ layer/s.	73
3.7	Profiles of reconstructed surface roughness square and mean slope square from the finite-dimensional approximation.	77
3.8	Profile of the expected mean slope square under closed-loop operation; $m_{\text{set}}^2 = 0.5$	82
3.9	Profile of the expected substrate temperature under closed-loop operation; $m_{\text{set}}^2 = 0.5$	82
3.10	Profile of the expected mean slope square under closed-loop operation; $m_{\text{set}}^2 = 5$	83
3.11	Profile of the expected substrate temperature under closed-loop operation; $m_{\text{set}}^2 = 5$	83

3.12	Profile of the expected mean roughness square under closed-loop operation; $r_{\text{set}}^2 = 100$	84
3.13	Profiles of $\langle r^2 \rangle$ and $\langle m^2 \rangle$ at the end of closed-loop simulations ($t = 1000s$) for different penalty weighting factors: $q_{m^2} = 1$ and $1 \leq q_{r^2} \leq 10000$	86
3.14	Dependence of light reflectance of thin film on the ratio of the weighting factors, $\lg(q_{r^2}/q_{m^2})$; $r_{\text{set}}^2 = 100$ and $m_{\text{set}}^2 = 0.5$	88
3.15	Light reflectance of thin films deposited under closed-loop operations with different weighting schemes.	89
3.16	Snapshots of the film microstructure at the end of simulations ($t = 1000s$) under open-loop and closed-loop operations	91
4.1	Profile of expected film surface roughness square from 100 closed-loop simulations. $q_{r^2} = 1$, $q_{m^2} = 0$ and $r_{\text{set}}^2 = 15$	105
4.2	Profiles of manipulated variables. $q_{r^2} = 1$, $q_{m^2} = 0$ and $r_{\text{set}}^2 = 15$	105
4.3	Comparison of histograms of r^2 at the end of the simulation between open-loop and closed-loop simulations	106
4.4	Profile of expected film surface rms slope square from 100 closed-loop simulations. $q_{r^2} = 0$, $q_{m^2} = 1$, and $m_{\text{set}}^2 = 0.2$	107
4.5	Profiles of manipulated variables. $q_{r^2} = 0$, $q_{m^2} = 1$, and $m_{\text{set}}^2 = 0.2$	107

4.6	Comparison of histograms of m^2 at the end of the simulation between open-loop and closed-loop simulations. $q_{r^2} = 0$, $q_{m^2} = 1$, and $m_{set}^2 = 0.2$.	108
4.7	$\langle r^2 \rangle$ and $\langle m^2 \rangle$ at the end of closed-loop simulations ($t = 100$ s) for different penalty weighting factors: $q_{m^2} = 1$ and $0.01 \leq q_{r^2} \leq 10^6$.	108
4.8	Light reflectance of thin films deposited under closed-loop operations with different weighting factor ratio.	110
5.1	Thin film deposition process on a 2D square lattice.	114
5.2	1D surface with roughness at different length scales	116
5.3	Reflection as a function of r_Δ and m_Δ of thin film surface.	119
5.4	Dependence of the steady state values of aggregate roughness and aggregate slope on aggregation length	120
5.5	c_2 and σ_2 as functions of lattice size l	128
5.6	c_2 and σ_2 as functions of deposition rate w_0	130
5.7	Steady state value of roughness $\langle r^2 \rangle$ as a function of lattice size l	131
5.8	$\langle r_\Delta^2 \rangle$ as a function of aggregation length Δ	132
5.9	Profile of expected film surface roughness square from 100 closed-loop simulations. $q_{r^2} = 1$, $q_{m^2} = 0$ and $r_{set}^2 = 0.04 \text{ nm}^2$.	137
5.10	Surface profile at the end of simulation, $t = 100$ s. $q_{r^2} = 1$, $q_{m^2} = 0$ and $r_{set}^2 = 0.04 \text{ nm}^2$.	138

5.11	Profile of expected film surface slope square from 100 closed-loop simulations. $q_{r^2} = 0$, $q_{m^2} = 1$ and $m_{set}^2 = 0.025$	139
5.12	Surface profile at the end of simulation, $t = 100$ s. $q_{r^2} = 0$, $q_{m^2} = 1$ and $m_{set}^2 = 0.025$	140
5.13	$\langle r_{\Delta}^2 \rangle$ and $\langle m_{\Delta}^2 \rangle$ at the end of closed-loop simulations ($t = 100$ s) for different penalty weighting factors: $q_{m^2} = 1$, $10^{-8} \leq q_{r^2} \leq 1$, $r_{set}^2 = 1.0$, $m_{set}^2 = 0.025$	141
5.14	Light reflectance of thin films deposited under closed-loop operations with different weighting factor ratios	142

ACKNOWLEDGEMENTS

It is my great fortune to work with Professor Panagiotis D. Christofides and Professor Gerassimos Orkoulas throughout my doctoral work. I would like to express my deepest gratitude to them for their guidance, encouragement and unwavering support.

I would like to thank Professor James F. Davis and Professor Tsu-Chin Tsao for agreeing to serve on my doctoral committee.

I also learned a lot from countless discussions with my colleagues, particularly Gangshi Hu, Jianqiao Huang, Patrick R. Sisljan, David Pham, Lutz Mädler and Mingheng Li. I consider myself lucky to be surrounded by these outstanding individuals.

Finally, I would like to thank my mother Xueming Dong and father Binyan Zhang for sharing with me their love of learning. I wouldn't be able to finish this work without their love and support.

Financial support from NSF, CBET-0652131, and from the UCLA Graduate Division through a 2010–2011 Doctoral Dissertation Year Fellowship, is gratefully acknowledged.

Chapter 2 is a version of: X. Zhang., G. Hu, G. Orkoulas and P. D. Christofides. Controller and Estimator Design for Regulation of Film Thickness, Surface Roughness and Porosity in a Multiscale Thin Film Growth Process. *Industrial & Engineering Chemistry Research*, 49:7795–7806, 2010.

Chapter 3 is a version of: X. Zhang., G. Hu, G. Orkoulas and P. D. Christofides. Predictive Control of Surface Mean Slope and Roughness in a Thin Film Deposition Process. *Chemical Engineering Science*, 65:4720–4731, 2010.

Chapter 4 is a version of: X. Zhang., G. Hu, G. Orkoulas and P. D. Christofides. Multivariable Model Predictive Control of Thin Film Surface Roughness and Slope for Light Trapping Optimization. *Industrial & Engineering Chemistry Research*, 49:10510–10516, 2010.

Chapter 5 is a version of: X. Zhang., J. Huang, G. Hu, G. Orkoulas and P. D. Christofides. Controlling Aggregate Thin Film Surface Morphology for Improved Light Trapping using a Patterned Deposition Rate Profile. *Chemical Engineering Science*, *in press*.

VITA

- 2007 Bachelor of Science, Automation
Zhejiang University
Hangzhou, China
- 2008–2010 Graduate Student Researcher
Department of Chemical and Biomolecular Engineering
University of California, Los Angeles
- 2008–2010 Teaching Assistant/Associate/Fellow
Department of Chemical and Biomolecular Engineering
University of California, Los Angeles
- 2010–2011 Dissertation Year Fellowship
University of California, Los Angeles

PUBLICATIONS AND PRESENTATIONS

1. G. Hu, X. Zhang, G. Orkoulas, and P. D. Christofides. Construction of stochastic differential equation models for porous thin film deposition processes. *AIChE Annual Meeting*, paper 546a, Philadelphia, Pennsylvania, 2008.
2. P. R. Sislian, X. Zhang, M. Li, D. Pham, L. Mädler, P. D. Christofides. Bacterial Aerosol Neutralization by Aerodynamic Shocks using a Novel Impactor System: Design and Computation. *Chemical Engineering Science*, 64:1953-1967, 2009
3. G. Hu, X. Zhang, G. Orkoulas, and P. D. Christofides. Simultaneous regulation of film thickness, surface roughness and porosity in a multiscale thin film growth process. *Proceedings of the 48th IEEE Conference on Decision and Control*, 2387–2394, Shanghai, China, 2009.

4. X. Zhang, G. Hu, G. Orkoulas, and P. D. Christofides. Multiscale modeling and control of a porous thin film deposition process. *AIChE Annual Meeting*, paper 140f, Nashville, Tennessee, 2009.
5. X. Zhang, G. Hu, G. Orkoulas, and P. D. Christofides. Controller and estimator design for regulation of film thickness, surface roughness and porosity in a multiscale thin film growth process. *Industrial & Engineering Chemistry Research*, 49:7795–7806, 2010.
6. X. Zhang., G. Hu, G. Orkoulas and P. D. Christofides. Predictive control of surface mean slope and roughness in a thin film deposition process. *Chemical Engineering Science*, 65:4720–4731, 2010.
7. X. Zhang., G. Hu, G. Orkoulas and P. D. Christofides. Multivariable Model Predictive Control of Thin Film Surface Roughness and Slope for Light Trapping Optimization. *Industrial & Engineering Chemistry Research*, 49:10510–10516, 2010.
8. P. R. Sislian, D. Pham, X. Zhang, M. Li, D. Pham, L. Mädler and P. D. Christofides. Bacterial Aerosol Neutralization by Aerodynamic Shocks using a Novel Impactor System: Experimental Results For E. Coli and Analysis. *Chemical Engineering Science*, 65: 1490-1502, 2010.
9. P. R. Sislian, J. Rau, X. Zhang, D. Pham, M. Li, L. Mädler and P. D. Christofides. Bacterial Aerosol Neutralization by Aerodynamic Shocks Using an Impactor

- System: Experiments Results for *B. atropheus* Spores. *Chemical Engineering Science*, 65: 4803-4815, 2010.
10. X. Zhang., J. Huang, G. Hu, G. Orkoulas and P. D. Christofides. Modeling and Control of Aggregate Surface Roughness and Slope in Thin Film Growth for Light Trapping Optimization. *AIChE Annual Meeting*, paper 291f, Salt Lake City, Utah, 2010.
 11. X. Zhang., G. Hu, G. Orkoulas and P. D. Christofides. Multivariable Model Predictive Control of Surface Roughness and Slope in a Thin Film Growth Process. *AIChE Annual Meeting*, paper 528e, Salt Lake City, Utah, 2010.
 12. P. Sislian, J. Rau, X. Zhang., D. Pham, M. Li, L. Mädler and P. D. Christofides. Bacterial Aerosol Neutralization by Aerodynamic Shocks Using An Impactor System: An Integrated Computational and Experimental Study On *B. Atropheus* Spores. *AIChE Annual Meeting*, paper 230e, Salt Lake City, Utah, 2010.
 13. X. Zhang., J. Huang, G. Orkoulas and P. D. Christofides. Controlling aggregate thin film surface morphology for improved light trapping using a patterned deposition rate profile. *Chemical Engineering Science*, *in press*.
 14. X. Zhang., G. Hu, G. Orkoulas and P. D. Christofides. Modeling and Control of Aggregate Thin Film Surface Morphology Using Stochastic PDEs and a Patterned Deposition Rate Profile. *AIChE Annual Meeting*, *accepted*, *Minneapolis, Minnesota, 2011*

ABSTRACT OF THE DISSERTATION

Multiscale Modeling and Control of Microstructural Defects and Surface
Morphology in Thin Film Deposition

by

Xinyu Zhang

Doctor of Philosophy in Chemical Engineering

University of California, Los Angeles, 2011

Professor Panagiotis D. Christofides, Co-Chair

Professor Gerassimos Orkoulas, Co-Chair

Thin film deposition is a key process used in the manufacturing of microelectronic devices as well as in the manufacturing of thin film solar cells. Improving the ability to operate and control thin film deposition such that the deposited films have desired levels of internal microstructure and surface morphology is an issue of major technological significance, with significant implications in the efficiencies of microelectronic devices and thin film solar cells. While significant progress has been made over the last ten years on modeling and control of thin film surface roughness and porosity, there is a number of important unresolved practical issues with respect to our ability to implement the existing solutions for porosity control in practice as well as with

respect to control of surface morphology metrics that directly regulate light trapping properties of thin films.

This dissertation presents a unified and practical framework for multiscale modeling and control of thin film internal microstructure and surface morphology in thin film deposition processes. Multiscale modeling provides the link between microscopic film properties like film porosity and surface morphology and macroscopically-controlled process variables like temperature and precursor flow rate and concentration. Within this multiscale modeling framework, model predictive control is used to develop novel control problem formulations and manipulated input trajectories which account for control actuator constraints and lead to a balanced trade-off in the closed-loop system between the possibly conflicting control objectives of film porosity and film surface roughness and/or slope. The proposed multiscale modeling and control methods are applied to a series of complex thin film deposition processes and extensive simulation studies are carried out to evaluate the resulting closed-loop system performance and robustness in terms of achieving key film quality metrics such as amount of internal defects and light trapping efficiency of film surface.

Chapter 1

Introduction

1.1 Motivation

Currently, there is an increasing need to improve the thin film semiconductor manufacturing process operation and yield due to its crucial role in a wide range of applications such as microelectronics, optical electronics, and solar cells [63]. In the microelectronics industry, the surface roughness and slope strongly influence the electrical and mechanical properties of microelectronic devices [2, 41]. The amount of internal defects, which can be characterized by film porosity, is another important parameter that needs to be tightly controlled. Porosity strongly influences film electrical properties. For example, low-k dielectric films of high porosity are being used in current interconnect technologies to meet resistive-capacitive delay goals and minimize cross-talk. In the case of gate dielectrics, it is important to reduce thin film

porosity as much as possible and eliminate the development of holes close to the interface.

Another area that requires stringent control of thin film microstructure is the photovoltaic cell manufacturing. Photovoltaic (solar) cells are an important source of sustainable energy and their share of the overall solar cell market is steadily increasing (e.g., [23, 68]). Currently, the limited conversion efficiency of the solar power prevents the wide application of solar cells. Thin-film silicon solar cells are currently the most developed and widely used solar cells. Research on optical and electrical modeling of thin-film silicon solar cells indicates that the scattering properties of the thin film interfaces are directly related to the light trapping process and the efficiencies of thin-film silicon solar cells [36, 51]. Recent studies on enhancing thin-film solar cell performance [79, 55, 51, 65, 60] have shown that film surface and interface morphology, characterized by root-mean-square roughness (RMS roughness, r) and root-mean-square slope (RMS slope, m) at length scales comparable to the wavelength of incident light [73], play an important role in enhancing absorption of the incident light by the semiconductor layers. Specifically, significant increase of conversion efficiency by introducing appropriately roughened interfaces has been reported in several works [66, 40, 37].

To provide a concrete example of this issue, we focus on a typical p-i-n thin-film solar cell (Fig. 1.1). In this thin-film solar cell, light comes into the hydrogenated amorphous silicon (a-Si:H) semiconductor layers (p, i, n layers) through a front trans-

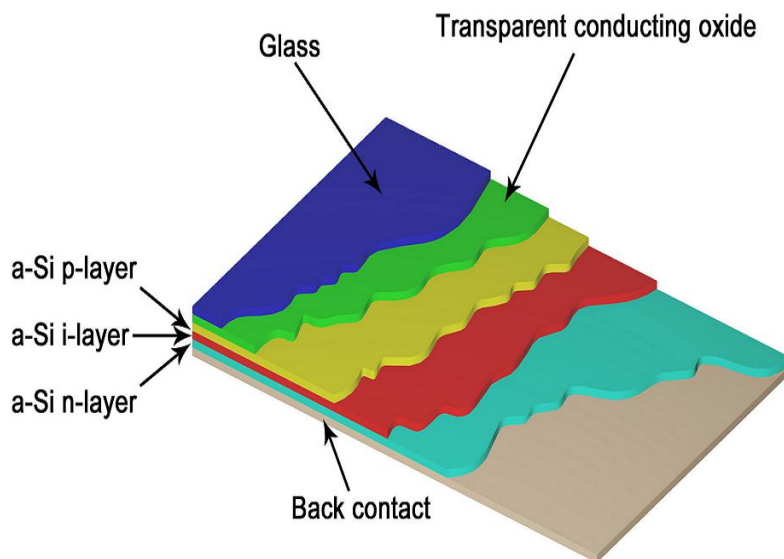


Figure 1.1: Typical structure of a p-i-n thin-film solar cell with front transparent conducting oxide (TCO) layer and back contact.

parent conducting oxide (TCO) layer (made, for example, of ZnO:Al), and part of this light is absorbed by the semiconductor layers before it reaches the back TCO layer. At the back TCO layer, the remaining light is either reflected back to the semiconductor layers to potentially be absorbed again or leaves the system by transmitting through the back TCO layer. The reflected light that is not absorbed reaches the front TCO layer again and this process of reflection and transmission is repeated until all the light leaves the cell or is absorbed by the cell. We focus on a thin film a-Si:H p-i-n solar cell with glass/ZnO:Al as the front TCO layer and ZnO:Al as the back TCO layer to demonstrate quantitatively the influence of surface/interface r and m on thin film light reflectance and transmittance. Light scattering (Rayleigh scattering) occurs when the incident light goes through a rough interface (e.g., the

front TCO surface or the TCO-p interface) where it is divided into four components: specular reflection, specular transmission, diffused reflection and diffused transmission; see Fig. 1.3 [66, 40]. If a rough thin film surface is illuminated with a beam of monochromatic light at normal incidence, the total reflectance, R , can be approximately calculated as follows [14]:

$$R = R_0 \exp\left[-\frac{4\pi r^2}{\lambda^2}\right] + R_0 \int_0^{\pi/2} 2\pi^4 \left(\frac{a}{\lambda}\right)^2 \left(\frac{r}{\lambda}\right)^2 (\cos\theta + 1)^4 \sin\theta \exp\left[-\frac{(\pi a \sin\theta)^2}{\lambda^2}\right] d\theta \quad (1.1)$$

where R_0 is the reflectance of a perfectly smooth surface of the same material, r is the RMS roughness, θ is the incident angle, λ is the light wavelength and a is the auto-covariance length. It can be proved that $a = \sqrt{2}r/m$, where m is the RMS slope of the profile of the surface [9]. The numerical integration result of eq (1.1) is shown in Figure 1.2. From this plot, it can be inferred that both r and m strongly influence the intensity of light reflection (and therefore, light transmission) by the surface/interface. Specifically, in a thin-film solar cell, the objective is to maximize the generation of electricity in the i-layer, so it is necessary to control the intensities and directions of light reflection and transmission at the front and back TCO layers, as well as at the TCO-p and n-TCO interfaces by attaining proper values of r and m during the thin-film manufacturing process. Specifically, when light first comes into the front TCO layer, appropriate values of r and m are needed for the surface of the TCO layer to maximize the transmission, T , through the TCO layer. At the back

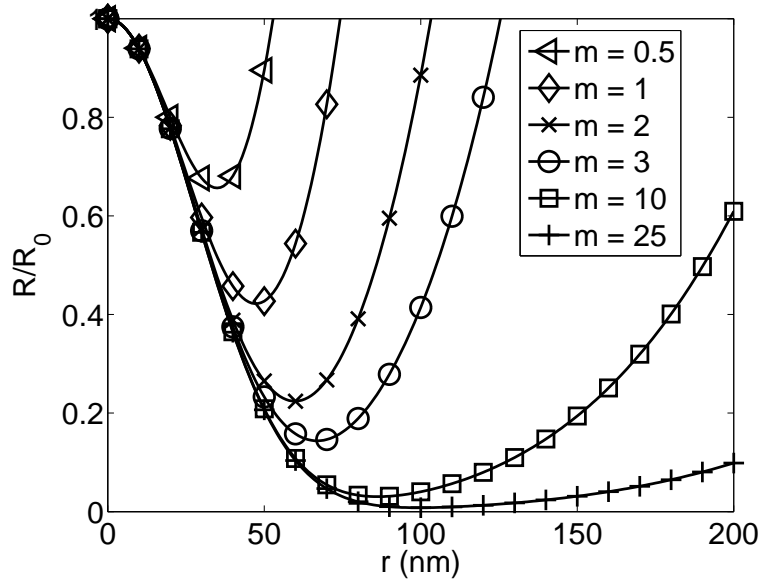


Figure 1.2: Reflectance of thin film surface as a function of r for different m .

n-TCO interface layer, certain surface morphology is also required to maximize the reflection, R , of light back to the cell. The distributions of the four components of light reflectance and transmittance are also affected by m and r [37, 38] even though this dependence cannot be expressed by an approximate equation like the one of Eq. (1.1). Therefore, it is important during the manufacturing of thin-film solar cells to regulate process input variables like precursor flow rates and temperature such that the surfaces/interfaces of the produced thin-film solar cells have appropriate values (set-points) of r and m that optimize light reflectance and transmittance.

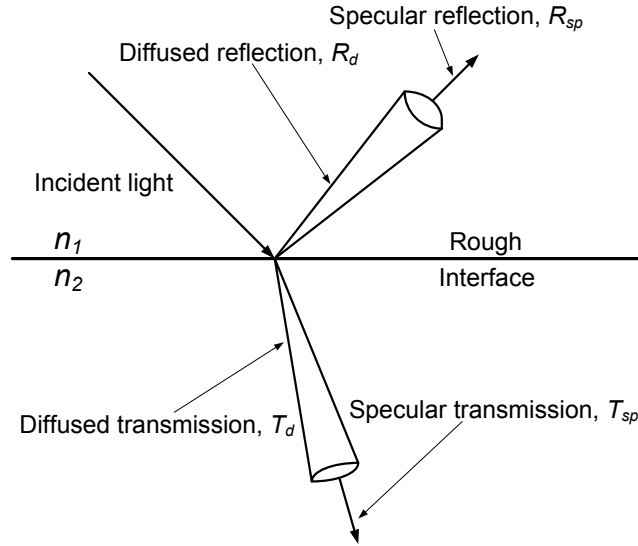


Figure 1.3: Light scattering at a rough interface: specular reflection, R_{sp} , diffused reflection, R_d , specular transmission, T_{sp} , and diffused transmission, T_d . n_1 and n_2 are the refractive indices of the two substances above and below the rough interface, respectively.

1.2 Control of thin film microstructure

Motivated by the above considerations, model-based real-time feedback control of thin film growth processes has become increasingly important in order to meet the stringent requirement on the quality of thin films and reduce thin film variability. The development of modern surface roughness measurement techniques has enabled real-time feedback of thin film growth conditions with a wide variety of sensors, such as x-ray and electron diffraction, and optical spectroscopy [8, 24]. For example, surface roughness can be measured by X-ray scattering (GISAXS) in real-time [58] or by combination of on-line measurement techniques for measuring gas phase compositions with off-line measurement techniques for measuring surface roughness [54].

In [54], the latter approach was used to measure carbon composition of thin films in plasma-enhanced chemical vapor deposition using combination of optical emission spectroscopy (OES) and X-ray photoelectron spectroscopy (XPS). Moreover, experimental methods have been developed to perform scanning tunneling microscopy (STM) measurements of the surface during epitaxial growth of semiconductor layers [72].

Deposition uniformity and composition control has been accomplished on the basis of continuum-type distributed parameter models (see [59, 3, 67, 12] for results on rapid thermal processing (RTP) and [5, 54] for results on plasma-enhanced chemical vapor deposition (PECVD)). However, precise control of thin film microstructure requires stochastic distributed models that can predict how the microscopic-level film state is influenced by changes in the macroscopic process parameters.

Control of macroscopic variables which are low statistical moments of the microscopic distributions (e.g., surface coverage, which is the zeroth moment of species distribution on a lattice) can be achieved using linear deterministic models. Such an approach was reported in [64, 7] to identify linear deterministic models from the output of kinetic Monte Carlo (kMC) simulators and design controllers using linear control theory. Other results based on construction of linear/nonlinear deterministic models from input/output data can be found in [15, 61, 77].

However, deterministic models may not be sufficient to control higher statistical moments of the microscopic distributions, such as the surface roughness (the second

moment of height distribution on a lattice), surface slope or film internal porosity. The effect of the stochastic nature of the microscopic processes becomes significant in these cases and cannot be ignored in the model construction and controller design. In the context of modeling the evolution of thin film height profiles, kinetic Monte Carlo models and stochastic partial differential equations are two widely-used methods. Feedback control of surface roughness based on kMC models was developed in [45, 44]. In [44] a real-time roughness estimator was proposed using multiple small lattice kMC simulators, adaptive filters and measurement error compensators. In [45] feedback controllers based on the real-time roughness estimators were designed. In addition, the effectiveness of the method was demonstrated in the context of surface roughness control of a GaAs deposition process model [46]. Kinetic Monte Carlo models have also been used in predictive control of surface roughness in a complex deposition process including multiple components with both short-range and long-range interactions [52]. Using kMC simulation as a realization of a stochastic process consistent with the master equation that describes the evolution of the probability distribution of the system at a certain micro-configuration, Gallivan [20] proposed a method to construct reduced-order approximation of the master equation. On the other hand, controller design methods based on stochastic PDEs can be found in [47, 48]. In this method, the linear PDE is first reformulated as a system of infinite linear stochastic ODEs by using modal decomposition and then a finite-dimensional approximation that captures the dominant mode contribu-

tion to the surface roughness is derived. Subsequently a state feedback controller is designed based on the finite-dimensional approximation. Finally, computationally-efficient optimization schemes for multiscale models have been developed based on the concept of in-situ adaptive tabulation [70, 69], based on the concept of coarse time-steppers [6, 10], and based on the concept of funneling [49, 50].

Model predictive control is widely used in chemical process control due to its ability to handle input and state constraints, achieve robustness against model inaccuracy and force the closed-loop system to follow an optimal trajectory (see reference [21, 4, 56, 62] for reviews of results on MPC). An MPC calculates the control action by repeatedly solving a finite horizon constrained open-loop optimization problem. Recent efforts on predictive control of distributed parameter systems have mainly focused on application to deterministic parabolic PDEs including linear systems with distributed [17] and boundary [16] actuation.

1.3 Modeling of thin film deposition processes

As discussed in the previous section, both kinetic Monte Carlo (kMC) methods [22, 57] and stochastic differential equation (SDE) models [18, 74, 39] have been widely used in thin film growth process modeling and controller design. kMC methods simulate thin film microscopic processes based on the microscopic rules and the thermodynamic and kinetic parameters obtained from experiments and molecular dynamics

simulations [43, 80, 42, 13]. Specifically, kinetic Monte Carlo (kMC) models based on a square lattice and utilizing the solid-on-solid (SOS) approximation for deposition were employed to describe the evolution of film microstructure and design feedback control laws for thin film surface roughness [44, 13]. kMC models have also been used to simulate porous thin films in many deposition processes, such as the molecular beam epitaxial (MBE) growth of silicon films [43] and copper thin film growth [80]. A triangular lattice kMC model that allows vacancies and overhangs to develop was introduced in [29, 81] to model porous thin film growth. However, since kMC models are not available in closed form, they cannot be readily used for feedback control design and system-level analysis.

On the other hand, stochastic PDEs can be used for the modeling of surface height evolution in thin film growth and sputtering processes. For example, many deposition processes can be modeled by the Edward-Wilkinson equation [18]. The nonlinear stochastic Kuramoto-Sivashinsky equation (KSE) has been used in [27, 26] to model a sputtering process. The closed form of the SDE models enables their use as the basis for the design of feedback controllers which can regulate thin film surface roughness, film porosity, and film thickness, using either deposition rate or substrate temperature as manipulated input [28, 29, 30]. Although stochastic PDE models are available, the construction of these models for thin film deposition processes is a challenging task. Most system identification results focus on stochastic ODE systems, e.g., Astrom's early work [1] provides theoretical foundations on the

analysis, parametric optimization, and optimal stochastic control for linear stochastic ODE systems. More recently, Bohlin [11] and Kristensen [35] proposed likelihood-based methods for parameter estimation of stochastic ODE models. To determine the model parameters, an optimization problem is solved in these methods to maximize a likelihood function or a posterior probability density function of a given sequence of measurements of a stochastic process. Since the dynamics of the state moment of a stochastic process may be described by deterministic equations, recent works [47, 53] proposed an identification method for linear stochastic PDEs employing parameter identification techniques for deterministic systems.

1.4 Dissertation objectives and structure

Motivated by the above considerations, this dissertation focuses on the modeling and control of film surface morphology and internal microstructure in thin film growth processes. Kinetic Monte Carlo models are developed to simulate the thin film growth processes on the basis of lattice structures; both solid-on-solid and triangular lattice models are used. Surface roughness, surface slope and film porosity are defined and computed from the kMC simulation data and are used to characterize the surface morphology and microstructure of the thin films. Stochastic and deterministic differential equation models are introduced to describe the evolution of the thin film surface morphology and internal microstructure and are used as the basis for feedback control design. The model parameters of the dynamic equation models can be estimated on

the basis of the kMC simulation data using least-square methods. MPC algorithms are developed to regulate and stabilize the thin film surface roughness, surface slope and film porosity at desired levels. Simultaneous control of these variables under a unified framework is addressed using MPC. The proposed control algorithms are successfully applied to the kMC models and SPDE models of the thin film deposition processes under consideration through numerical simulations.

This dissertation has the following structure:

Chapter 2 focuses on simultaneous regulation of film thickness, surface roughness and porosity in a multiscale model of a thin film growth process using the inlet precursor concentration as the manipulated input. Specifically, under the assumption of continuum, a partial differential equation model is first derived to describe the dynamics of the precursor concentration in the gas phase. The thin film growth process is modeled via a microscopic kinetic Monte Carlo simulation model on a triangular lattice with vacancies and overhangs allowed to develop inside the film. Closed-form dynamic models of the thin film surface profile and porosity are developed and used as the basis for the design of model predictive control algorithms to simultaneously regulate film thickness, surface roughness, and porosity. Both state feedback and porosity estimation-based output feedback control algorithms are presented. Simulation results demonstrate the applicability and effectiveness of the proposed modeling and control approach by applying the proposed controllers to the multiscale model of the thin film growth process.

Chapter 3 focuses on the development of a model predictive control algorithm to simultaneously regulate the surface slope and roughness of a thin film growth process to optimize thin film light reflectance and transmittance. Specifically, a thin film deposition process modeled on a one-dimensional triangular lattice that involves two microscopic processes: an adsorption process and a migration process, is considered. Kinetic Monte Carlo (kMC) methods are used to simulate the thin film deposition process. To characterize the surface morphology and to evaluate the light trapping efficiency of the thin film, surface roughness and surface slope are introduced as the root mean squares of the surface height profile and surface slope profile. An Edwards–Wilkinson (EW)-type equation is used to describe the dynamics of the surface height profile and predict the evolution of the root-mean-square (RMS) roughness and RMS slope. A model predictive control algorithm is then developed on the basis of the EW equation model to regulate the RMS slope and the RMS roughness at desired levels by optimizing the substrate temperature at each sampling time. The model parameters of the EW equation are estimated from simulation data through least-square methods. Closed-loop simulation results demonstrate the effectiveness of the proposed model predictive control algorithm in successfully regulating the RMS slope and the RMS roughness at desired levels that optimize thin film light reflectance and transmittance.

Chapter 4 focuses on the development of a multivariable model predictive controller that simultaneously regulates thin film surface roughness and mean slope to

optimize light reflectance and transmittance during thin film manufacturing by manipulating substrate temperature and deposition rate. Surface roughness and surface slope are defined as the root-mean-squares of the surface height profile and the surface slope profile, respectively. The dynamics of the evolution of the thin film surface height profile are assumed to be described by an Edwards–Wilkinson-type equation (a second-order stochastic partial differential equation) in two spatial dimensions. Analytical solutions of the expected surface roughness and surface slope are obtained on the basis of the Edwards–Wilkinson equation and are used in the controller design. The model parameters of the Edwards–Wilkinson equation depend on the substrate temperature and deposition rate. This dependence is used in the formulation of the predictive controller to predict the influence of the control action on the surface roughness and slope at the end of the growth process. The model predictive controller involves constraints on the magnitude and rate of change of the control action and optimizes a cost that involves penalty on both surface roughness and mean slope from the set-point values. The controller is applied to the two-dimensional Edwards–Wilkinson equation and is shown to successfully regulate surface roughness and mean slope to set-point values at the end of the deposition that yield desired film reflectance and transmittance.

Chapter 5 focuses on modeling and control of aggregate thin film surface morphology for improved light trapping using a patterned deposition rate profile. The dynamics of the evolution of the thin film surface height profile are modeled by an

Edwards-Wilkinson-type equation in two spatial dimensions. The thin film surface morphology is characterized in terms of aggregate surface roughness and surface slope. These variables are computed with respect to appropriate visible light-relevant characteristic length scales and defined as the root-mean-squares of height deviation and slope of aggregate surface height profiles, respectively. Analytical solutions of the expected aggregate surface roughness and surface slope are obtained by solving the Edwards-Wilkinson equation and are used in the controller design. The model parameters of the Edwards-Wilkinson equation are estimated from kinetic Monte-Carlo simulations using a novel parameter estimation procedure. This parameter dependence on the deposition rate is used in the formulation of the predictive controller to predict the influence of the control action on the surface roughness and slope at the end of the growth process. The cost function of the controller involves penalties on both aggregate surface roughness and mean slope from set-point values as well as constraints on the magnitude and rate of change of the control action. The controller is applied to the two-dimensional Edwards-Wilkinson equation. Simulation results demonstrate that the proposed controller successfully regulates aggregate surface roughness and slope to set-point values at the end of the deposition that yield desired levels of thin film reflectance and transmittance.

Finally, Chapter 6 summarizes the contributions of this dissertation.

Chapter 2

Control of Film Thickness, Surface Roughness and Porosity in a Multiscale Thin Film Growth Process

2.1 Introduction

In the context of modeling of thin film porosity, kMC models have been widely used to model the evolution of porous thin films in many deposition processes [43, 80, 42, 76]. Deterministic and stochastic ordinary differential equation (ODE) models of film porosity were recently developed [28] to model the evolution of film porosity and

its fluctuation and design model predictive control (MPC) algorithms to control film porosity to a desired level and reduce run-to-run porosity variability. More recently, simultaneous control of film thickness, surface roughness, and porosity within a unified control framework was addressed on the basis of a kMC thin film growth model using the deposition rate as the manipulated input [29]. However, in a practical thin film growth setting, the surface deposition rate cannot be manipulated directly but indirectly through manipulation of the inlet precursor concentration.

This chapter addresses this practical consideration and focuses on simultaneous regulation of film thickness, surface roughness, and porosity in a multiscale model of a thin film growth process using the inlet precursor concentration as the manipulated input. Specifically, under the continuum hypothesis, a partial differential equation model is used to describe the dynamics of the precursor concentration in the gas phase. The thin film growth process is modeled via a microscopic kinetic Monte Carlo simulation model on a triangular lattice with vacancies and overhangs allowed to develop inside the film. The macroscopic and microscopic models are connected through boundary conditions. Distributed parameter and lumped dynamic models are developed to describe the evolution of the film surface profile and porosity, respectively. The developed dynamic models are then used as the basis for the design of state and output feedback model predictive control algorithms to simultaneously regulate film thickness, surface roughness, and porosity. Simulation results demonstrate the applicability and effectiveness of the proposed modeling and control approach by

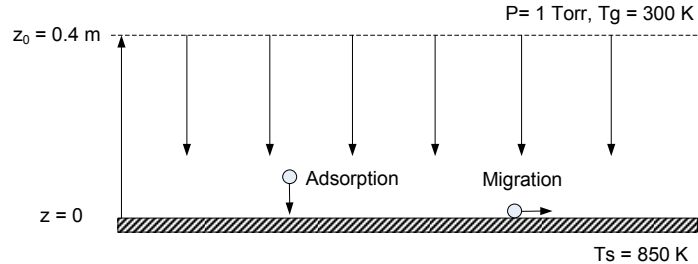


Figure 2.1: Schematic of thin film growth process in an LPCVD reactor.

applying the proposed controllers to the multiscale process model.

2.2 Preliminaries

We consider a silicon thin film growth process in a low-pressure chemical vapor deposition (LPCVD) reactor, which is shown in figure 2.1. Due to the large discrepancies of the time and length scales between the gas-phase and the thin-film growth phenomena, two different models are employed to describe the evolutions of the gas phase and of the thin film. Under the continuum hypothesis, a PDE model derived from a mass balance is used to describe the precursor concentration in the gas-phase. The thin film growth model is simulated through an on-lattice kMC model that uses a triangular lattice and allows overhangs and vacancies to develop inside the film. The two models are connected through boundary conditions, i.e., the adsorption rate in the kMC model depends on the reactant concentration right above the surface following an appropriate deposition rate law.

2.2.1 Gas-phase model

For the gas-phase model, a vertical, one-dimensional, stagnant flow geometry is considered. The inlet flow consists of two components, hydrogen and silane. Silane diffuses through a stagnant gas film of hydrogen. The temperature is constant throughout the gas phase. Thus, under the assumption of continuum, the silane concentration in the gas phase can be modeled via the following parabolic PDE:

$$\frac{\partial X}{\partial t} = D \frac{\partial^2 X}{\partial z^2} - KX \quad (2.1)$$

where X is the molar fraction of silane, D is the diffusivity of silane, and the term $-KX$ accounts for the consumption of silane in the gas phase, i.e., via gas-phase reaction and undesired sediments on reactor walls (we assume that this term has a first-order dependence on silane concentration, but other rate laws can be readily used in the present framework).

The diffusivity, D , is calculated using a second order polynomial of temperature as follows [34]:

$$D = c_0 + c_1 T_g + c_2 T_g^2, \quad (2.2)$$

where T_g is the gas phase temperature set at 300 K, and c_0 , c_1 , and c_2 are the coefficients of the polynomial whose values are given in Table 2.1.

T_g	300 K	P	1 Torr
T_s	850 K	z_0	0.4 m
c_0	-2.90	K	0.5
c_1	2.06×10^{-2}	K_H	0.19 [Pa ^{-1/2}]
c_2	2.81×10^{-5}	K_s	0.70 [Pa ⁻¹]

Table 2.1: Gas-Phase Model Parameters.

The diffusion equation of eq (2.1) is subject to the initial condition

$$X(z, 0) = 0, \quad (2.3)$$

the boundary condition at the inlet ($z = z_0 = 0.4$ m)

$$X(z_0, t) = X_{in}, \quad (2.4)$$

where X_{in} is the inlet concentration of silane, and the boundary condition at the wafer surface ($z = 0$)

$$CD \frac{\partial X}{\partial z}(0, t) = R_W, \quad (2.5)$$

where C is the molar concentration of the gas phase right above the surface and R_W is the deposition rate on the wafer surface. Under the assumption of ideal gas, $C = P/(RT_g)$, where P is the gas phase pressure and R is the ideal gas constant.

When silane diffuses to the wafer surface, it decomposes into silicon and hydrogen as follows:



Then, the silicon atoms are deposited onto the thin film. The deposition rate law on the surface is given as follows [34]:

$$R_W = \frac{kPX_s}{1 + K_H(P(1 - X_s))^{1/2} + K_sPX_s}, \quad (2.7)$$

where X_s is the silane concentration at the wafer surface, and k , K_H , and K_s are coefficients in the rate law. The coefficient k follows an Arrhenius-type law as follows [34]:

$$k = 1.6 \times 10^4 \exp(-18500/T_s) \quad \text{mole} \cdot \text{m}^{-2} \cdot \text{s}^{-1} \cdot \text{Pa}^{-1}, \quad (2.8)$$

where T_s is the temperature of the wafer surface. The values of the parameters and coefficients of the gas-phase model can be found in table 2.1.

2.2.2 On-lattice kinetic Monte Carlo model of thin film growth

The film growth model used in this work is an on-lattice kMC model in which all particles occupy discrete lattice sites [25, 29]. The on-lattice kMC model is valid for a low temperature region, $T < 0.5T_m$ (T_m is the melting point of the crystal). A triangular lattice is selected to represent the crystalline structure of the film, as shown in figure 2.2. The new particles are always deposited from the top side of the lattice where the gas phase is located. The number of sites in the lateral direction is defined as the lattice size and is denoted by L . In the triangular lattice, a bottom layer in the lattice is initially set to be fully packed and fixed, as shown in figure 2.2. There

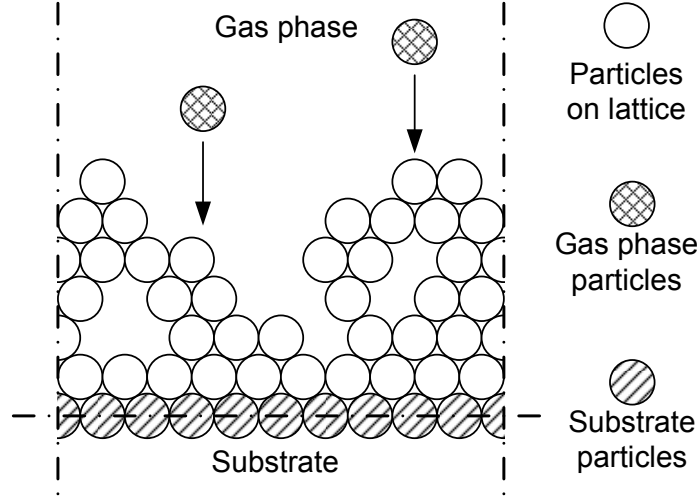


Figure 2.2: Thin film growth process on a triangular lattice.

are no vacancies in this layer, and the particles in this layer cannot migrate. This layer acts as the substrate for the deposition and is not counted in the computation of the number of the deposited particles, i.e., this fixed layer does not influence the film microscopic properties. Two types of microscopic processes (Monte Carlo events) are considered: an adsorption process, in which particles are incorporated into the film from the gas phase, and a migration process, in which surface particles move to adjacent sites [43, 42, 76, 78].

In an adsorption process, an incident particle comes in contact with the film and is incorporated onto the film. The microscopic adsorption rate, W , which is in units of layers per unit time, is equal to the deposition rate, R_W (i.e., $W = R_W$). The incident particles are initially placed at random positions above the film lattice and move toward the lattice in the vertical direction until contacting the first particle on the film. Upon contact, the particle moves (relaxes) to the nearest vacant site. Surface

relaxation is conducted if this site is unstable, i.e., site with only one neighboring particle. When a particle is subject to surface relaxation, the particle moves to its most stable neighboring vacant site and is finally incorporated into the film.

In a migration process, a particle overcomes the energy barrier of the site and jumps to its vacant neighboring site. The migration rate (probability) of a particle follows an Arrhenius-type law with a precalculated activation energy barrier that depends on the local environment of the particle and the substrate temperature. Since the film is thin, the temperature is assumed to be uniform throughout the film. The interior particles (the particles fully surrounded by 6 nearest neighbors) and the substrate layer particles cannot migrate.

When a particle is subject to migration, it can jump to either of its vacant neighboring sites with equal probability, unless the vacant neighboring site has no nearest neighbors, i.e., the surface particle cannot jump off the film and it can only migrate on the surface. The deposition process is simulated using the continuous-time Monte Carlo (CTMC) method (see [29] for details on the microscopic model and simulation algorithm).

2.2.3 Definitions of surface height profile and film site occupancy ratio

Utilizing the continuous-time Monte Carlo algorithm, simulations of the kMC model of a porous silicon thin film growth process can be carried out. Snapshots of film

microstructure, i.e., the configurations of particles within the triangular lattice, are obtained from the kMC model at various time instants during process evolution. To quantitatively evaluate the thin film microstructure, two variables, surface roughness and film porosity, are introduced in this subsection.

Surface roughness, which measures the texture of the thin film surface, is represented by the root-mean-square of the surface height profile of the thin film. Determination of surface height profile is slightly different in the triangular lattice model compared to a solid-on-solid (SOS) model. In the SOS model, the surface of the thin film is naturally described by the positions of the top particles of each column. In the triangular lattice model, however, due to the existence of vacancies and overhangs, the definition of the film surface needs further clarification (see [30] for details). Specifically, taking into account practical considerations of surface roughness measurements, the surface height profile of a triangular lattice model is defined based on the particles that can be reached in the vertical direction, as shown in figure 2.3. In this definition, a particle is considered as a surface particle only if it is not blocked by the particles in the neighboring columns. Therefore, the surface height profile of a porous thin film is the line that connects the sites that are occupied by the surface particles. With this definition, the surface height profile can be treated as a function of the spatial coordinate. Surface roughness, as a measurement of the surface texture, is defined as the standard deviation of the surface height profile from its average height. The mathematical definition of surface roughness is given later in section 2.3.1.

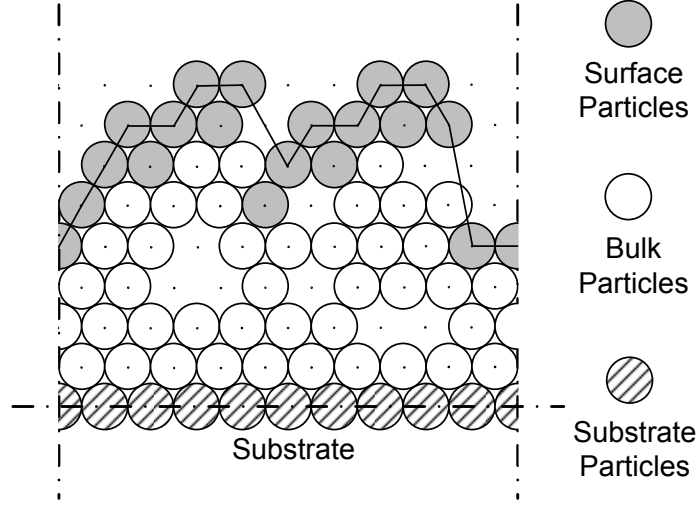


Figure 2.3: Definition of surface height profile. A surface particle is a particle that is not blocked by particles from both of its neighboring columns in the vertical direction.

In addition to film surface roughness, the film site occupancy ratio (SOR) was introduced in [28] to represent the extent of the porosity inside the thin film. The mathematical expression of film SOR is defined as follows:

$$\rho = \frac{N}{LH} \quad (2.9)$$

where ρ denotes the film SOR, N is the total number of deposited particles on the lattice, L is the lattice size, and H denotes the number of deposited layers. Note that the deposited layers are the layers that contain only deposited particles and do not include the initial substrate layers. The variables in the expression of eq (2.9) can be found in figure 2.4. Since each layer contains L sites, the total number of sites in the film that can be contained within the H layers is LH . Thus, film SOR is the ratio of the occupied lattice sites, N , over the total number of available sites, LH . Film

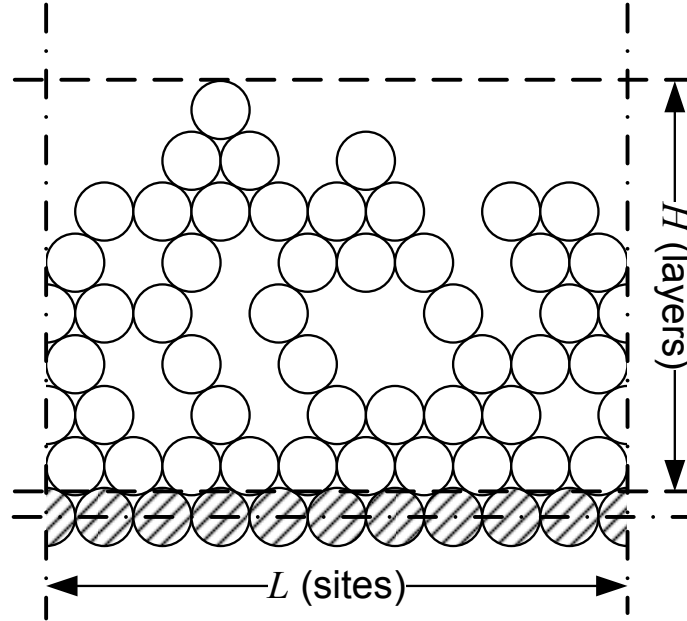


Figure 2.4: Illustration of the definition of film SOR of eq (2.9).

SOR ranges from 0 to 1. Specifically, $\rho = 1$ denotes a fully occupied film with a flat surface. The value of zero is assigned to ρ at the beginning of the deposition process since there are no particles deposited on the lattice.

2.3 Closed-form dynamic model construction

2.3.1 Edwards–Wilkinson-type equation of surface height

The Edwards–Wilkinson (EW)-type equation, a second-order stochastic PDE, can be used to describe the surface height evolution in many microscopic processes that involve thermal balance between adsorption (deposition) and migration (diffusion). Following our previous works [28, 30], an EW-type equation is chosen to describe the

dynamics of the fluctuation of surface height (the validation of this choice can be found in [25]):

$$\frac{\partial h}{\partial t} = r_h + \nu \frac{\partial^2 h}{\partial x^2} + \xi(x, t) \quad (2.10)$$

subject to periodic boundary conditions

$$h(-\pi, t) = h(\pi, t), \quad \frac{\partial h}{\partial x}(-\pi, t) = \frac{\partial h}{\partial x}(\pi, t) \quad (2.11)$$

and the initial condition

$$h(x, 0) = h_0(x) \quad (2.12)$$

where $x \in [-\pi, \pi]$ is the spatial coordinate, t is the time, r_h and ν are the model parameters, and $\xi(x, t)$ is a Gaussian white noise with the following mean and covariance:

$$\begin{aligned} \langle \xi(x, t) \rangle &= 0 \\ \langle \xi(x, t) \xi(x', t') \rangle &= \sigma^2 \delta(x - x') \delta(t - t') \end{aligned} \quad (2.13)$$

where σ^2 is a parameter which measures the intensity of the Gaussian white noise and $\delta(\cdot)$ denotes the standard Dirac delta function. The values of r_h , ν and σ will be computed so that the solutions of eq (2.10) approximate well data obtained from the kMC simulations of the thin film growth process.

To proceed with control design, a stochastic ODE approximation of eq (2.10) is first derived using modal decomposition. Consider the eigenvalue problem of the

linear operator of eq (2.10), which takes the following form:

$$\mathcal{A}\bar{\phi}_n(x) = \nu \frac{d^2 \bar{\phi}_n(x)}{dx^2} = \lambda_n \bar{\phi}_n(x) \quad (2.14)$$

$$\bar{\phi}_n(-\pi) = \bar{\phi}_n(\pi), \quad \frac{d\bar{\phi}_n}{dx}(-\pi) = \frac{d\bar{\phi}_n}{dx}(\pi)$$

where λ_n denotes an eigenvalue and $\bar{\phi}_n$ denotes an eigenfunction. A direct computation of the solution of the above eigenvalue problem yields $\lambda_0 = 0$ with $\psi_0 = 1/\sqrt{2\pi}$, and $\lambda_n = -\nu n^2$ (λ_n is an eigenvalue of multiplicity two) with eigenfunctions $\phi_n = (1/\sqrt{\pi}) \sin(nx)$ and $\psi_n = (1/\sqrt{\pi}) \cos(nx)$ for $n = 1, \dots, \infty$. Note that the $\bar{\phi}_n$ in eq (2.14) denotes either ϕ_n or ψ_n . The solution of eq (2.10) is expanded in an infinite series in terms of the eigenfunctions of the operator of eq (2.14) as follows:

$$h(x, t) = \sum_{n=1}^{\infty} \alpha_n(t) \phi_n(x) + \sum_{n=0}^{\infty} \beta_n(t) \psi_n(x) \quad (2.15)$$

where $\alpha_n(t)$, $\beta_n(t)$ are time-varying coefficients. Substituting the above expansion for the solution, $h(x, t)$, into eq (2.10) and taking the inner product with the adjoint eigenfunctions, $\phi_n^*(x) = (1/\sqrt{\pi}) \sin(nx)$ and $\psi_n^*(x) = (1/\sqrt{\pi}) \cos(nx)$, the following system of infinite stochastic ODEs is obtained:

$$\begin{aligned} \frac{d\beta_0}{dt} &= \sqrt{2\pi} r_h + \xi_\beta^0(t) \\ \frac{d\beta_n}{dt} &= \lambda_n \beta_n + \xi_\beta^n(t) \\ \frac{d\alpha_n}{dt} &= \lambda_n \alpha_n + \xi_\alpha^n(t), n = 1, \dots, \infty \end{aligned} \quad (2.16)$$

where

$$\xi_{\alpha}^n(t) = \int_{-\pi}^{\pi} \xi(x, t) \phi_n^*(x) dx, \quad \xi_{\beta}^n(t) = \int_{-\pi}^{\pi} \xi(x, t) \psi_n^*(x) dx. \quad (2.17)$$

The covariances of $\xi_{\alpha}^n(t)$ and $\xi_{\beta}^n(t)$ can be obtained as follows: $\langle \xi_{\alpha}^n(t) \xi_{\alpha}^n(t') \rangle = \sigma^2 \delta(t - t')$ and $\langle \xi_{\beta}^n(t) \xi_{\beta}^n(t') \rangle = \sigma^2 \delta(t - t')$. Due to the orthogonality of the eigenfunctions of the operator in the EW equation of eq (2.10), $\xi_{\alpha}^n(t)$ and $\xi_{\beta}^n(t)$, $n = 0, 1, \dots$, are stochastically independent.

Since the stochastic ODE system is linear, the analytical solution of state variance can be obtained from a direct computation as follows:

$$\begin{aligned} \langle \alpha_n^2(t) \rangle &= \frac{\sigma^2}{2\nu n^2} + \left(\langle \alpha_n^2(t_0) \rangle - \frac{\sigma^2}{2\nu n^2} \right) e^{-2\nu n^2(t-t_0)} \\ \langle \beta_n^2(t) \rangle &= \frac{\sigma^2}{2\nu n^2} + \left(\langle \beta_n^2(t_0) \rangle - \frac{\sigma^2}{2\nu n^2} \right) e^{-2\nu n^2(t-t_0)} \end{aligned} \quad (2.18)$$

$$n = 1, 2, \dots, \infty$$

where $\langle \alpha_n^2(t_0) \rangle$ and $\langle \beta_n^2(t_0) \rangle$ are the state variances at time t_0 . The analytical solution of state variance of eq (2.18) will be used in the parameter estimation and the MPC design.

When the dynamic model of surface height profile is determined, surface roughness of the thin film is defined as the standard deviation of the surface height profile from

its average height and is computed as follows:

$$r(t) = \sqrt{\frac{1}{2\pi} \int_{-\pi}^{\pi} [h(x, t) - \bar{h}(t)]^2 dx} \quad (2.19)$$

where $\bar{h}(t) = \frac{1}{2\pi} \int_{-\pi}^{\pi} h(x, t) dx$ is the average surface height. According to eq (2.15), we have $\bar{h}(t) = \beta_0(t)\psi_0$. Therefore, $\langle r^2(t) \rangle$ can be rewritten in terms of $\langle \alpha_n^2(t) \rangle$ and $\langle \beta_n^2(t) \rangle$ as follows:

$$\begin{aligned} \langle r^2(t) \rangle &= \frac{1}{2\pi} \left\langle \int_{-\pi}^{\pi} (h(x, t) - \bar{h}(t))^2 dx \right\rangle \\ &= \frac{1}{2\pi} \left\langle \sum_{i=1}^{\infty} (\alpha_i^2(t) + \beta_i^2(t)) \right\rangle \\ &= \frac{1}{2\pi} \sum_{i=1}^{\infty} [\langle \alpha_i^2(t) \rangle + \langle \beta_i^2(t) \rangle] \end{aligned} \quad (2.20)$$

where $\bar{h} = \frac{1}{2\pi} \int_{-\pi}^{\pi} h(x, t) dx = \beta_0(t)\psi_0$ is the average of surface height. Thus, eq (2.20) provides a direct link between the state variance of the infinite stochastic ODEs of eq (2.16) and the expected surface roughness of the thin film. However, due to the presence of infinite terms in the summation of eq (2.20), the solution of the expected surface roughness of eq (2.20) cannot be directly used in the MPC design. Thus, a reduced-order model is needed and is introduced in the MPC design later in section 2.4.1. Note that the parameter r_h does not appear in the expression of surface roughness, since only the zeroth state, β_0 , is affected by r_h but this state is not included in the computation of the expected surface roughness square of eq (2.20).

Film thickness, which is represented by the average of surface height, \bar{h} , is another objective under consideration in this work. The dynamics of the expected value of averaged surface height can be obtained from the analytical solution of the zeroth state, β_0 , from eq (2.16), as follows:

$$\frac{d\langle\bar{h}\rangle}{dt} = r_h. \quad (2.21)$$

The analytical solution of expected value of film thickness, $\langle\bar{h}\rangle$, can be obtained directly from eq (2.21) as follows:

$$\langle\bar{h}(t)\rangle = \langle\bar{h}(t_0)\rangle + r_h(t - t_0). \quad (2.22)$$

2.3.2 Dynamic model of film site occupancy ratio

The concept of film site occupancy ratio (SOR) is used to characterize film porosity. According to the definition of film SOR of eq (2.9), film SOR accounts for all deposited layers during the entire deposition process. Thus, film SOR is a cumulative property, the evolution of which can be characterized by an integral form. Before further derivation of the dynamic model of film SOR, a concept of instantaneous film SOR of the film layers deposited between time t and $t + dt$, denoted by ρ_d , is first introduced as the spatial derivative of the number of deposited particles in the growing direction

as follows:

$$\rho_d = \frac{dN}{d(HL)} \quad (2.23)$$

In eq (2.23), the lattice size L is a constant and the derivative dH can be written as a linear function of the time derivative dt as follows:

$$dH = r_H dt \quad (2.24)$$

where r_H is the growth rate of the thin film from the top layer point of view. Note that r_H is different from the model coefficient r_h in eq (2.10). Thus, the expressions of N and H can be obtained by integrating eqs (2.23) and (2.24) as follows:

$$\begin{aligned} N(t) &= L \int_0^t \rho_d r_H ds \\ H(t) &= \int_0^t r_H ds \end{aligned} \quad (2.25)$$

With the definition of ρ of eq (2.9) and the expressions of N and H of eq (2.25), the film SOR of eq (2.9) can be rewritten in an integral form as follows:

$$\rho = \frac{\int_0^t \rho_d r_H ds}{\int_0^t r_H ds} \quad (2.26)$$

To simplify the subsequent development and develop an SOR model that is suitable for control purposes, we assume (this assumption will be verified in the closed-loop simulation results below where the performance of the controller will be evalu-

ated) that the dynamics of the instantaneous film SOR, ρ_d , can be approximated by a linear first-order process, i.e.:

$$\tau \frac{d\rho_d(t)}{dt} = \rho_d^{ss} - \rho_d(t) \quad (2.27)$$

where τ is the time constant and ρ_d^{ss} is the steady-state value of the instantaneous film SOR. We note that the first-order ODE model of eq (2.27) was introduced and justified with numerical results in [28] and [25] for the modeling of the partial film SOR, which is defined to characterize the evolution of the film porosity of layers that are close to the film surface. The instantaneous film SOR is a similar concept to the partial film SOR, because it also describes the contribution to the bulk film porosity of the newly deposited layers. Therefore, the first-order ODE model is a suitable choice to describe the evolution of the instantaneous film SOR.

From eq (2.26), it follows that at large times as ρ_d approaches ρ_d^{ss} , the steady-state film SOR (ρ^{ss}) approaches the steady-state value of the instantaneous film SOR (i.e., $\rho^{ss} = \rho_d^{ss}$). The deterministic ODE system of eq (2.27) is subject to the following initial condition:

$$\rho_d(t_0) = \rho_{d0} \quad (2.28)$$

where t_0 is the initial time and ρ_{d0} is the initial value of the instantaneous film SOR.

From eqs (2.27) and (2.28) and the fact that $\rho^{ss} = \rho_d^{ss}$ at large times, it follows that

$$\rho_d(t) = \rho^{ss} + (\rho_{d0} - \rho^{ss}) e^{-(t-t_0)/\tau}. \quad (2.29)$$

For controller implementation purposes, the expression of the film SOR can be derived as follows:

$$\begin{aligned} \rho(t) &= \frac{\int_0^{t_0} \rho_d r_H ds + \int_{t_0}^t \rho_d r_H ds}{\int_0^{t_0} r_H ds + \int_{t_0}^t r_H ds} \\ &= \frac{\rho_0 H_0 + \int_{t_0}^t \rho_d r_H ds}{H_0 + \int_{t_0}^t r_H ds} \end{aligned} \quad (2.30)$$

where t_0 is the current time, ρ_0 and H_0 are film SOR and film height at time t_0 , respectively.

Substituting the solution of ρ_d of eq (2.29) into eq (2.30) and assuming that r_H is constant for $t > \tau > t_0$, which is taken to be the case in the parameter estimation and the MPC formulations below, the analytical solution of film SOR at time t can be obtained as follows:

$$\rho = \frac{\rho_0 H_0 + r_H [\rho^{ss}(t - t_0) + (\rho^{ss} - \rho_0)\tau(e^{-(t-t_0)/\tau} - 1)]}{H_0 + r_H(t - t_0)} \quad (2.31)$$

which is directly utilized in the model predictive control formulation of eq (2.34) below.

2.4 Model predictive controller design

In this section, model predictive controllers are designed to regulate the expected values of film roughness square, SOR, and thickness to desired levels by manipulating the inlet silane concentration. Two different ways of implementing the desired film thickness requirement are presented and compared. A reduced-order model of the EW equation is used in the MPC formulation to approximate the dynamics of the surface roughness. State feedback control is considered in this section to present the control algorithms, i.e., the surface height profile and the value of film SOR are assumed to be available to the controller. Porosity estimation-based model predictive control is considered in section 2.6.

2.4.1 Reduced-order model for surface roughness

In the MPC formulation, the expected surface roughness may be computed from the EW equation of eq (2.10) by substituting the solution of the state variance of eq (2.18) into the expression of the expected surface roughness square of eq (2.20). However, the EW equation is a distributed parameter dynamic model, which contains infinite dimensional stochastic states. Therefore, the solution of the EW equation leads to a model predictive controller of infinite order that cannot be realized in practice (i.e., the practical implementation of a control algorithm based on such a system will require the computation of infinite sums which cannot be done by a computer). To this end, a reduced-order model of the infinite dimensional ODE model of eq (2.16) is

instead derived and used to calculate the prediction of the expected surface roughness in the model predictive controller.

Due to the structure of the eigenspectrum of the linear operator of the EW equation of eq (2.10), the dynamics of the EW equation are characterized by a finite number of dominant modes. By neglecting the high-order modes ($n \geq m + 1$), the system of eq (2.16) can be approximated by a finite-dimensional system as follows:

$$\begin{aligned} \frac{d\alpha_n}{dt} &= \lambda_n \alpha_n + \xi_\alpha^n(t), & \frac{d\beta_n}{dt} &= \lambda_n \beta_n + \xi_\beta^n(t) \\ n &= 1, \dots, m. \end{aligned} \tag{2.32}$$

Note that the ODE for the zeroth state is also neglected, since the zeroth state does not contribute to surface roughness.

Using the finite-dimensional system of eq (2.32), the expected surface roughness square, $\langle r^2(t) \rangle$, can be approximated with the finite-dimensional state variance as follows:

$$\langle \tilde{r}^2(t) \rangle = \frac{1}{2\pi} \sum_{i=1}^m [\langle \alpha_i^2(t) \rangle + \langle \beta_i^2(t) \rangle] \tag{2.33}$$

where the tilde symbol in $\langle \tilde{r}^2(t) \rangle$ denotes its association with a finite-dimensional system.

2.4.2 MPC formulation

We consider the control problem of film surface roughness, porosity, and thickness regulation by using a model predictive control design. The expected values, $\langle r^2 \rangle$, $\langle \rho \rangle$, and $\langle \bar{h} \rangle$, are chosen as the control objectives. The adsorption rate is computed by the controller, which, in turn, is used to calculate the inlet silane concentration via eq (2.7) (i.e., the presence of the gas phase is neglected in the calculation of the control action, X_{in} , but it is accounted for in the multiscale process model, where the control action is applied). The substrate temperature is fixed at 850 K during the entire closed-loop simulation. The control action is obtained by solving a finite-horizon optimal control problem.

The cost function in the optimal control problem (eq (2.34) below) includes penalty on the deviation of $\langle r^2 \rangle$ and $\langle \rho \rangle$ from their respective set-point values. However, since the manipulated input variable is the adsorption rate and the film deposition process is a batch operation (i.e., the film growth process is terminated within a certain time), a desired value of the film thickness is also required to prevent an undergrown thin film at the end of the deposition process. Therefore, in the MPC shown in eq (2.34), the desired film thickness is regarded as the set-point value of the film thickness, i.e., the deviation of the film thickness from the desired value is included in the cost function. However, only the negative deviation (when the film thickness is less than the desired value) is penalized; no penalty is imposed on the deviation when the thin film thickness exceeds the desired thickness. Different weighting factors

are assigned to the penalties on the deviations of the expected values of film surface roughness, SOR, and thickness from their desired values. Relative deviations are used in the formulation of the cost function to make the magnitude of the different terms comparable. The optimization problem is subject to the dynamics of the reduced-order model of surface roughness of eq (2.32), the dynamics of the film thickness of eq (2.21), and the dynamics of the film SOR of eq (2.26). The optimal profile of the adsorption rate is calculated by solving a finite-dimensional optimization problem in a receding horizon fashion. Specifically, the MPC problem is formulated as follows:

$$\min_{W_1, \dots, W_i, \dots, W_p} J = \sum_{i=1}^p \{q_{r^2, i} F_{r^2, i} + q_{h, i} F_{h, i} + q_{\rho, i} F_{\rho, i}\} \quad (2.34)$$

subject to:

$$F_{r^2, i} = \left[\frac{r_{set}^2 - \langle \tilde{r}^2(t_i) \rangle}{r_{set}^2} \right]^2$$

$$F_{h, i} = \begin{cases} \left[\frac{h_{min} - \langle \bar{h}(t_i) \rangle}{h_{min}} \right]^2, & h_{min} > \langle \bar{h}(t_i) \rangle \\ 0, & h_{min} \leq \langle \bar{h}(t_i) \rangle \end{cases}$$

$$F_{\rho, i} = \left[\frac{\rho_{set} - \langle \rho(t_i) \rangle}{\rho_{set}} \right]^2$$

$$\langle \alpha_n^2(t_i) \rangle = \frac{\sigma^2}{2\nu n^2} + \left(\langle \alpha_n^2(t_{i-1}) \rangle - \frac{\sigma^2}{2\nu n^2} \right) e^{-2\nu n^2 \Delta}$$

$$\langle \beta_n^2(t_i) \rangle = \frac{\sigma^2}{2\nu n^2} + \left(\langle \beta_n^2(t_{i-1}) \rangle - \frac{\sigma^2}{2\nu n^2} \right) e^{-2\nu n^2 \Delta}$$

$$\langle \bar{h}(t_i) \rangle = \langle \bar{h}(t_{i-1}) \rangle + r_h \Delta$$

$$\langle \rho(t_i) \rangle = \frac{1}{\langle \bar{h}(t_{i-1}) \rangle + r_h \Delta} \cdot \left\{ \langle \rho(t_{i-1}) \rangle \langle \bar{h}(t_{i-1}) \rangle + r_h [\rho^{ss} \Delta + (\rho^{ss} - \langle \rho(t_{i-1}) \rangle) \tau_p (e^{-\Delta/\tau_p} - 1)] \right\}$$

$$W_{min} < W_i < W_{max}, \quad i = 1, 2, \dots, p$$

where t is the current time, Δ is the sampling time, p is the number of prediction steps, $p\Delta$ is the specified prediction horizon, t_i , $i = 1, 2, \dots, p$, is the time of the i th prediction step ($t_i = t + i\Delta$), respectively, W_i , $i = 1, 2, \dots, p$, is the adsorption rate at the i th step ($W_i = W(t + i\Delta)$), respectively, $q_{r^2,i}$, $q_{h,i}$, and $q_{\rho,i}$, $i = 1, 2, \dots, p$, are the weighting penalty factors for the deviations of $\langle r^2 \rangle$, $\langle h \rangle$ and $\langle \rho \rangle$ from their respective set-points r_{set}^2 and ρ_{set} , $\langle \bar{h} \rangle$ from its desired h_{min} , at the i th prediction step, and W_{min} and W_{max} are the lower and upper bounds on the deposition rate, respectively. Note that we choose $\langle \bar{h} \rangle$, r_h and $\rho(t_0)$ to replace H , r_H and ρ_{d0} in the MPC formulation of eq (2.34), respectively.

The optimal set of (W_1, W_2, \dots, W_p) , is obtained from the solution of the multi-variable optimization problem of eq (2.34), and only the first value of the manipulated input trajectory, W_1 , is used to compute the inlet silane concentration and is applied to the deposition process from time t until the next sampling time, when new measurements are received and the MPC problem of eq (2.34) is solved for the computation of the next optimal input trajectory.

The dependence of the model coefficients, r_h , ν , σ^2 , ρ^{ss} , and τ , on adsorption rate is used in the formulation of the model predictive controller of eq (2.34). Thus,

parameter estimation from open-loop kMC simulation results of the thin film growth process for a variety of operation conditions is performed to obtain the dependence of the model coefficients on adsorption rate using least square methods [30].

Remark 2.1 *In the MPC formulation shown in eq (2.34), the desired thickness requirement is implemented by including penalty on the negative deviation of the expected film thickness from its set point in the cost function. This formulation cannot guarantee that the final film thickness is greater than the set-point value, thus it can be viewed as a soft constraint formulation. To ensure that the thickness requirement would be satisfied, a thickness constraint should be implemented as a lower bound on deposition rate, which is the smallest deposition rate needed to reach the desired thickness at the end of the deposition process. The modified MPC, accounting for the gas phase via a constant gain, can be then formulated as follows:*

$$\min_{W_1, \dots, W_i, \dots, W_p} J = \sum_{i=1}^p \{q_{r^2, i} F_{r^2, i} + q_{\rho, i} F_{\rho, i}\} \quad (2.35)$$

subject to:

$$F_{r^2, i} = \left[\frac{r_{set}^2 - \langle \tilde{r}^2(t_i) \rangle}{r_{set}^2} \right]^2$$

$$F_{\rho, i} = \left[\frac{\rho_{set} - \langle \rho(t_i) \rangle}{\rho_{set}} \right]^2$$

$$\langle \alpha_n^2(t_i) \rangle = \frac{\sigma^2}{2\nu n^2} + \left(\langle \alpha_n^2(t_{i-1}) \rangle - \frac{\sigma^2}{2\nu n^2} \right) e^{-2\nu n^2 \Delta}$$

$$\langle \beta_n^2(t_i) \rangle = \frac{\sigma^2}{2\nu n^2} + \left(\langle \beta_n^2(t_{i-1}) \rangle - \frac{\sigma^2}{2\nu n^2} \right) e^{-2\nu n^2 \Delta}$$

$$\langle \bar{h}(t_i) \rangle = \langle \bar{h}(t_{i-1}) \rangle + r_h \Delta$$

$$\langle \rho(t_i) \rangle = \frac{1}{\langle \bar{h}(t_{i-1}) \rangle + r_h \Delta} \cdot \{ \langle \rho(t_{i-1}) \rangle \langle \bar{h}(t_{i-1}) \rangle + r_h [\rho^{ss} \Delta + (\rho^{ss} - \langle \rho(t_{i-1}) \rangle) \tau_p (e^{-\Delta/\tau_p} - 1)] \}$$

$$W_{min} < W_i < W_{max}, \quad i = 1, 2, \dots, p$$

$$r_h > \frac{h_{min} - h(t_i)}{(t_{end} - t_i)}, \quad i = 1, 2, \dots, p$$

It is important to note that it is possible that the required minimum deposition rate is larger than the upper bound imposed on W , thereby resulting in an infeasible optimization problem. If this happens, the lower bound is reset to $W_{max} - 0.001$.

Remark 2.2 *A multivariable control algorithm can be developed for more improved closed-loop control by simultaneously manipulating two or more process input variables. For example, the adsorption rate, W , and the substrate temperature, T , may be used as two simultaneous manipulated inputs in a multivariable control design. The MPC framework presented in this work is suitable for multivariable control system design. However, parameter estimation for a wider range of operating conditions is required to capture the parameter dependence on the adsorption rate and the substrate temperature. Such a parameter dependence may be tabulated via interpolation or formulated via linear or nonlinear regression [53].*

Remark 2.3 *Another possible improvement for the control of a thin film growth process is to take into account the transition and crossover of the thin film growth be-*

havior. Specifically, we have recently found [25] that at different regions of operating conditions, *i.e.*, adsorption rate and substrate temperature, the growth behavior of thin films may be described by different dynamic models. At low temperatures, the surface profile of a porous thin film follows closely the EW dynamics. As temperature increases, the growth behavior deviates from the EW equation. Other dynamic models (Kardar-Parisi-Zhang-type equations or stochastic Kuramoto-Sivashinsky equation) may be more suitable to describe the evolution of thin film surface profile. Therefore, the transition and crossover may be incorporated into the control design by switching the dynamic models at different regions of operation conditions. While the control system designed in this work is successful in achieving the control objectives, the use of even more accurate dynamic models of the film growth at different regimes may help further improve the accuracy of predictions in the MPC.

2.5 Closed-loop simulations

In this section, the proposed model predictive controllers of eqs (2.34) and eq (2.35) are applied to the multiscale model of the thin film growth process described in section 2.2. The value of the adsorption rate is obtained from the solution of the optimization problem at each sampling time. The corresponding inlet concentration of silane is calculated from the adsorption rate based on the rate law of eq (2.7) and is applied to the closed-loop system until the next sampling time. The optimization problems in the MPC formulations of eqs (2.34) and (2.35) are solved via a local

constrained minimization algorithm using a broad set of initial guesses.

The desired values (set-point values) in the closed-loop simulations are $r_{set}^2 = 50$ layer² and $\rho_{set} = 0.985$, with a desired film thickness of $h_{min} = 800$ layers. The substrate temperature is fixed at 850 K. The variation of adsorption rate is from 0.1 to 0.45 layer/s (0.45 layer/s is the maximum adsorption rate that can be obtained according to the rate law of eq (2.7) at $X_s = 1$ and the given conditions of the gas phase in table 2.1). The number of prediction steps is set to be $p = 5$. The prediction horizon of each step is fixed at $\Delta = 5$ s. The closed-loop simulation duration is 3000 s. All expected values are obtained from 1000 independent simulation runs.

2.5.1 Regulation of film surface roughness and thickness

Closed-loop simulations of regulating film surface roughness and thickness are first carried out. In these control problems, the control objective is to regulate the expected surface roughness square and expected film thickness to desired values. Thus, the cost functions of these problems contain penalties on the deviations of the expected surface roughness square from the set-point value and of the expected film thickness from the desired value. The weighting factors are $q_{r^2,i} = 0.1$, $q_{h,i} = 1$ and $q_{\rho,i} = 0$ for all i .

Figure 2.5 shows the closed-loop simulation results of the roughness-thickness control problem. From figure 2.5, it can be seen that the model predictive controller drives the expected film thickness close to the desired value, at the end of the simulation. However, due to the requirement of achieving a desired film thickness value,

which includes a higher penalty factor, the controller computes a higher adsorption rate, and thus, it results in a higher expected surface roughness square at the end of the closed-loop simulation. The effect of the penalty on film thickness can be observed by comparing figure 2.5 to figure 2.6, which shows the closed-loop simulation results without penalty on film thickness. It can be clearly seen that, without penalty on the deviation of film thickness from its desired value, the expected surface roughness square approaches closer to the set-point value at the end of the simulation, while the expected film thickness is lower than the desired value. Figure 2.7 shows the corresponding profiles of the mean value of inlet precursor concentration for both cases, which demonstrates that in the simulation runs of figure 2.5 (where a higher penalty is used on film thickness) the controller uses a higher deposition rate. Figure 2.8 shows the histogram of film thickness from 1000 independent simulation runs at the end of the simulations ($t = 3000$ s) using the MPC formulation of eq (2.34) with $q_{r^2,i} = 0.1$, $q_{h,i} = 1$ and $q_{\rho,i} = 0$. Although the mean value is around 800, the distribution is wide and there are many simulations in which the thickness set-point is not reached. The histogram of roughness square is shown in figure 2.9. In this case, the mean value is 60.37.

2.5.2 Regulation of film porosity

In this subsection, it is demonstrated that the precise regulation of SOR to its set-point can be achieved. Figure 2.10 shows the closed-loop simulation results of the

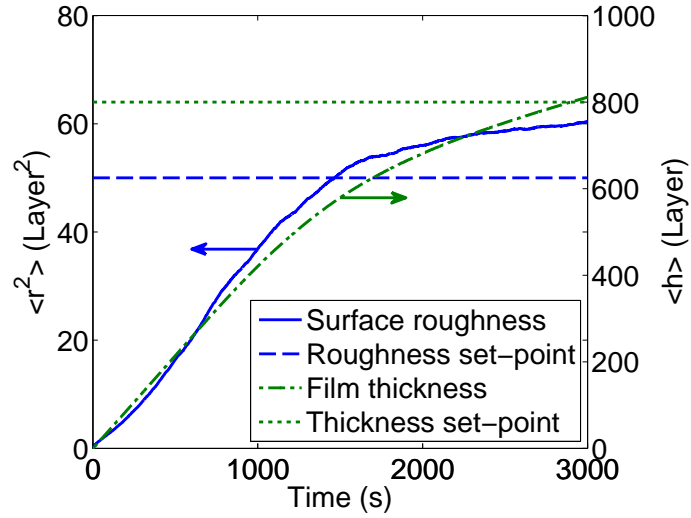


Figure 2.5: Profiles of the expected values of surface roughness square (solid line, left y -axis) and of film thickness (dash-dotted line, right y -axis) under closed-loop operation using the MPC formulation of eq (2.34) with $q_{r^2,i} = 0.1$, $q_{h,i} = 1$ and $q_{\rho,i} = 0$.

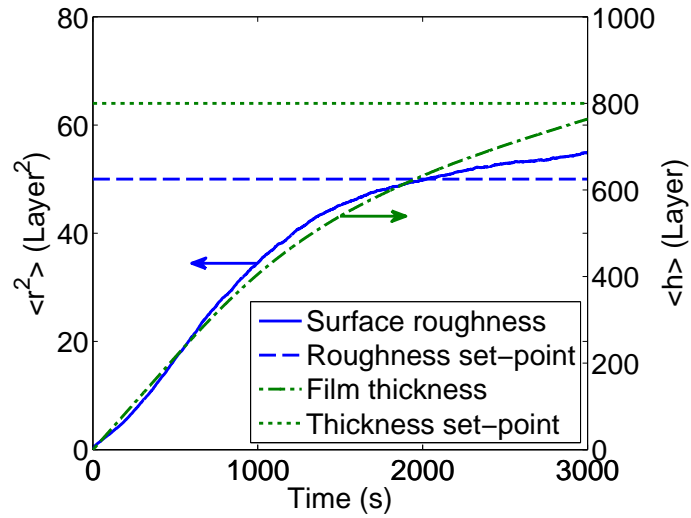


Figure 2.6: Profiles of the expected values of surface roughness square (solid line, left y -axis) and of film thickness (dash-dotted line, right y -axis) under closed-loop operation using the MPC formulation of eq (2.34) with $q_{r^2,i} = 1$, $q_{h,i} = 0$ and $q_{\rho,i} = 0$.

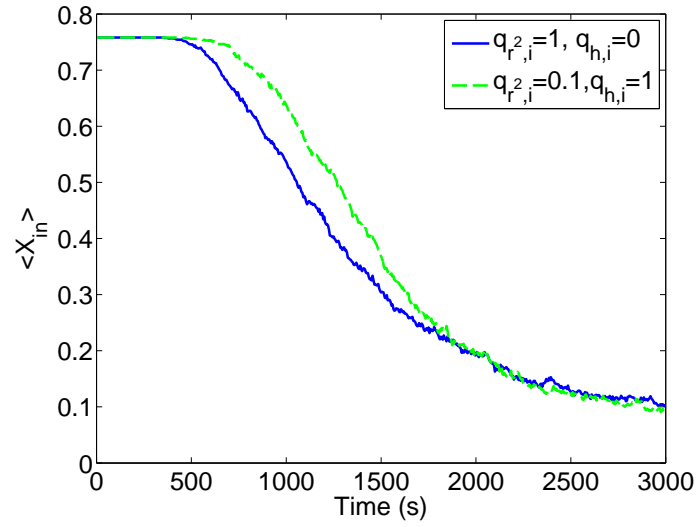


Figure 2.7: Profiles of expected inlet silane concentrations under closed-loop operation using the MPC formulation of eq (2.34) with $q_{r^2,i} = 0.1, q_{h,i} = 1$ and $q_{\rho,i} = 0$ and the MPC formulation of eq (2.34) with $q_{r^2,i} = 1, q_{h,i} = 0$ and $q_{\rho,i} = 0$ (dashed line).

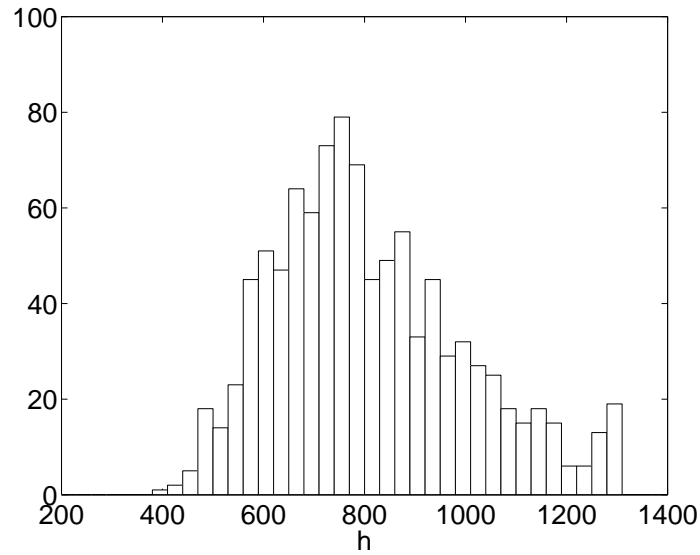


Figure 2.8: Histogram of closed-loop film thickness at the end of simulation ($t = 3000$ s) using the MPC formulation of eq (2.34) with $q_{r^2,i} = 0.1, q_{h,i} = 1$ and $q_{\rho,i} = 0$.

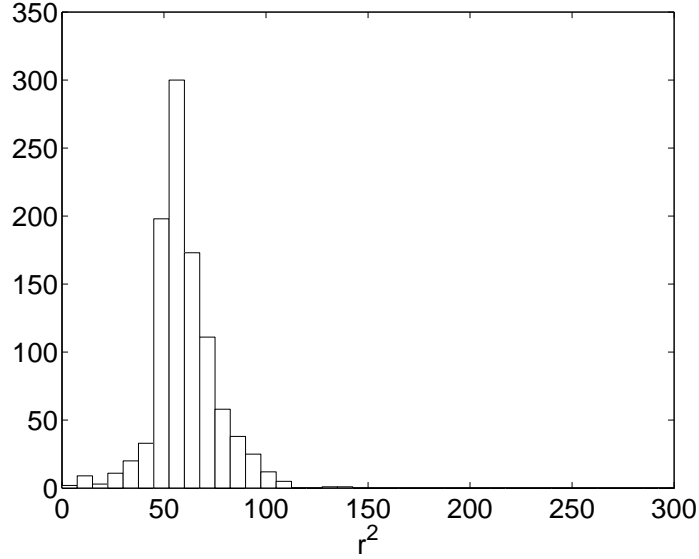


Figure 2.9: Histogram of closed-loop surface roughness square at the end of simulation ($t = 3000$ s) using the MPC formulation of eq (2.34) with $q_{r^2,i} = 0.1$, $q_{h,i} = 1$ and $q_{\rho,i} = 0$.

porosity control problem where the cost function includes only a penalty on the deviation of film SOR from the desired value, 0.985. The histogram of SOR is also presented in figure 2.11, and the mean value is 0.9845. We conclude from these two figures that the model predictive controller successfully drives the expected film SOR to the set-point value.

2.5.3 Simultaneous regulation of film surface roughness, porosity and thickness

Closed-loop simulations of simultaneous regulation of film thickness, surface roughness and SOR are carried out with the same weighting factors. Since the inlet silane

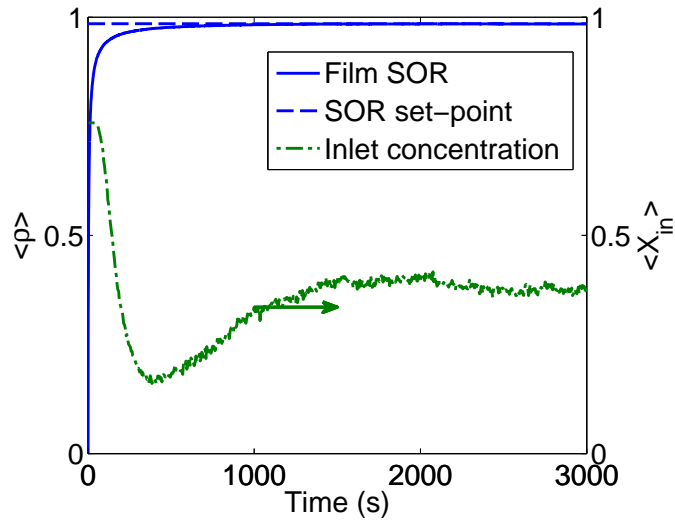


Figure 2.10: Profiles of the expected values of film SOR (solid line, left y -axis) and of inlet silane concentration (dash-dotted line, right y -axis) under closed-loop operation using the MPC formulation of eq (2.34) with $q_{r^2,i} = 0$, $q_{h,i} = 0$ and $q_{\rho,i} = 1$.

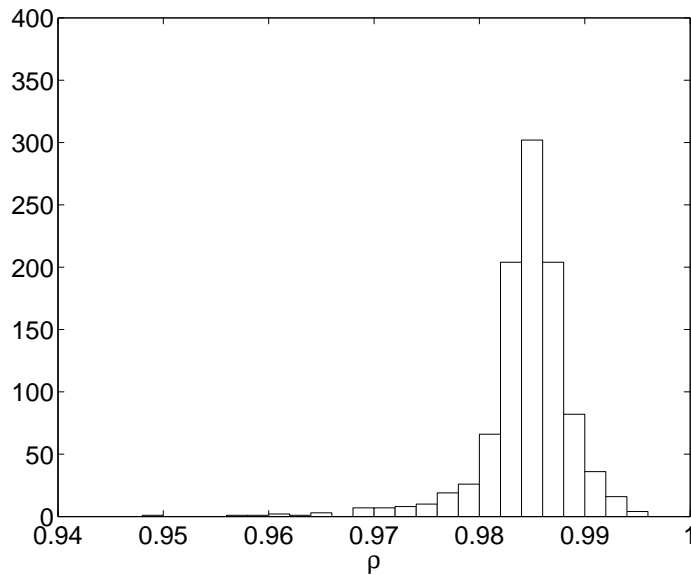


Figure 2.11: Histogram of closed-loop SOR at the end of simulation ($t = 3000$ s) using the MPC formulation of eq (2.34) with $q_{r^2,i} = 0$, $q_{h,i} = 0$ and $q_{\rho,i} = 1$.

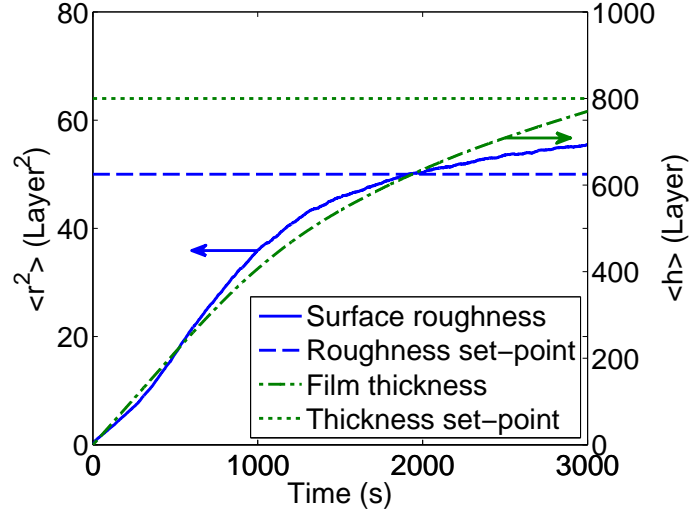


Figure 2.12: Profiles of the expected values of surface roughness square (solid line, left y -axis) and of film thickness (dash-dotted line, right y -axis) under closed-loop operation using the MPC formulation of eq (2.34) with $q_{r^2,i} = 1$, $q_{h,i} = 1$ and $q_{\rho,i} = 1$.

concentration is the only manipulated input, the desired values of r_{set}^2 and ρ_{set} cannot be achieved simultaneously, i.e., the values of inlet silane concentration needed to achieve the desired surface roughness and film thickness are not the same. Therefore, a trade-off between the two set-points is made by the controller. Figure 2.12 and figure 2.13 show the simulation results for this scenario. The expected values of both surface roughness square and film SOR approach their corresponding set-points and the expected film thickness is lower than the desired one. Figure 2.14 shows the histogram of SOR, where a very narrow distribution around the mean value is observed.

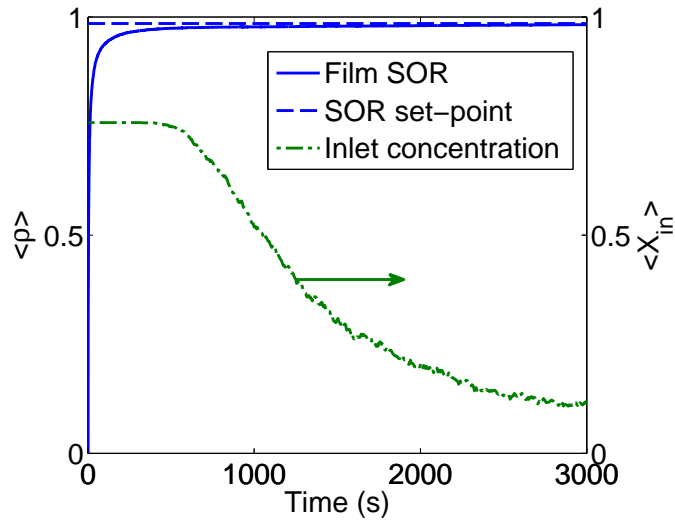


Figure 2.13: Profiles of the expected values of film SOR (solid line, left y -axis) and of inlet silane concentration (dash-dotted line, right y -axis) under closed-loop operation using the MPC formulation of eq (2.34) with $q_{r^2,i} = 1$, $q_{h,i} = 1$ and $q_{\rho,i} = 1$.

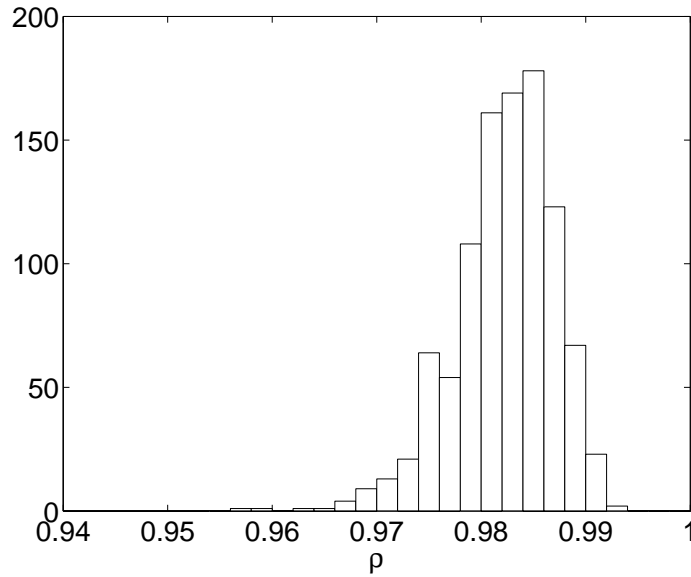


Figure 2.14: Histogram of closed-loop SOR at the end of simulation ($t = 3000$ s) using the MPC formulation of eq (2.34) with $q_{r^2,i} = 1$, $q_{h,i} = 1$ and $q_{\rho,i} = 1$.

2.5.4 Regulation of roughness with constraint on film thickness

In this subsection, the modified model predictive controller of eq (2.35) is applied to the regulation of surface roughness and film thickness. The cost function penalizes only roughness deviation, and the weighting factors are $q_{r^2,i} = 0.1$, $q_{\rho,i} = q_{h,i} = 0$.

Figure 2.15 shows the profile of the mean value of thickness and roughness. The MPC drives the thickness above the desired minimum value. The offset of roughness square at the end of simulation is larger compared to the result shown in figure 2.5 where the film thickness is penalized in the cost function. Figure 2.16 shows the histogram of film thickness for 1000 simulation runs. Almost every run reaches the minimum thickness requirement and the maximum negative offset is less than 1. This can be compared with the result of the MPC formulation of eq (2.34), where about 50% of the simulation runs do not satisfy the thickness requirement. Figure 2.17 shows the histograms of roughness square. Its distribution is wider compared with the result of MPC of eq (2.34), shown in figure 2.9. It should be pointed out that the relative weighting between thickness and roughness deviation plays a key role in the MPC of eq (2.34). For example, by increasing the relative weighting of thickness over roughness from 10 to 1000, the mean value of the film thickness can be larger than the set point at the expense of a much higher surface roughness.

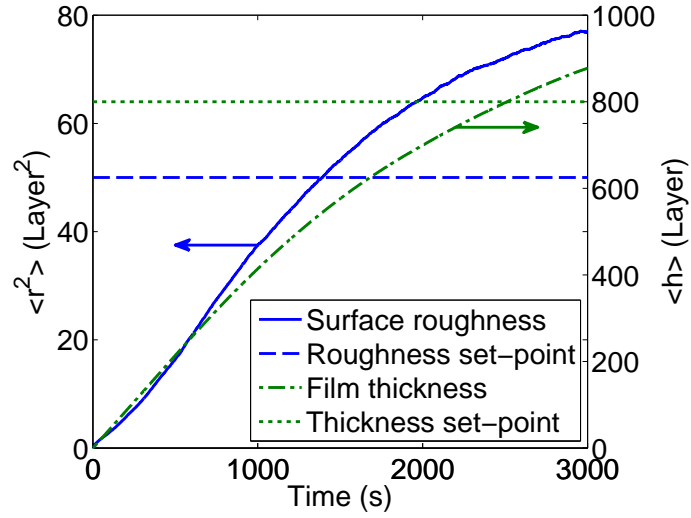


Figure 2.15: Profiles of the expected values of surface roughness square (solid line, left y -axis) and of film thickness (dash-dotted line, right y -axis) under closed-loop operation using the MPC formulation of eq (2.35) with $q_{r^2,i} = 0.1$, $q_{h,i} = 0$ and $q_{\rho,i} = 0$.

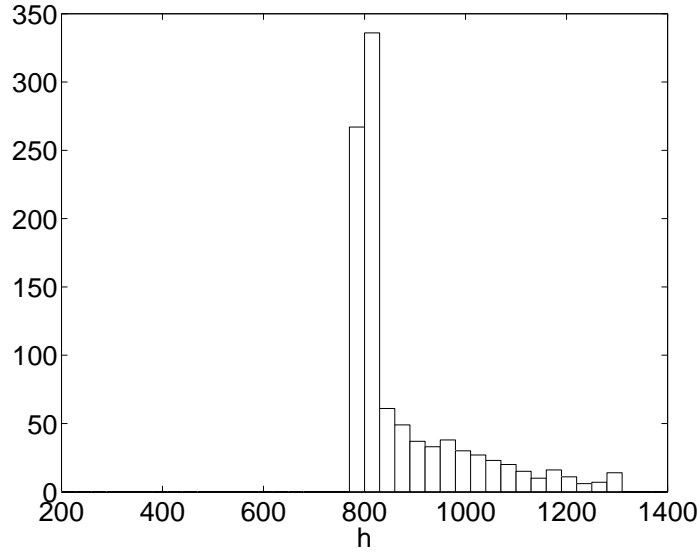


Figure 2.16: Histogram of closed-loop film thickness at the end of simulation ($t = 3000$ s) using the MPC formulation of eq (2.35) with $q_{r^2,i} = 0.1$, $q_{h,i} = 0$ and $q_{\rho,i} = 0$.

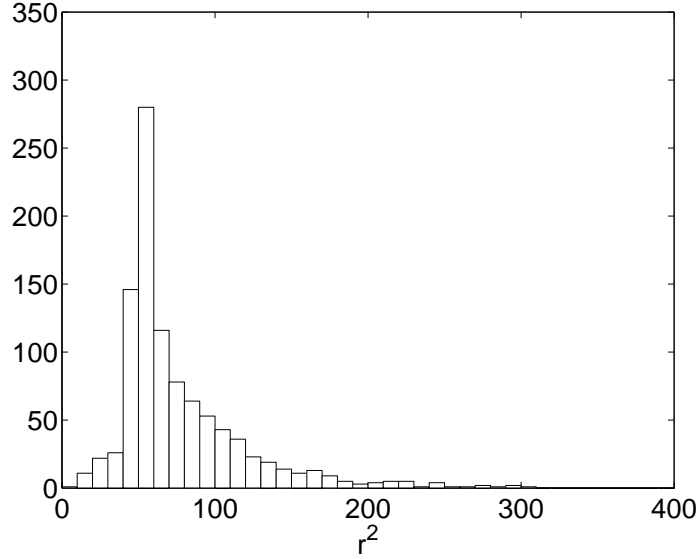


Figure 2.17: Histogram of closed-loop surface roughness square at the end of simulation ($t = 3000$ s) using the MPC formulation of eq (2.35) with $q_{r^2,i} = 0.1$, $q_{h,i} = 0$ and $q_{\rho,i} = 0$.

2.6 Porosity estimation-based model predictive control

The MPC formulations of eqs (2.34) and (2.35) have been derived under the state feedback assumption. In this assumption, all the required information about the thin film state can be measured in real time during the closed-loop operation. However, it may be difficult to measure the film porosity online with currently available techniques, and thus, state feedback control of film SOR may not be possible to be directly implemented in practice. To address this problem, an estimation scheme is needed to estimate the film porosity from other available film measurements, e.g., the surface profile of the thin film. The proposed MPC formulations will then use the estimates

of the film SOR in the optimization problem to compute the optimal solution for the manipulated input.

To estimate the film porosity, we need the following assumptions:

1. The number of deposited layers, H , is available or can be measured from the surface profile of the thin film.
2. The adsorption rate at the wafer surface, W , can be obtained, either from the simulation of the gas phase model or by measuring the surface precursor concentration.

By substituting the number of deposited particles, N , with the integral of the adsorption rate for the entire deposition duration in the definition of film SOR of eq (2.9), film SOR can be estimated by the following equation:

$$\widehat{\rho}(t_i) = \frac{\int_0^{t_i} W(t_i) dt}{H(t_i)} \approx \frac{\widehat{\rho}(t_{i-1})H(t_{i-1}) + \sum_1^i W(t_i)\Delta}{H(t_i)} \quad (2.36)$$

where $\widehat{\rho}(t_i)$ is the estimated film SOR.

To compare the estimated film SOR with its actual value computed by the multi-scale process model, we plot the profiles of the estimated and of the actual SOR value from a single simulation run in figure 2.18. It can be seen that the estimate follows closely the actual film SOR but reaches a lower steady-state value at large times.

Using the estimation scheme of film SOR of eq (2.36), we can construct an output feedback controller by combining the MPC formulations of eqs (2.34) or (2.35) and

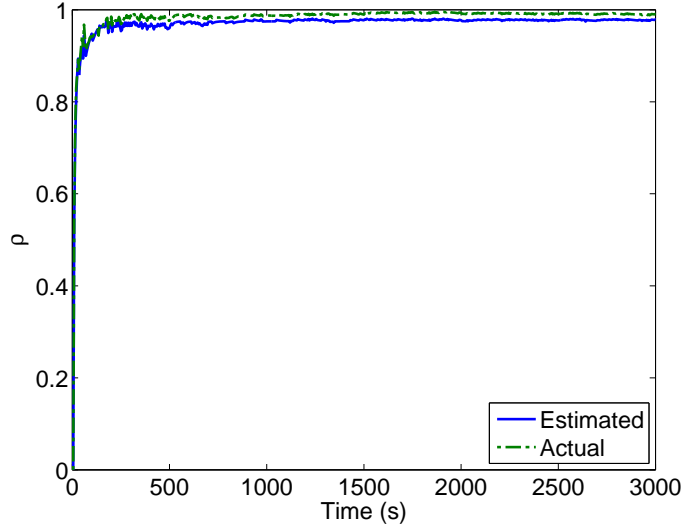


Figure 2.18: Profiles of SOR estimated via eq (2.36) (solid line) and computed directly from the multiscale process model (dash-dotted line).

the estimation scheme. To demonstrate the effectiveness of the estimation scheme and of the output feedback controller, we first consider the porosity-only control problem. The MPC formulation of eq (2.34) is used in the output feedback controller. The same operating conditions are used in the output feedback control problem as in the state feedback control problem in section 2.5. Figure 2.19 shows the profiles of the film SOR and of the inlet concentration of silane. The output feedback controller successfully stabilizes the porosity close to the set-point value, 0.985. Figure 2.20 shows the histogram of SOR at $t = 3000$ s under the output feedback controller. It can be clearly seen that the output feedback controller results in a wider distribution of film SOR at the end of the simulation compared to the one under state feedback control, which is expected due to the error introduced by porosity estimation.

To further demonstrate the applicability of the output feedback controller, we

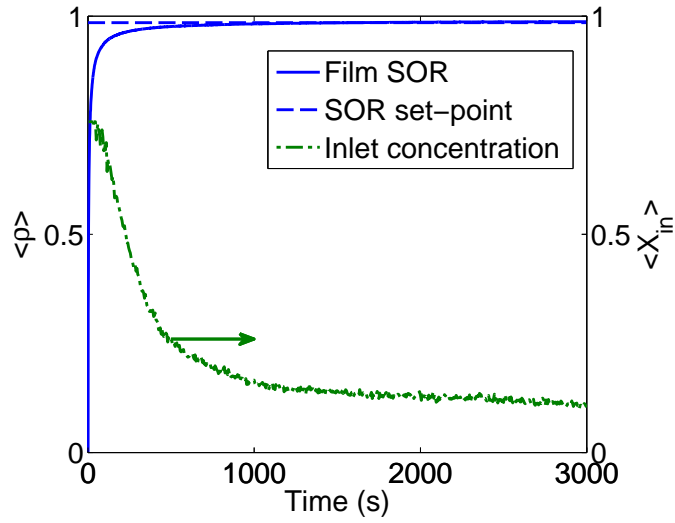


Figure 2.19: Profiles of the expected value of film SOR (solid line, left y -axis) and of inlet silane concentration (dash-dotted line, right y -axis) under closed-loop operation using the MPC formulation of eq (2.34) with $q_{r^2,i} = 0$, $q_{h,i} = 0$ and $q_\rho = 1$ and porosity estimation.

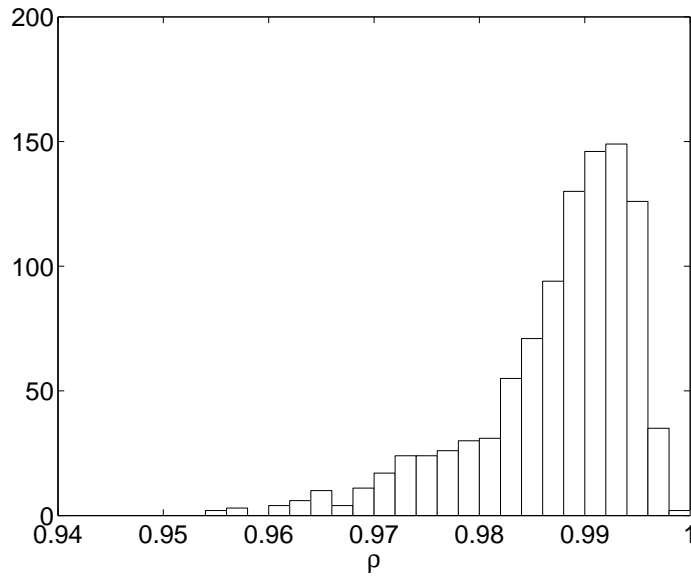


Figure 2.20: Histogram of closed-loop SOR at the end of simulation ($t=3000$ s) using the MPC formulation of eq (2.34) with $q_{r^2,i} = 0$, $q_{h,i} = 0$ and $q_\rho = 1$ and porosity estimation.

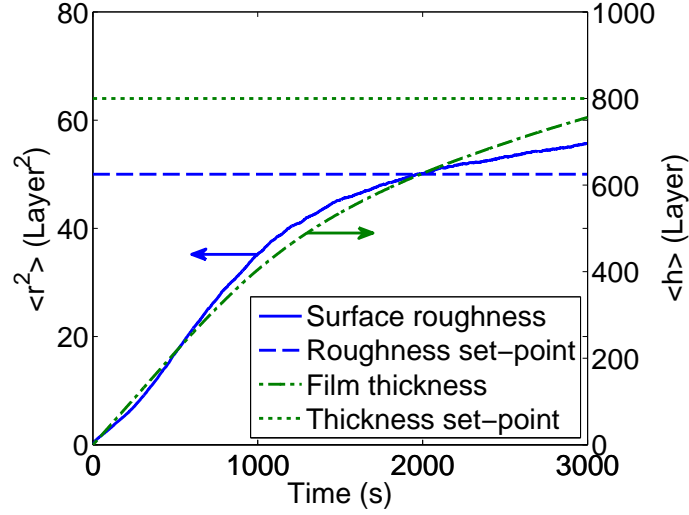


Figure 2.21: Profiles of the expected values of film SOR (solid line, left y -axis) and of inlet silane concentration (dash-dotted line, right y -axis) under closed-loop operation using the MPC formulation of eq (2.34) with $q_{r^2,i} = 1$, $q_{h,i} = 1$ and $q_\rho = 1$ and porosity estimation.

also consider simultaneous output feedback control of film surface roughness, porosity and thickness. The closed-loop simulation results can be found in figure 2.21 and figure 2.22, which show the profiles of the expected value of the film thickness, roughness square, film SOR, and of the inlet silane concentration, respectively. The closed-loop profiles under output feedback control are close to the results under state feedback control presented in section 2.5.3, which is reasonable since the film porosity is estimated quite well. The histogram of the film SOR is also shown in figure 2.23; it has a wider spread compared to the one under state feedback control (figure 2.14) owing to the error introduced by the estimation.

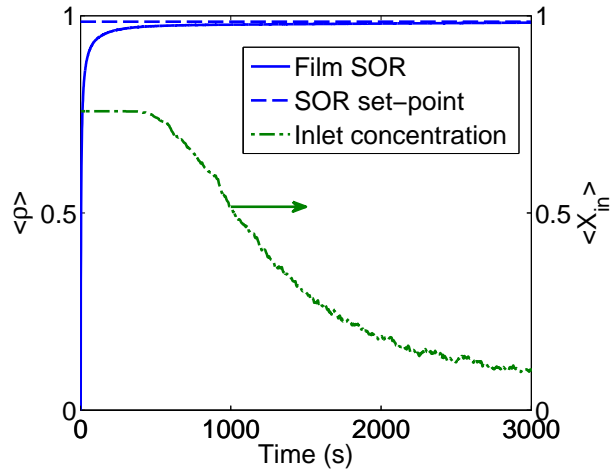


Figure 2.22: Profiles of the expected values of film SOR (solid line, left y -axis) and of inlet silane concentration (dash-dotted line, right y -axis) under closed-loop operation using the MPC formulation of eq (2.34) with $q_{r^2,i} = 1$, $q_{h,i} = 1$ and $q_\rho = 1$ and porosity estimation.

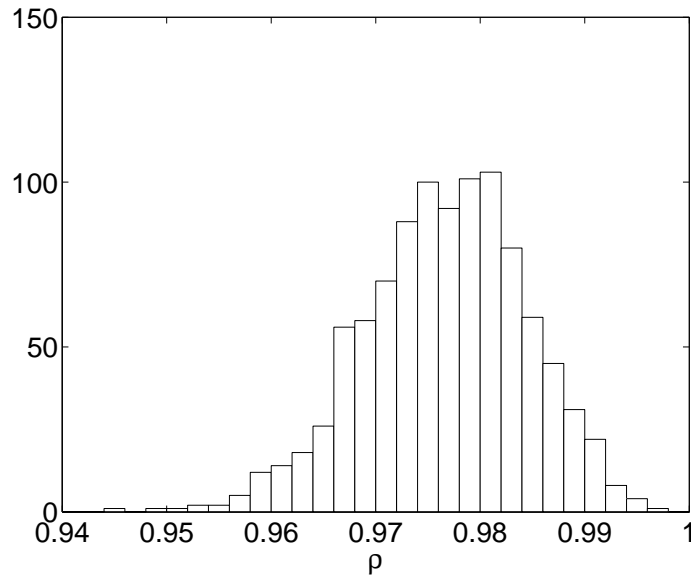


Figure 2.23: Histogram of closed-loop SOR at the end of simulation ($t=3000$ s) using the MPC formulation of eq (2.34) with $q_{r^2,i} = 1$, $q_{h,i} = 1$ and $q_\rho = 1$ and porosity estimation.

2.7 Conclusions

In this chapter, we developed model predictive control algorithms to simultaneously control film surface roughness, porosity, and thickness in a multiscale model of a thin film growth process. On the macroscopic side, the gas phase dynamics was modeled by a continuous PDE model derived from a mass balance. On the microscopic side, the thin film deposition process was simulated via a kinetic Monte Carlo model developed on a triangular lattice with vacancies and overhangs allowed to develop inside the film. Dynamic models of film surface height and film porosity were developed and used in the MPC algorithms. The regulation of film thickness was addressed in two different ways. One way is to include penalty on the deviation of the film thickness into the cost function and the other one is to impose a constraint on the adsorption rate to ensure the desired film thickness at the end of the film growth process. The proposed model predictive controllers were applied to the multiscale thin film growth model to evaluate their performance. In addition, an estimation scheme of film SOR was introduced and used successfully in conjunction with the MPC schemes.

Chapter 3

Control of Surface Roughness and Slope with 1D kMC Model

3.1 Introduction

This chapter focuses on the development of a model predictive control algorithm to simultaneously regulate the surface slope and roughness of a thin film growth process to optimize thin film light reflectance and transmittance. Specifically, a thin film deposition process modeled on a one-dimensional triangular lattice that involves two microscopic processes: an adsorption process and a migration process, is considered. Kinetic Monte Carlo methods are used to simulate the thin film deposition process. To characterize the surface morphology and to evaluate the light trapping efficiency of the thin film, surface roughness and surface slope are introduced as the root mean

squares of the surface height profile and surface slope profile. An Edwards–Wilkinson (EW)-type equation is used to describe the dynamics of the surface height profile and predict the evolution of the RMS roughness and RMS slope. A model predictive control algorithm is then developed on the basis of the EW equation model to regulate the RMS slope and the RMS roughness at desired levels by optimizing the substrate temperature at each sampling time. The model parameters of the EW equation are estimated from simulation data through least-square methods. Closed-loop simulation results are presented to demonstrate the effectiveness of the proposed model predictive control algorithm in successfully regulating the RMS slope and the RMS roughness at desired levels that optimize thin film light reflectance and transmittance.

3.2 Thin film deposition process

In this section, a thin film growth process is considered and modeled by using an on-lattice kMC model on a triangular lattice. Vacancies and overhangs are allowed to develop inside the film [30, 25]. Definitions of surface height profile, root-mean-square roughness, and RMS slope are also introduced in this section.

3.2.1 On-lattice kinetic Monte Carlo model

The one-dimensional triangular lattice in which the thin film deposition process takes place is shown in Fig. 3.1. Film growth occurs in the direction perpendicular to the

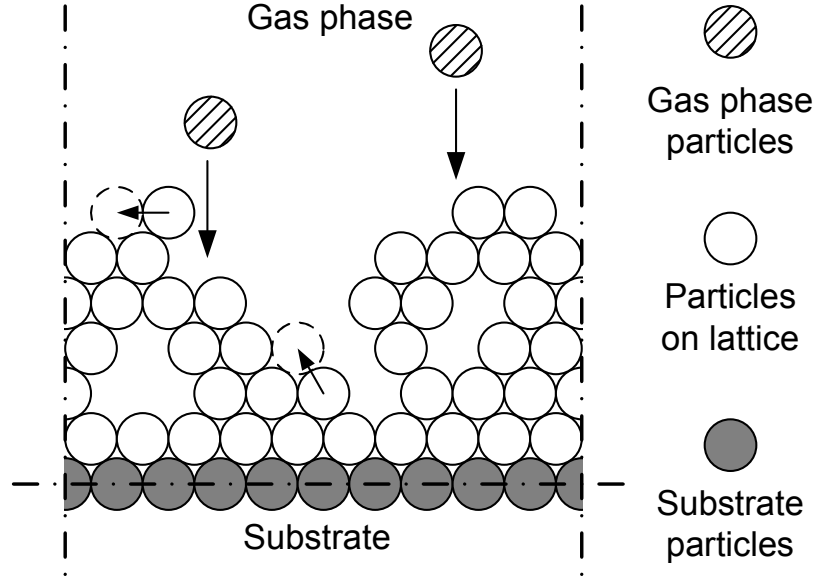


Figure 3.1: Thin film growth process on a triangular lattice. The arrows denote adsorption and migration processes.

lateral direction, i.e., the vertical direction as shown in Fig. 3.1. Periodic boundary conditions are applied in the lateral direction, i.e., the horizontal direction as shown in Fig. 3.1. In the triangular lattice, the maximum number of nearest neighboring particles around a given particle is six. In the one-dimensional triangular lattice model, a particle with only one nearest neighbor (and the rest five neighboring sites being vacant) is considered unstable and is subject to instantaneous surface relaxation. When a particle is subject to instantaneous surface relaxation, it moves to the nearest vacant site that is the most stable, i.e., the site with the most nearest neighbors; see [33] for a detailed description of the relaxation process. To initiate the thin film deposition process, a fully packed and fixed substrate layer is placed in the bottom of the lattice at the beginning of the deposition process.

In this thin film deposition process, two different micro-processes take place and significantly influence the thin film surface morphology [76, 78]: an adsorption process, where vertically incident particles are deposited from the gas phase into the thin film, and a migration process, where particles on the thin film overcome their energy barriers of the sites and move to neighboring vacant sites. In an adsorption process, the initial positions of the incident particles are randomly determined with a uniform probability distribution function in the gas phase domain. In a migration process, the probability that an on-film particle is subject to migration (i.e., migration rate) follows an Arrhenius-type law, where the pre-exponential factor and the activation energy are taken from a silicon film [25]. However, substrate particles and the particles fully surrounded by six nearest neighbors cannot move.

The stochastic nature of the microscopic deposition process is captured by using a kinetic Monte Carlo (kMC) algorithm to simulate the evolution of the deposition process. The microscopic rules of these micro-processes are used in the kMC algorithm to simulate the thin film deposition process. In the kMC simulation, each Monte Carlo event represents a specific microprocess, e.g., adsorption of a particle from the gas phase or migration of a particle on the thin film. In the kMC simulation, the time increment after a successfully executed Monte Carlo event depends on the total rate of all possible events in the lattice model of the thin film at the time of the execution of the event. In this work, a continuous-time Monte Carlo (CTMC)-type method (e.g., [71]) is used to implement the kMC simulations.

The thin film surface morphology depends on the adsorption and the migration processes. As a result of the complex interplay between the adsorption process and the migration process, the thin film surface morphology achieves a thermal balance. This thermal balance can be represented by certain values of surface roughness and surface slope, the definitions of which are introduced in the next subsection. The macroscopic variables of the deposition process have a strong influence on the resulting film surface morphology. The two variables that are considered in this work are the adsorption rate and the substrate temperature. Specifically, the adsorption rate, which is denoted by W , is defined as the number of deposited layers per second. The substrate temperature, which is denoted by T , influences the migration rate via the Arrhenius rate law.

We note that the deposition rate as an operating condition in this work is different from the rate of change of film thickness. The deposition rate here refers to the number of fully packed layers deposited per second and, in a vapor deposition process model, is determined from the flux rate at the gas-phase/surface boundary. With a constant deposition rate, the same amount of particles is deposited in the same time period (in the sense of expected value). Meanwhile, with different substrate temperatures, different film microstructures may form with different film porosity and film thickness. Thus, process operating conditions like the deposition rate or the substrate temperature, can be constant or vary with respect to time. These operating variables can be used as the manipulated variables for the control of the

thin film surface morphology expressed in terms of RMS surface slope and RMS surface roughness.

3.2.2 Definition of variables

In this section, two variables, RMS surface roughness and RMS surface slope, are precisely defined to characterize the film surface morphology and calculate the reflectance of a surface/interface. The surface height profile is used to represent the film surface morphology in the one-dimensional lattice model and is defined as the connection of the centers of the surface particles. Surface particles are the particles that can be reached from above in the vertical direction without being fully blocked by other particles on the film [30, 25]. Fig. 3.2 shows an example of the surface height profile of a given thin film configuration. The RMS surface roughness and RMS surface slope can be then defined on the basis of the surface height profile of the thin film.

Surface roughness is a commonly used measure of thin film surface morphology. In this work, surface roughness is defined as the root mean square of the surface height profile. Specifically, the definition of RMS surface roughness is given as follows:

$$r = \left[\frac{1}{2L} \sum_{i=1}^{2L} (h_i - \bar{h})^2 \right]^{1/2}, \quad (3.1)$$

where r denotes the RMS surface roughness, h_i , $i = 1, 2, \dots, 2L$, is the surface

height at the i -th position in the unit of layer, L is the number of sites on the lateral direction, and $\bar{h} = \frac{1}{2L} \sum_{i=1}^{2L} h_i$ is the average surface height.

From the expression of surface light reflectance of Eq. (1.1) and the dependence of light reflectance in Fig. 1.2, the RMS surface slope is also an important variable that determines the surface morphology in addition to the RMS roughness. In this work, the RMS slope represents the extent of surface slope and is defined as the root-mean-square of surface slope profile similarly to the definition of the RMS roughness of Eq. (3.1) in the following form:

$$m = \left[\frac{1}{2L} \sum_{i=1}^{2L} (h_i^s)^2 \right]^{1/2} \quad (3.2)$$

where m denotes the RMS slope and h_i^s , $i = 1, 2, \dots, 2L$, is the surface slope at the i -th position. Both m and h_i^s are dimensionless variables. The surface slope profile is obtained from the surface height profile using a first-order finite-difference approximation as follows:

$$h_i^s = \frac{(h_{i+1} - h_i)\sqrt{3}/2}{1/2} = \sqrt{3}(h_{i+1} - h_i), \quad (3.3)$$

where the constant, $\sqrt{3}$, is derived from the geometric ratio between the single-layer height and the interval between adjacent height positions in the triangular lattice. Due to the use of PBCs, the slope at the right most boundary position (h_{2L}^s) is computed from the right most and the left most surface heights, i.e., $h_{2L}^s = \sqrt{3}(h_1 -$

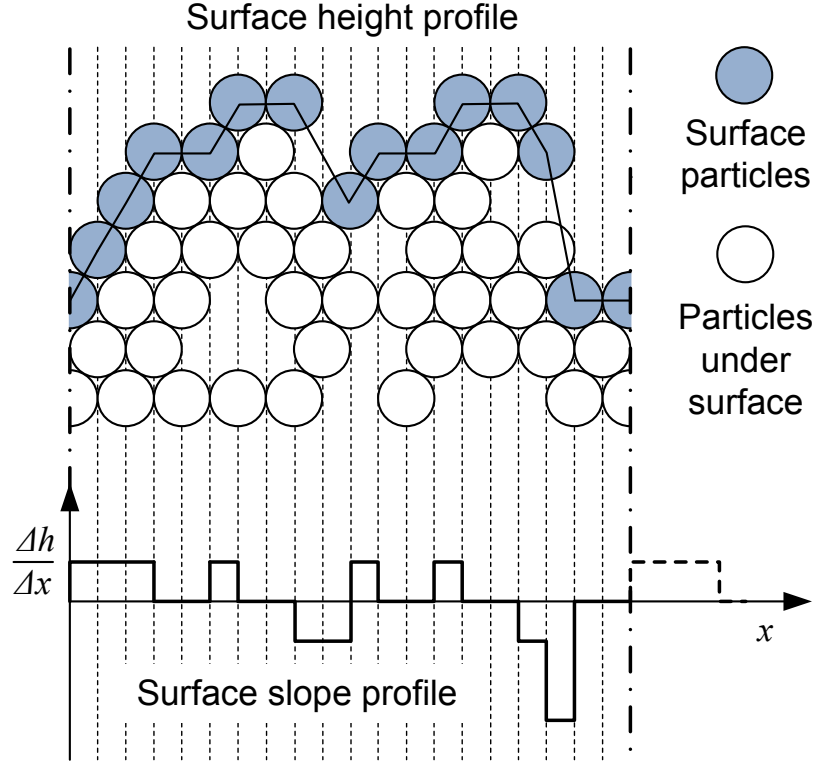


Figure 3.2: An example showing the definition of the surface height profile and the calculation of the corresponding surface slope profile.

h_{2L}). Fig. 3.2 also shows an example of the surface slope profile obtained from the surface height profile.

The behavior of RMS slope, i.e., its dynamics and dependence on the operating conditions and on the lattice size, has been studied in previous work [33]. For the purpose of theoretical analysis and control design, the square of RMS roughness (surface roughness square, r^2) and the square of RMS slope (mean slope square, m^2), are used in the analysis and controller design later in this work. Specifically, the expected mean slope square increases from zero and reaches a steady state at large times. The dynamics and the steady-state values of the expected mean slope

square depend on the operating conditions, i.e., the substrate temperature and the adsorption rate. Thus, the substrate temperature and/or the adsorption rate may be used as the manipulated inputs in the model predictive control design.

3.3 Closed-form dynamic model construction

The Edward-Wilkinson equation model as described in detail in Chapter 2 is used to model the thin film growth process. However, the domain is changed from $[-\pi, \pi]$ to $[0, 2L]$. We will focus on the model parameter estimation aspect in this section.

The expected mean slope square can then be expressed as the sum of weighted modal state variances as follows [33]:

$$\langle m^2(t) \rangle = \sum_{n=1}^{\infty} K_n \langle \alpha_n^2(t) \rangle, \quad (3.4)$$

where $K_n = \frac{2}{L(\Delta x)^3} \sin^2\left(\frac{n\pi}{2L}\right)$.

Using the analytical solutions of the expected surface roughness square of Eq. (2.20) and of the expected mean slope square of Eq. (3.4), we can obtain the behavior of the surface roughness square and of the mean slope square from the EW equation and from the lattice model. These analytical solutions will be later used to predict the evolution of the expected surface roughness square and of the expected mean slope square in the model parameter estimation and in the controller design.

3.3.1 Model parameter estimation and dependence on substrate temperature

In the EW equation of Eq. (2.10), there are three parameters r_h , ν , and σ^2 . The dependence of the model parameters, ν and σ^2 , on the operating conditions, i.e., the adsorption rate and the substrate temperature, is determined from the kMC simulation data. In this work, we only consider the temperature dependence of model parameters and use the substrate temperature as the manipulated input for control purposes (see section 3.4 below). Deposition rate is another choice for manipulated variable, and it can be implemented via the control of inlet flow rate and/or precursor concentration. Multivariable feedback control with temperature and deposition rate as manipulated variables can be done but it is outside the scope of this work.

In this work, the model parameter estimation is conducted on the basis of the RMS slope so that the dynamics of the surface slope can be captured by the EW equation in a more accurate fashion. Specifically, these parameters are estimated by matching the predicted evolution profiles of mean slope square to the ones obtained from the kMC simulations of the thin film deposition process in a least-square sense where the following cost is minimized:

$$\min_{\nu, \sigma^2} \sum_{k=1}^{N_1} \left[\langle m^2(t_k) \rangle - \sum_{n=1}^{\infty} K_n \langle \alpha_n^2(t_k) \rangle \right]^2, \quad (3.5)$$

where N_1 is the number of data points used for parameter estimation and $\langle m^2(t_k) \rangle$

is the expected mean slope square computed from 100 independent kMC simulations with identical and time-invariant operating conditions. The prediction of the state variance, $\langle \alpha_n^2(t_k) \rangle$, is obtained from the analytical solution of Eq. (2.18). In this work, the deposition rate is fixed at $W_0 = 1$ layer/s for all simulations. Eleven substrate temperature values ranging from 300K to 700K are sampled for the computation of the dependence of the parameters on substrate temperature.

Fig. 3.3 shows the steady-state values of the expected mean slope square at different substrate temperatures computed from the EW equation with the estimated parameters and from the kMC simulations; the agreement is excellent for all substrate temperatures. The dependence of the model parameters on the substrate temperature is shown in Fig. 3.4 and is used in the formulation of the model predictive controller. The EW-type equation with parameters estimated under time-invariant operating conditions is suitable for the purpose of model predictive control design because the control input in the MPC formulation is piecewise constant, i.e., the manipulated substrate temperature remains constant between two consecutive sampling times, and thus, the dynamics of the microscopic process can be predicted using the closed-form dynamic models with estimated parameters.

The temperature dependence of model parameters can be verified by comparing the predictions of the expected mean slope square from the EW equation with the estimated parameters to the corresponding profiles obtained from the kMC simulations, as shown in Figs. 3.5 and 3.6. We see that the EW equation with the estimated

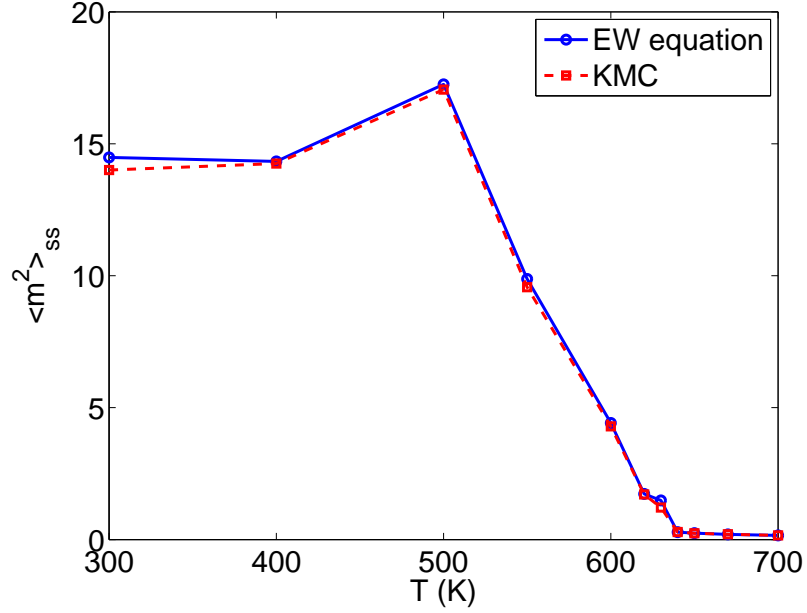


Figure 3.3: Steady-state values of the expected mean slope square computed from the EW equation (solid line) and from the kMC simulations (dashed line) at different substrate temperatures; $W = 1$ layer/s.

parameters is consistent with the kMC simulations in terms of the expected mean slope square at varying substrate temperatures.

It has been demonstrated that for a broad range of temperature variation the porous thin film growth process exhibits EW-type behavior [25]. Thus, each time a new temperature condition (control actuation) is applied to the thin film growth process, the process follows the EW equation behavior but with different model parameters, which depend on the new temperature condition.

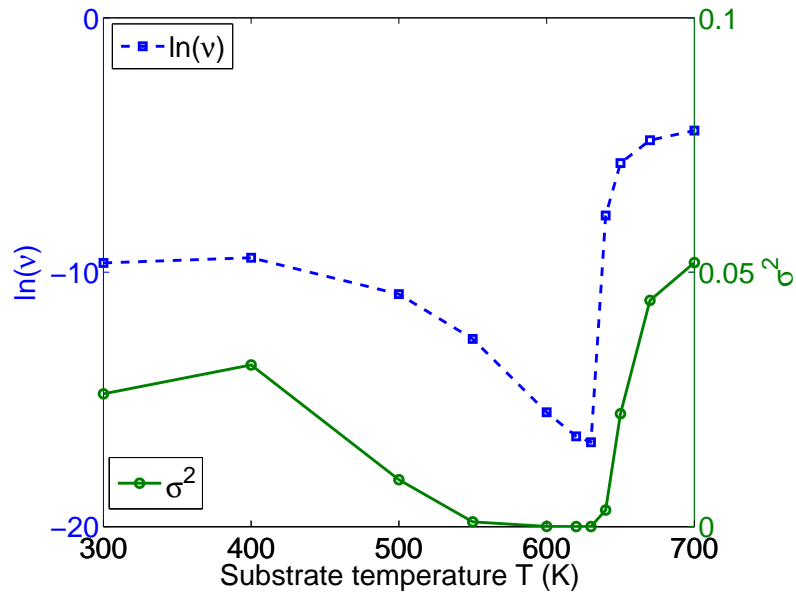


Figure 3.4: Dependence of $\ln(\nu)$ and σ^2 on substrate temperature; $W = 1$ layer/s.

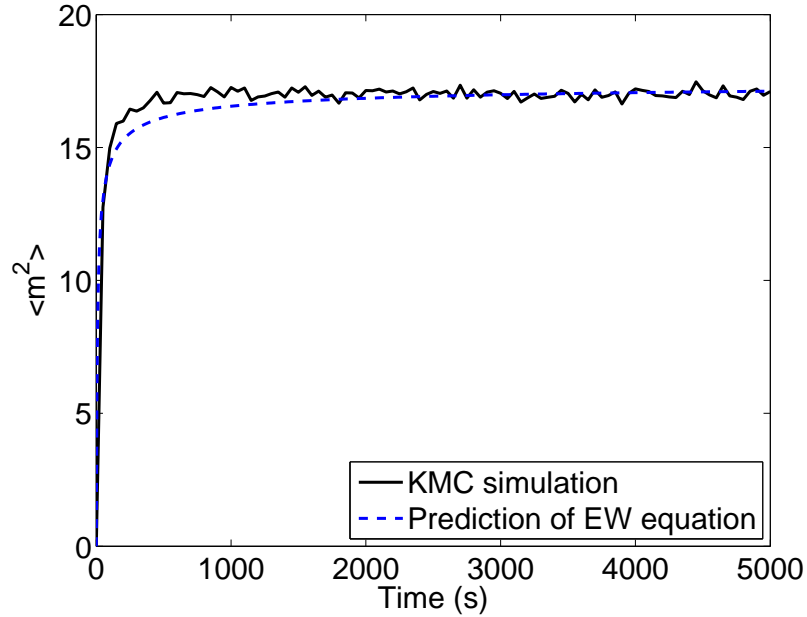


Figure 3.5: Comparison of EW-model prediction and kMC simulation results for $\langle m^2 \rangle$; $T = 500\text{K}$ and $W = 1$ layer/s.

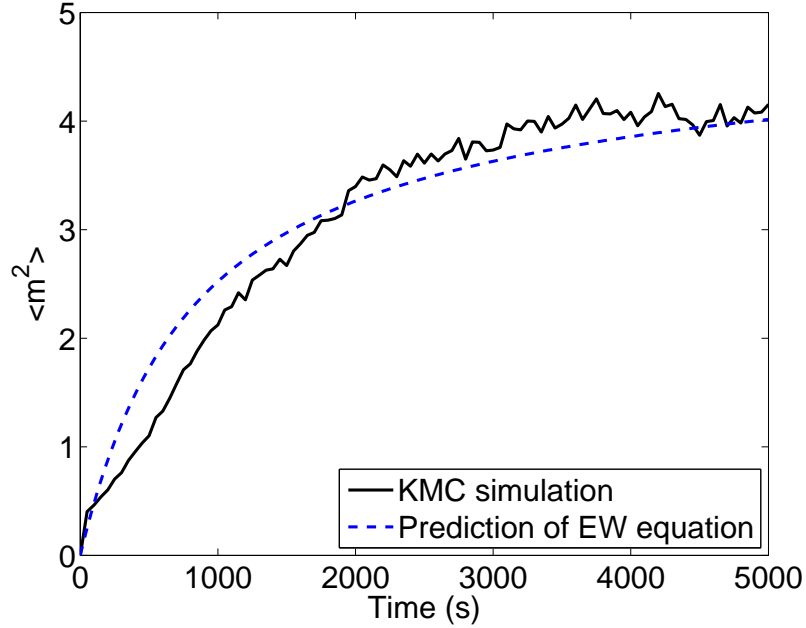


Figure 3.6: Comparison of EW-model prediction and kMC simulation results for $\langle m^2 \rangle$; $T = 600\text{K}$ and $W = 1$ layer/s.

3.4 Model predictive controller design

In this section, a model predictive controller is developed on the basis of the constructed closed-form dynamic model. The control objective is to regulate the expected mean slope square and the expected surface roughness square of the thin film to desired levels which optimize the light trapping efficiency, i.e., minimizing or maximizing the light reflectance of the surface or interface in thin-film solar cells. The dynamics of the mean slope square and of the surface roughness square are described by the EW equation of the surface height profile of Eq. (2.10) with appropriately estimated parameters.

3.4.1 MPC formulation

In this subsection, we consider the problem of regulation of RMS slope and RMS roughness of the thin film to desired levels within a model predictive control framework. The expected values of mean slope square and of surface roughness square, $\langle m^2 \rangle$ and $\langle r^2 \rangle$, are chosen as the control objectives. The substrate temperature is used as the manipulated input. When temperature is used as the manipulated input, the deposition rate is fixed at a certain value, W_0 , during the entire closed-loop simulation. To account for a number of practical considerations, several constraints are added to the controller. First, there is a constraint on the range of variation of the substrate temperature. This constraint ensures validity of the on-lattice kMC model. Another constraint is imposed on the rate of change of the substrate temperature to account for actuator limitations. The control action at time t is obtained by solving a finite-horizon optimal control problem. The cost function in the optimal control problem includes penalty on the deviation of $\langle r^2 \rangle$ and $\langle m^2 \rangle$ from their set-point values, which are computed to optimize the light reflectance of the thin film. The optimization problem is subject to the dynamics of the surface height. The optimal temperature profile is calculated by solving a finite-dimensional optimization problem in a receding horizon fashion. Specifically, the MPC problem is formulated as follows:

$$\min_{T_1, \dots, T_i, \dots, T_p} J = \sum_{i=1}^p \left\{ q_{m^2, i} \left[\frac{m_{\text{set}}^2 - \langle m^2(t_i) \rangle}{m_{\text{set}}^2} \right]^2 + q_{r^2, i} \left[\frac{r_{\text{set}}^2 - \langle r^2(t_i) \rangle}{r_{\text{set}}^2} \right]^2 \right\} \quad (3.6)$$

subject to:

$$\begin{aligned}\frac{\partial h}{\partial t} &= r_h + \nu \frac{\partial^2 h}{\partial x^2} + \xi(x, t) \\ r^2(t) &= \frac{1}{2L_0} \int_{-L_0}^{L_0} [h(x, t) - \bar{h}(t)]^2 dx \\ m^2(t) &= \frac{1}{2L} \sum_{i=1}^{2L} \left(\frac{h_{i+1} - h_i}{\Delta x} \right)^2\end{aligned}$$

$$T_{\min} < T_i < T_{\max}, \quad |(T_{i+1} - T_i)/\Delta| \leq L_T, \quad i = 1, 2, \dots, p,$$

where t is the current time, Δ is the length of the sampling interval, p is the number of prediction steps, $p\Delta$ is the specified prediction horizon, t_i , $i = 1, 2, \dots, p$, is the time of the i th prediction step ($t_i = t + i\Delta$), T_i , $i = 1, 2, \dots, p$, is the substrate temperature at the i th step ($T_i = T(t_i)$), $q_{r^2, i}$ and $q_{m^2, i}$, $i = 1, 2, \dots, p$, are the weighting penalty factors for the deviations of $\langle r^2 \rangle$ and $\langle m^2 \rangle$ from their respective set-points, r_{set}^2 and m_{set}^2 , at the i th prediction step, T_{\min} and T_{\max} are the lower and upper bounds on the substrate temperature, respectively, and L_T is the limit on the rate of change of the substrate temperature. The optimal temperature profile, (T_1, T_2, \dots, T_p) , is obtained from the solution of the optimization problem of (3.6), which minimizes the deviation of the expected mean slope square and of the expected surface roughness square from their respective set-point values within the prediction horizon.

The EW equation model is a stable system, guaranteed by the eigenspectrum of the second-order spatial differential operator with a positive coefficient. In this work, the optimization formulations in the MPC algorithms are solved on an open-

loop operating basis at each sampling time (even though feedback is included at each sampling time via the measurements). Thus, the inherent stability of the EW-equation model ensures a stable closed-loop operation under the model predictive controller.

3.4.2 MPC formulation based on finite-dimensional approximations

The surface roughness square and the mean slope square in terms of the state variance, Eqs. (2.20) and (3.4), respectively, require computation of infinite sums. Thus, the model predictive controller of (3.6) is infinite-dimensional and cannot be implemented in practice. To this end, finite-dimensional approximations (with a sufficiently large number of slow modes) can be used to approximately predict the dynamics of the surface roughness square and of the mean slope square as follows:

$$\langle \tilde{r}^2(t) \rangle = \frac{1}{2L_0} \sum_{n=1}^N \langle \alpha_n^2(t) \rangle, \quad \langle \tilde{m}^2(t) \rangle = \sum_{n=1}^N K_n \langle \alpha_n^2(t) \rangle, \quad (3.7)$$

where N denotes the dimension of the approximation and the tilde symbols denote the association of these variables with a finite-dimensional system.

Fig. 3.7 shows the profiles of the reconstructed surface roughness square and mean slope square obtained from the finite-dimensional approximations of Eq. (3.7) and compares them with the values of the surface roughness square and of the mean slope

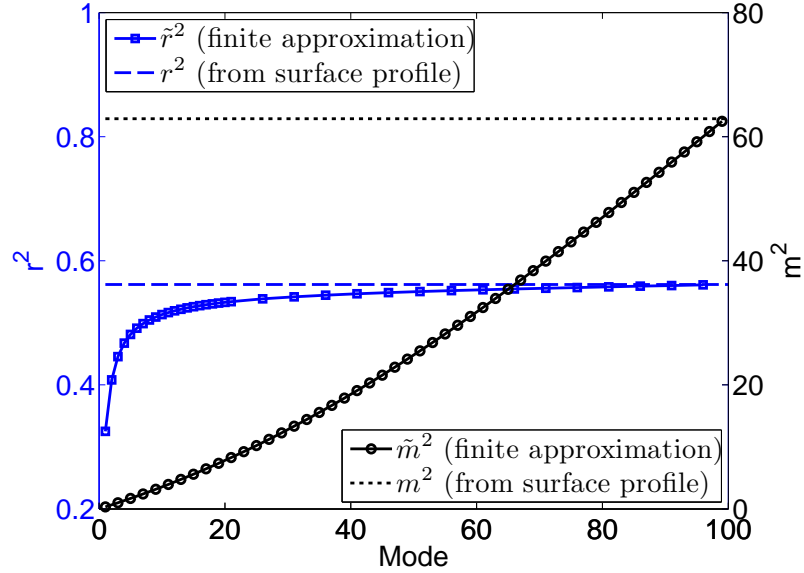


Figure 3.7: Profiles of reconstructed surface roughness square and mean slope square from the finite-dimensional approximation.

square computed from the definitions of Eqs. (3.1) and (3.2). It can be seen from Fig. 3.7 that as the order of the approximation increases, the reconstructed values are approaching the actual values computed from the definitions. Thus, the finite-dimensional approximation, that contains a finite number of modes, can be used for model prediction in the model predictive control formulation. Note that, although a higher-order model generally yields a more accurate approximation, the choice of the dimension of the reduced-order model is limited by the lattice size/discretization size. In the closed-loop simulations, the values of states are reconstructed from the discrete surface height profile by taking the inner product with the adjoint eigenfunctions. Due to the finite number of discrete surface height points, there is a limited number (half of the discrete surface height points) of states (modes) that can be used to obtain correct estimates of the surface roughness square and of the mean slope

square. This limited availability of the states is an additional reason for using a reduced-order model in the MPC formulation. The MPC formulation based on the finite-dimensional approximation of the EW equation has the following form:

$$\min_{T_1, \dots, T_i, \dots, T_p} J = \sum_{i=1}^p \left\{ q_{m^2, i} \left[\frac{m_{\text{set}}^2 - \langle \tilde{m}^2(t_i) \rangle}{m_{\text{set}}^2} \right]^2 + q_{r^2, i} \left[\frac{r_{\text{set}}^2 - \langle \tilde{r}^2(t_i) \rangle}{r_{\text{set}}^2} \right]^2 \right\} \quad (3.8)$$

subject to:

$$\langle \alpha_n^2(t_i) \rangle = -\frac{\sigma^2}{2\lambda_n} + \left(\alpha_n^2(t) + \frac{\sigma^2}{2\lambda_n} \right) e^{2\lambda_n i \Delta}$$

$$\langle \tilde{r}^2(t_i) \rangle = \frac{1}{2L_0} \sum_{n=1}^N \langle \alpha_n^2(t_i) \rangle$$

$$\langle \tilde{m}^2(t_i) \rangle = \sum_{n=1}^N K_n \langle \alpha_n^2(t_i) \rangle$$

$$T_{\min} < T_i < T_{\max}, \quad |(T_{i+1} - T_i)/\Delta| \leq L_T, \quad i = 1, 2, \dots, p.$$

3.5 Closed-loop simulations

In this section, we apply the proposed predictive controller of eq (3.8) to the kMC model of the thin film deposition process to regulate the surface slope and roughness at desired levels. The substrate temperature is used as the manipulated variable, which can be implemented via a heating/cooling system. The adsorption rate is kept constant during all deposition runs. The controlled variables are the expected values of the mean slope square and of the surface roughness square at the end of the

deposition process.

In the closed-loop simulations, the surface height profile is obtained from the surface morphology of the thin film from the kMC simulations and is transferred to the controller (state feedback control) at each sampling time. A finite number of slow modes are reconstructed from the surface height profile and are used to calculate the predictions of the mean slope square and of the surface roughness square along the prediction horizon. The estimated parameters and the dependence of the parameters on substrate temperature is used when solving the optimization problem in the model predictive controller. The constrained optimization problem formulated in the MPC of eq. (3.8) is solved and the optimal input temperature profile is obtained and is applied to the closed-loop system. The optimization problem is solved via a local constrained minimization algorithm with a broad set of initial guesses. The measurement of thin film surface morphology is a challenging issue, especially in real-time. Several techniques have been developed that enable surface height measurements during the operation of a deposition process like atomic force microscopy. The surface information can be also obtained by combining on-line probing and off-line measurements.

After being computed from the solution of the optimization problem, the optimal manipulated input is applied to the thin film growth process in a sample-and-hold fashion, i.e., the substrate temperature remains constant until the next sampling time. The EW model constructed from the open-loop simulation data can be used in the

MPC design since the manipulated input in the closed-loop system changes slowly with respect to the dynamics of the evolution of surface roughness and slope.

3.5.1 Separate regulation of surface slope and roughness

We first consider the control problems of separately regulating surface roughness and slope. Specifically, closed-loop simulations of the slope-only control problem are carried out by assigning the following values to the weighting factors in the MPC formulation of eq. (3.8): $q_{r^2} = 0.0$ and $q_{m^2} = 1.0$. Two set-point values, $m_{\text{set}}^2 = 0.5$ and 5, are considered. The order of finite-dimensional approximation used in the MPC formulation is $N = 100$. The deposition rate is fixed at $W = 1$ layer/s, which is appropriate from a practical standpoint, and the initial substrate temperature is $T = 500$ K. The variation of temperature is from 400 K to 700 K. The maximum rate of change of the temperature is $L_T = 1$ K/sec, which is also appropriate from a practical standpoint. The number of prediction steps is $p = 5$ and the prediction step size is $\Delta = 5$ s. The sampling time is also 5 s. Since the sampling time equals the prediction step size, only the first value of the manipulated input trajectory, T_1 , is applied to the deposition process (i.e., kMC model) during the time interval between two successive sampling times, $(t, t + \Delta)$. At the time $t + \Delta$, the surface height profile is sampled and the MPC problem of eq. (3.6) is solved to obtain the next optimal manipulated input trajectory. The closed-loop simulation duration is 1000 s. All expected values are obtained from 200 independent simulation runs to evaluate the

statistics of closed-loop performance.

Figs. 3.8 and 3.9 show, respectively, the profiles of the expected mean slope square and of the expected substrate temperature in the closed-loop simulation where the set-point of the mean slope square is 0.5. In Fig. 3.9, the substrate temperature increases linearly from the initial temperature of 500 K due to the constraint on the rate of change of the temperature. At large times ($t > 500$ s), the substrate temperature reaches a steady-state value around 620 K. Correspondingly, the expected surface mean slope square initially overshoots and is later regulated at the desired value of 0.5, which can be observed from Fig. 3.8. The overshoot of the expected mean slope square is the consequence of the constrained increase of the substrate temperature. A less-tight constraint on the rate of change of the substrate temperature or a higher initial substrate temperature may reduce or even avoid this overshoot.

Figs. 3.10 and 3.11 show the closed-loop simulation results with a higher set-point value for the mean slope square, $m_{\text{set}}^2 = 5$. The proposed model predictive controller also successfully drives the expected mean slope square to the desired value of 5 within 1000 s.

In addition to the slope-only control problem, the roughness-only control problem is considered with the following weighting factors: $q_{r^2} = 1.0$ and $q_{m^2} = 0.0$. As shown in Fig. 3.12, the expected surface roughness square is regulated close to the set-point value of 100; a final offset is observed due to the selection of the EW-model parameters that are more sensitive with respect to surface slope. This offset can be

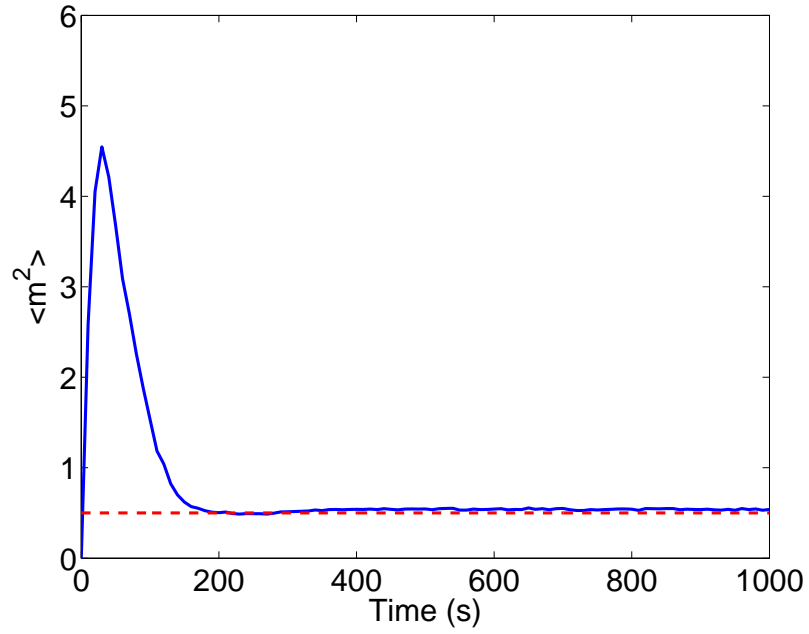


Figure 3.8: Profile of the expected mean slope square under closed-loop operation (solid line); $m_{\text{set}}^2 = 0.5$ (dashed line).

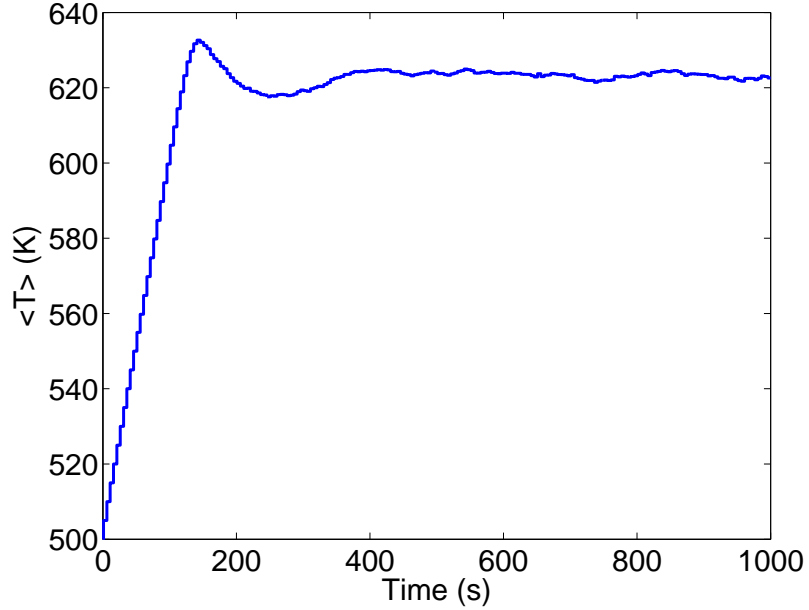


Figure 3.9: Profile of the expected substrate temperature under closed-loop operation; $m_{\text{set}}^2 = 0.5$.

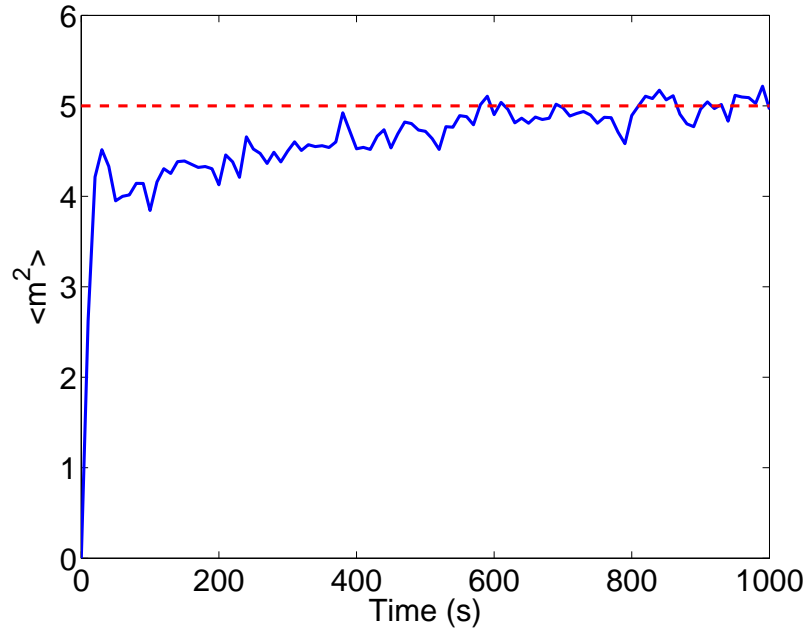


Figure 3.10: Profile of the expected mean slope square under closed-loop operation (solid line); $m_{\text{set}}^2 = 5$ (dashed line).

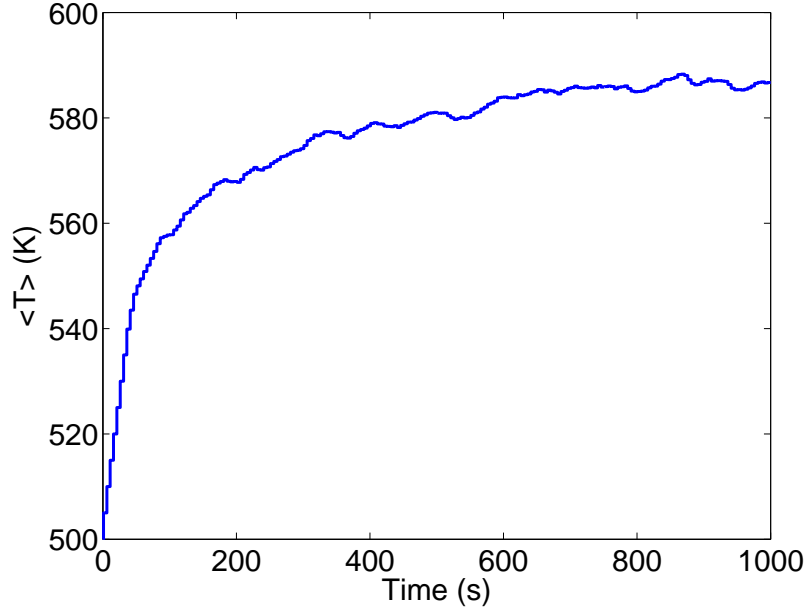


Figure 3.11: Profile of the expected substrate temperature under closed-loop operation; $m_{\text{set}}^2 = 5$.

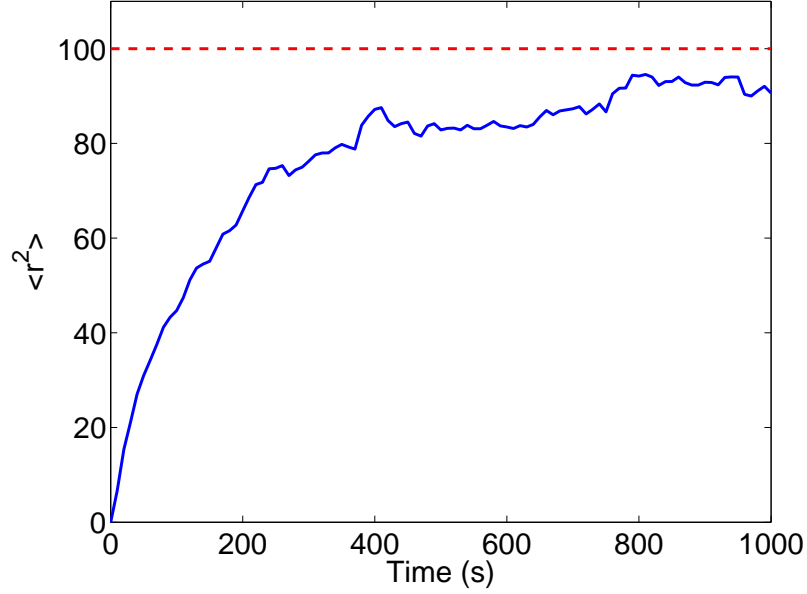


Figure 3.12: Profile of the expected mean roughness square under closed-loop operation (solid line); $r_{\text{set}}^2 = 100$ (dashed line).

eliminated if we replace $\langle m^2(t_k) \rangle$ by $\langle r^2(t_k) \rangle$ in the optimization problem of Eq. (3.5) used for estimating the EW-model parameters. Specifically, there is a deviation of the expected surface roughness square from the set-point value at the end of the simulation. This deviation is due to the fact that the parameter set is estimated solely on the basis of the dynamics of the mean slope square and this parameter set may result in deviations in the prediction of surface roughness square, especially for the intermediate region of the substrate temperature ($500 \text{ K} < T < 650 \text{ K}$). In addition, because there is no penalty on the deviation of RMS slope, $\langle m^2 \rangle$ is far away from its set-point of 0.5 at the end of the roughness-only closed-loop simulations.

3.5.2 Simultaneous regulation of surface slope and roughness for light trapping efficiency

Finally, closed-loop simulations of simultaneous regulation of surface slope and roughness are carried out. The set-points of the mean slope square and of the surface roughness square are $m_{\text{set}}^2 = 0.5$ and $r_{\text{set}}^2 = 100$, respectively. Since the substrate temperature is the only manipulated input, the mean slope square and the surface roughness square under closed-loop operation may not reach their respective set-point values. Therefore, a tradeoff between the surface slope and roughness is made by the controller on the basis of the weighting factors of the mean slope square and of the surface roughness square. To simplify the development, the same values of weighting factors of the mean slope square (and the same weighting factors of the surface roughness square) are used for all prediction steps, i.e., $q_{m^2,1} = q_{m^2,2} = \dots = q_{m^2,5} = q_{m^2}$ ($q_{r^2,1} = q_{r^2,2} = \dots = q_{r^2,5} = q_{r^2}$). The weighting factor of mean slope square is kept at 1, while the factor of surface roughness square varies from 1 to 10000. Fig. 3.13 shows the final expected values of the mean slope square and of the surface roughness square at the end of the closed-loop simulations ($t = 1000$ s) at different ratios of the weighting factors, $\lg(q_{r^2}/q_{m^2})$. It is clear that as the weighting on the surface roughness square increases, i.e., a higher value of $\lg(q_{r^2}/q_{m^2})$, the expected surface roughness square approaches more closely its set-point value of 100, while the expected mean slope square deviates from its set-point value of 0.5.

Since the mean slope square and the surface roughness square cannot reach their

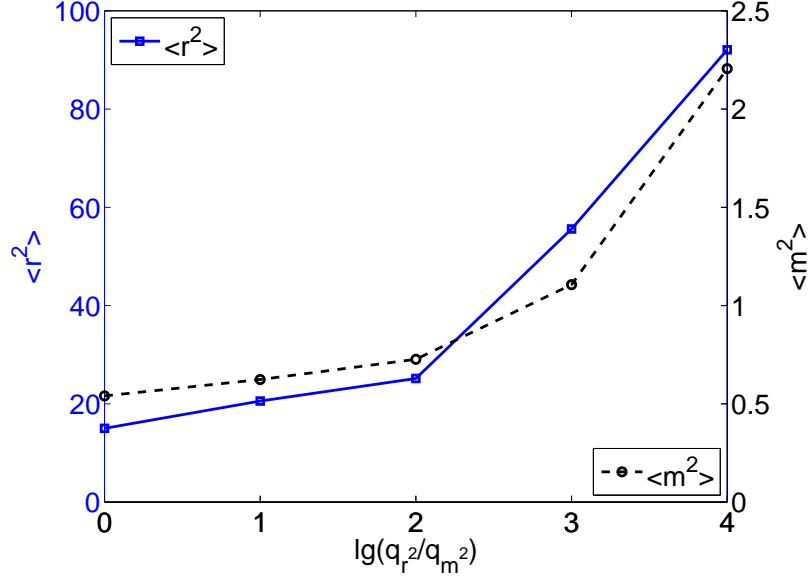


Figure 3.13: Profiles of $\langle r^2 \rangle$ (solid line) and $\langle m^2 \rangle$ (dashed line) at the end of closed-loop simulations ($t = 1000s$) for different penalty weighting factors: $q_{m^2} = 1$ and $1 \leq q_{r^2} \leq 10000$.

respective set-points, Fig. 3.13 also shows different values of the mean slope square and of the surface roughness square which are obtained at the end of the closed-loop simulations with different weighting factors of the mean slope square and of the surface roughness square. The light reflectance of these thin films obtained from the closed-loop simulations of simultaneous regulation can be computed from the resulting RMS surface slope and RMS roughness using Eq. (1.1), as shown in Fig. 3.14. In Fig. 3.14, the RMS slope, m , and the RMS roughness, r , are computed as the square roots of $\langle m^2 \rangle$ and $\langle r^2 \rangle$, respectively. The RMS roughness is also scaled with (by multiplying) a physical factor, 6.5 nm, so that the set-point value, r_{set}^2 , together with m_{set}^2 , corresponds to an optimal value (maximum) of the light reflectance in Eq. (1.1).

It can be seen from Fig. 3.14 that different values of light reflectance of the thin film are obtained at different ratios of the weighting factors, $\lg(q_{r^2}/q_{m^2})$. A plot with contours of the light reflectance is given in Fig. 3.15, which shows the dependence of the RMS slope, the RMS roughness, and the corresponding light reflectance of the thin film on the weighting factors. We note that the values of the RMS roughness in Figs. 3.14 and 3.15 are also scaled with the same factor as the one for r_{set}^2 . An optimal weighting scheme can be determined based on Figs. 3.14 and 3.15. For example, in the case where a high light reflectance is desired to improve the light trapping efficiency (e.g., for the back TCO layer that reflects the transmitted light back to the p-i-n layers of the thin film), a combination of the weighting factors, $q_{r^2} = 1$ and $q_{m^2} = 1$, can be used in the closed-loop operation.

For a perspective of the surface morphology of the thin films, representative snapshots of the film surface microstructure at the end of single open-loop and closed-loop simulations ($t = 1000\text{s}$) are shown in Fig. 3.16. Three closed-loop cases are compared: (1) slope-only control, (2) roughness-only control, and (3) simultaneous control of slope and roughness. It can be seen in Fig. 3.16 that different values of the mean slope square and of the surface roughness square are achieved at the end of simulations. In the open-loop simulation, the substrate temperature and the adsorption rate are fixed and the surface slope and roughness evolve following the open-loop dynamics. In the slope-only and roughness-only control, the mean slope square and the surface roughness square are regulated around their respective set-point values,

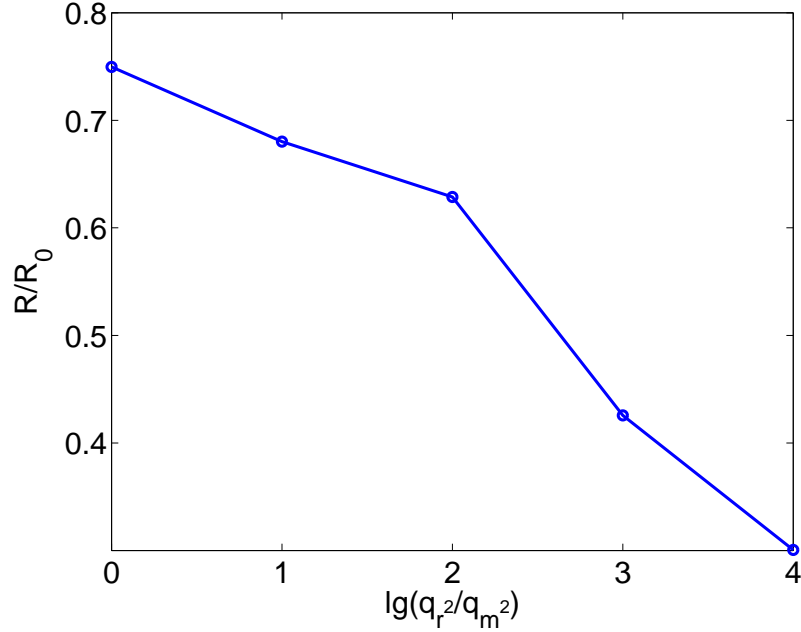


Figure 3.14: Dependence of light reflectance of thin film on the ratio of the weighting factors, $\lg(q_{r^2}/q_{m^2})$; $r_{\text{set}}^2 = 100$ and $m_{\text{set}}^2 = 0.5$.

$m_{\text{set}}^2 = 0.5$ and $r_{\text{set}}^2 = 100$, at the end of the simulation. In the case of simultaneous control of slope and roughness, a trade-off is made between the mean slope square and the surface roughness square. Specifically, different surface height profiles can be observed in Fig. 3.16 under open-loop operation and under different closed-loop operations. A nearly smooth surface height profile is obtained under slope-only control with a low RMS slope (since the RMS slope set-point, 0.5, is quite low) and a certain level of RMS roughness; these values of RMS slope and roughness result in a reflectance value of $R/R_0 = 0.69$ which could be appropriate for a back TCO layer. On the other hand, roughness-only control results in a rough surface height profile with both large slope fluctuation (high RMS slope) and large height fluctuation (high

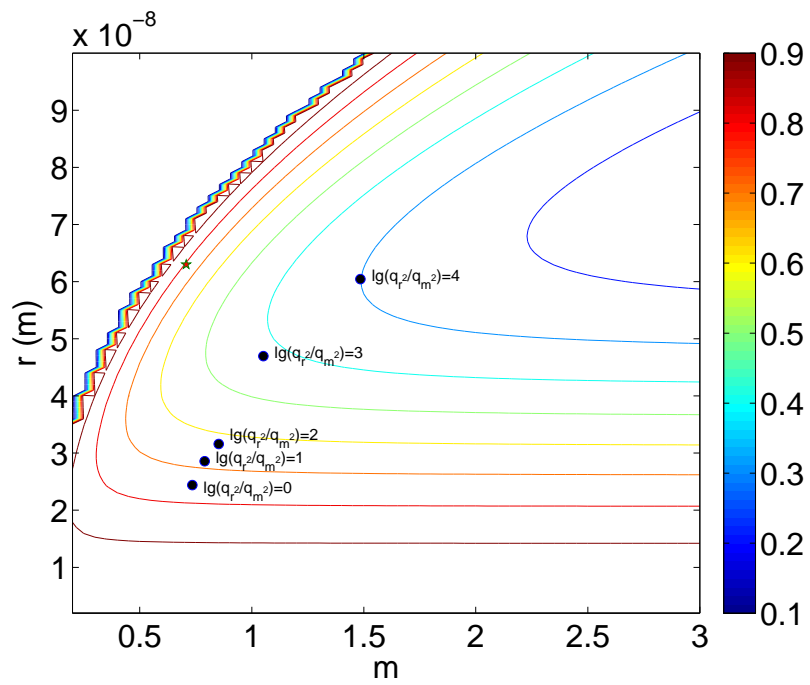


Figure 3.15: Light reflectance of thin films deposited under closed-loop operations with different weighting schemes.

RMS roughness); these values of RMS slope and roughness result in a reflectance value of $R/R_0 = 0.18$ which could be appropriate for a front TCO layer. The surface height profile under simultaneous control of slope and roughness with weighting factor ratio $\lg(q_r^2/q_m^2) = 3$ results in an “intermediate” surface height profile, as can be seen in Fig. 3.16, between slope-only control and roughness-only control, and a reflectance value of $R/R_0 = 0.46$ which could be appropriate for an intermediate solar cell layer. Therefore, by appropriately choosing the set-points for RMS roughness and RMS slope as well as the weighting factors, we can produce layers that have a broad range of reflectance values.

Remark 3.1 *In this work, the expected values of roughness and slope are compared to their respective set-points at the end of the deposition ($t = 1000$ s). The film thickness is not considered as a control objective. In some applications, there are stringent requirements for specific film thickness. If this is the case, model predictive controllers can be developed for simultaneous regulation of surface roughness, film porosity, and film thickness by including cost penalty on the deviation of film thickness from a desired minimum value or by implementing the thickness requirement as a constraint [29, 81].*

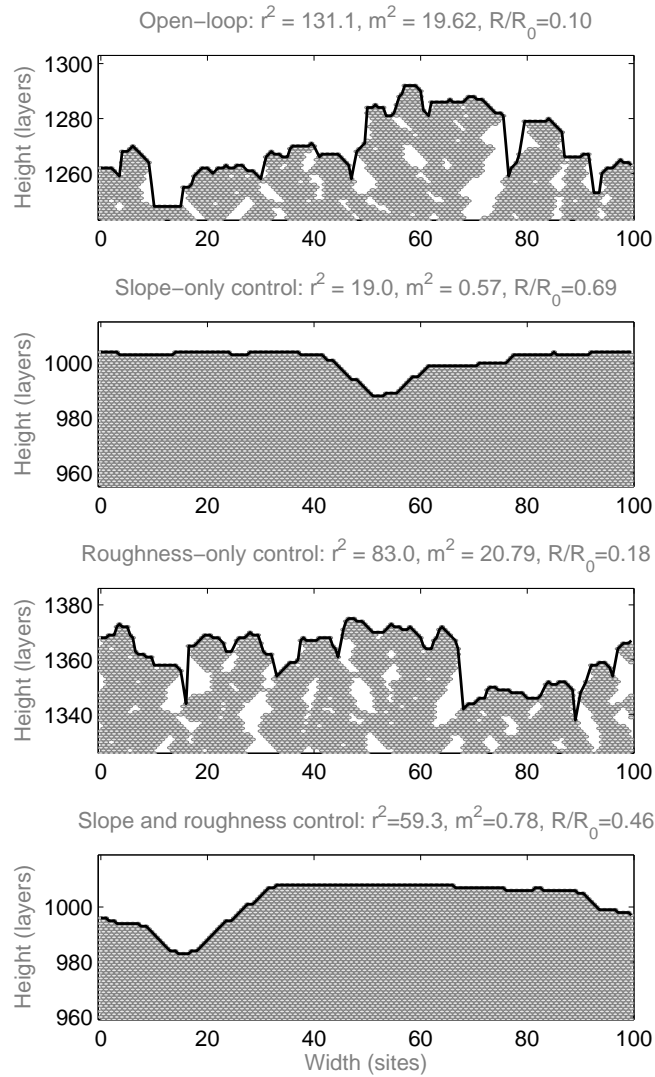


Figure 3.16: Snapshots of the film microstructure at the end of simulations ($t = 1000$ s) under open-loop and closed-loop operations. The open-loop operating conditions: $T = 500$ K and $W = 1.0$ layer/s; the set-points in closed-loop simulation: $r_{\text{set}}^2 = 100$ and $m_{\text{set}}^2 = 0.5$; the weighting factor ratio in the simultaneous regulation: $\lg(q_{r^2}/q_{m^2}) = 3$.

3.6 Conclusions

A model predictive control algorithm was developed to regulate the surface slope and roughness of a thin film growth process. The thin film deposition process was modeled on a one-dimensional triangular lattice that involves two microscopic processes: an adsorption process and a migration process. Kinetic Monte Carlo methods were used to simulate the thin film deposition process. To characterize the surface morphology and to evaluate the light trapping efficiency of the thin film, surface roughness and surface slope were introduced as the root mean squares of the surface height profile and surface slope profile. An EW-type equation was used to describe the dynamics of the surface height profile and predict the evolution of the RMS roughness and RMS slope. A model predictive control algorithm was then developed on the basis of the EW equation model to simultaneously regulate the RMS slope and the RMS roughness at desired levels by optimizing the substrate temperature at each sampling time. The model parameters of the EW equation were estimated from simulation data through least-square methods. Closed-loop simulation results were presented to demonstrate the effectiveness of the proposed model predictive control algorithm in successfully regulating the RMS slope and the RMS roughness at desired levels that optimize thin film light reflectance and transmittance.

Chapter 4

Control of Surface Roughness and Slope with 2D SPDE Model

4.1 Introduction

This chapter focuses on the development of a multivariable model predictive controller that simultaneously regulates thin film surface roughness and mean slope to optimize light reflectance and transmittance during thin-film manufacturing by manipulating the substrate temperature and the deposition rate. The dynamics of the evolution of the thin film surface height profile are assumed to be described by an Edwards–Wilkinson-type equation in two spatial dimensions. Analytical solutions of the expected surface roughness and surface slope are obtained on the basis of the Edwards–Wilkinson equation and are used in the design of a model predictive

controller that manipulates the substrate temperature and the deposition rate. The model predictive controller optimizes a cost function that involves penalty on both surface roughness and mean slope from desired set-point values and imposes constraints on the magnitude and the rate of change of the control action. The controller is applied to the two-dimensional Edwards–Wilkinson equation and is shown to successfully regulate the surface roughness and mean slope to set-point values at the end of the deposition that yield desired film reflectance and transmittance.

4.2 Preliminaries

4.2.1 2D Edwards–Wilkinson equation for surface height dynamics

The Edwards–Wilkinson (EW) equation, which is a second-order stochastic PDE, provides an adequate description of the dynamics of the evolution of the surface height profile in many thin-film growth processes that involve a thermal balance between atom adsorption and surface migration.[18, 19, 25, 32] In this work, the EW-type equation in two spatial dimensions takes the following form:

$$\frac{\partial h}{\partial t} = c + c_2 \left(\frac{\partial^2 h}{\partial x^2} + \frac{\partial^2 h}{\partial y^2} \right) + \xi(x, y, t) \quad (4.1)$$

where $x \in [0, \pi]$, $y \in [0, \pi]$ are the spatial coordinates, t is the time, $h(x, y, t)$ is the surface height, and $\xi(x, y, t)$ is a Gaussian white noise with a zero mean and the following covariance:

$$\langle \xi(x, y, t) \xi(x', y', t') \rangle = \sigma^2 \delta(x - x') \delta(y - y') \delta(t - t') \quad (4.2)$$

where $\delta(\cdot)$ denotes the Dirac delta function. c , c_2 , and σ^2 are model parameters that have explicit dependence on the macroscopic operating variables, i.e., the substrate temperature, T , and the deposition rate, W . Specifically, c is related to the growth rate of the average surface height and c_2 is related to the effect of surface relaxation/migration. These model parameters can be determined from kinetic Monte Carlo simulation or experimental data [53, 27]. The stochastic PDE, eq. (4.1), is subject to periodic boundary conditions (PBCs) of the form:

$$h(0, y, t) = h(\pi, y, t) \quad h(x, 0, t) = h(x, \pi, t) \quad (4.3)$$

$$\frac{\partial h}{\partial x}(0, y, t) = \frac{\partial h}{\partial x}(\pi, y, t) \quad \frac{\partial h}{\partial y}(x, 0, t) = \frac{\partial h}{\partial y}(x, \pi, t) \quad (4.4)$$

and the initial condition

$$h(x, y, 0) = h_0(x, y). \quad (4.5)$$

To analyze the dynamics and obtain a finite-dimensional approximation of the EW equation, we first consider the eigenvalue problem of the linear operator of eq (4.1)

subject to the periodic boundary conditions of eqs (4.3) and (4.4):

$$\mathcal{A}\phi_{m,n}(x, y) = c_2\left(\frac{\partial^2}{\partial x^2} + \frac{\partial^2}{\partial y^2}\right)\phi_{m,n}(x, y) = \lambda_{m,n}\phi_{m,n}(x, y), \quad (4.6)$$

$$\nabla^j \phi_{m,n}(0, y) = \nabla^j \phi_{m,n}(\pi, y), \quad j = 0, 1 \quad (4.7)$$

$$\nabla^j \phi_{m,n}(x, 0) = \nabla^j \phi_{m,n}(x, \pi), \quad j = 0, 1 \quad (4.8)$$

where $\lambda_{m,n}$ denotes an eigenvalue, $\phi_{m,n}$ denotes an eigenfunction, and ∇^j , $j = 0, 1$, denotes the gradient of a given function. The solution of the eigenvalue problem is as follows:

$$\lambda_{m,n} = 4c_2(m^2 + n^2) \quad (4.9)$$

$$\phi_{1,m,n} = \frac{2}{\pi} \sin(2mx) \sin(2ny) \quad (4.10)$$

$$\phi_{2,m,n} = \begin{cases} \frac{1}{\pi} & m = 0 \text{ and } n = 0 \\ \frac{2}{\pi} \cos(2mx) \cos(2ny) & m \neq 0 \text{ and } n \neq 0 \\ \frac{\sqrt{2}}{\pi} \cos(2mx) \cos(2ny) & m = 0, n \neq 0 \text{ or } m \neq 0, n = 0 \end{cases} \quad (4.11)$$

$$\phi_{3,m,n} = \begin{cases} 0 & m = 0 \\ \frac{2}{\pi} \sin(2mx) \cos(2ny) & m \neq 0, n \neq 0 \\ \frac{\sqrt{2}}{\pi} \sin(2mx) & m \neq 0, n = 0 \end{cases} \quad (4.12)$$

$$\phi_{4,m,n} = \begin{cases} 0 & n = 0 \\ \frac{2}{\pi} \cos(2mx) \sin(2ny) & n \neq 0, m \neq 0 \\ \frac{\sqrt{2}}{\pi} \sin(2ny) & n \neq 0, m = 0. \end{cases} \quad (4.13)$$

The solution of the EW equation of eq. (4.1) can be expanded in an infinite series in terms of the eigenfunctions of the operator of eq (4.6) as follows:

$$h(x, y, t) = \sum_{m=0}^{+\infty} \sum_{n=0}^{+\infty} \phi_{1,m,n} z_{1,m,n} + \phi_{2,m,n} z_{2,m,n} + \phi_{3,m,n} z_{3,m,n} + \phi_{4,m,n} z_{4,m,n}, \quad (4.14)$$

where $z_{1,m,n}$, $z_{2,m,n}$, $z_{3,m,n}$, and $z_{4,m,n}$ are time-varying coefficient.

Substituting the above expansion for the solution $h(x, y, t)$ into eq (4.1) and taking the inner product with the adjoint eigenfunctions, the following system of infinite stochastic linear ordinary differential equations (ODEs) for the temporal evolution of the time-varying coefficients is obtained:

$$\frac{dz_{2,0,0}}{dt} = \pi c + \xi_{2,0,0}(t), \quad (4.15)$$

$$\frac{dz_{p,m,n}}{dt} = \lambda_{m,n} z_{p,m,n} + \xi_{p,m,n}(t), \quad p = 1, 2, 3, 4, \quad m, n = 0, 1, \dots, \infty, \quad m^2 + n^2 \neq 0, \quad (4.16)$$

where $\xi_{p,m,n} = \int_0^\pi \int_0^\pi \xi(x, y, t) \phi_{p,m,n} dx dy$ is the projection of the noise $\xi(x, y, t)$ on the ODE for $z_{p,m,n}$. The noise term, $\xi_{p,m,n}$, has zero mean and covariance

$$\langle \xi_{p,m,n}(t) \xi_{p,m,n}(t') \rangle = \sigma^2 \delta(t - t'). \quad (4.17)$$

The temporal evolution of the variance of mode $z_{p,m,n}$ can be obtained from the

solution of the linear ODE of eqs (4.15) and (4.16) as follows:

$$\langle (z_{p,m,n}^2(t)) \rangle = e^{2\lambda_{m,n}(t-t_0)} \langle (z_{p,m,n}^2(t_0)) \rangle + \sigma^2 \frac{e^{2\lambda_{m,n}(t-t_0)} - 1}{2\lambda_{m,n}}, \quad m^2 + n^2 \neq 0. \quad (4.18)$$

For feedback control purposes (see Section 4.3 below), the modes can be calculated from a surface height measurement as follows:

$$z_{p,m,n}(t) = \int_0^\pi \int_0^\pi h(x, y, t) \phi_{p,m,n}(x, y) dx dy. \quad (4.19)$$

In many circumstances, only discrete height profile measurements are available, thus eq (4.19) can be approximated by

$$z_{p,m,n}(t) = \frac{\pi^2}{K^2} \sum_{i=0}^{L-1} \sum_{j=0}^{L-1} \hat{h}(i, j, t) \phi_{p,m,n}(i, j) \quad (4.20)$$

where L is the number of spatial height sampling (measurement) points in $[0, \pi]$ in both x and y coordinates and $\hat{h}(i, j, t) = h(x_i, y_j, t) = h(\frac{i\pi}{L}, \frac{j\pi}{L}, t)$. It is worth pointing out that, when discrete height measurements are available, the highest number of modes that can be accurately calculated is limited by the spatial sampling points, $m, n \leq L/2$.

The dependence of c , c_2 and σ^2 on substrate temperature T and deposition rate W can be identified from either experiments or kinetic Monte Carlo simulations of the thin film growth process. The expressions reported in [53] that were obtained

from kinetic Monte Carlo simulations are used here:

$$c(T, W) = W \left(1 - \frac{k_w}{W^{a_w}} e^{k_B T / E_w} \right) \quad (4.21)$$

$$c_2(T, W) = \frac{k_c}{L^2 W^{a_c}} e^{k_B T / E_c} \quad (4.22)$$

$$\sigma^2(T, W) = \frac{\pi^2}{L^2} \left[1 + e^{(a_t + k_t W)T - a_v - k_v W} \right] \quad (4.23)$$

where k_B is Boltzmann's constant (8.617343×10^{-5} eV/K), $k_w = 3.3829 \times 10^{-12}$, $a_w = 0.6042$, $E_w = 2.7 \times 10^{-3}$ eV, $k_c = 1.0274 \times 10^{-13}$, $a_c = 0.1669$, $E_c = 1.9 \times 10^{-3}$ eV, $a_v = 15.55493$, $k_v = 20.64504$ s, $a_t = 0.02332$ K $^{-1}$ and $k_t = 0.0261$ s·K $^{-1}$.

4.2.2 Film surface roughness and rms slope

Thin film surface morphology can be characterized by roughness and rms slope.

Roughness is defined as the root-mean-square of the surface height profile:

$$\begin{aligned} r(t) &= \sqrt{\frac{1}{\pi^2} \int_0^\pi \int_0^\pi (h(x, y, t) - \bar{h}(t))^2 dx dy} \\ &\approx \sqrt{\frac{1}{L^2} \sum_{i=0}^{L-1} \sum_{j=0}^{L-1} (\hat{h}(i, j, t) - \bar{h})^2} \end{aligned} \quad (4.24)$$

where \bar{h} denotes the average surface height. Substituting eq (4.14) into eq (4.24), the expected value of r^2 can be rewritten in terms of the state covariance as follows:

$$\langle r^2 \rangle = \frac{1}{\pi^2} \sum_{m,n=0, m^2+n^2 \neq 0}^{L/2} (\langle z_{1,m,n}^2 \rangle + \langle z_{2,m,n}^2 \rangle + \langle z_{3,m,n}^2 \rangle + \langle z_{4,m,n}^2 \rangle). \quad (4.25)$$

The rms slope is defined as the root mean square of the slope of the surface height:

$$\begin{aligned}
m(t) &= \sqrt{\frac{1}{\pi^2} \int_0^\pi \int_0^\pi \left(\frac{\partial h}{\partial x}(x, y, t) \right)^2 dx dy} \\
&\approx \sqrt{\frac{1}{\pi^2} \sum_{i=0}^{L-1} \sum_{j=0}^{L-1} \left(\frac{\hat{h}(i+1, j, t) - \hat{h}(i, j, t)}{\Delta x} \right)^2 \frac{\pi^2}{L^2}}.
\end{aligned} \tag{4.26}$$

The expected rms slope square can also be expressed in terms of the state covariance as follows:

$$\langle m^2 \rangle = \sum_{m,n=0, m^2+n^2 \neq 0}^{L/2} (K_{1,m,n} \langle z_{1,m,n}^2 \rangle + K_{2,m,n} \langle z_{2,m,n}^2 \rangle + K_{3,m,n} \langle z_{3,m,n}^2 \rangle + K_{4,m,n} \langle z_{4,m,n}^2 \rangle) \tag{4.27}$$

where $K_{p,m,n}$ can be computed by

$$K_{p,m,n} = \frac{1}{\pi^2} \sum_{i=0}^{L-1} \sum_{j=0}^{L-1} (\phi_{p,m,n}(i+1, j) - \phi_{p,m,n}(i, j))^2 = \frac{4}{\pi^2} \sin^2 \left(\frac{\pi m}{L} \right). \tag{4.28}$$

4.3 Model predictive controller design

In this section, a model predictive controller is developed based on the dynamic model of the expected roughness square and rms slope square. Substrate temperature and deposition rate are used as the manipulated variables. The control objective is to minimize the deviation of the expected roughness square and/or rms slope square from desired set-point values. Because the thin film deposition process is a batch process, the interval between current time and the end of the batch run is used as

the prediction horizon. During each predictive controller evaluation, the manipulated variable is assumed to stay fixed until the end of the batch. To account for practical considerations, two types of input constraints are imposed: (a) both the temperature and the deposition rate have lower and upper limits, and (b) the rates of change of both inputs are constrained to be less than certain upper limits due to actuator limitations. The resulting MPC formulation is as follows:

$$\min_{T(t), W(t)} J(t) = q_{r^2} (\langle r^2(t_f) \rangle - r_{\text{set}}^2)^2 + q_{m^2} (\langle m^2(t_f) \rangle - m_{\text{set}}^2)^2 \quad (4.29)$$

where

$$\langle r^2(t_f) \rangle = \frac{1}{\pi^2} \sum_{m,n=0, m^2+n^2 \neq 0}^{L/2} (\langle z_{1,m,n}^2 \rangle + \langle z_{2,m,n}^2 \rangle + \langle z_{3,m,n}^2 \rangle + \langle z_{4,m,n}^2 \rangle) \quad (4.25)$$

$$\begin{aligned} \langle m^2(t_f) \rangle = & \sum_{m,n=0, m^2+n^2 \neq 0}^{L/2} (K_{1,m,n} \langle z_{1,m,n}^2(t_f) \rangle + K_{2,m,n} \langle z_{2,m,n}^2(t_f) \rangle \\ & + K_{3,m,n} \langle z_{3,m,n}^2(t_f) \rangle + K_{4,m,n} \langle z_{4,m,n}^2(t_f) \rangle) \end{aligned} \quad (4.27)$$

$$\text{cov}(z_{p,m,n}(t_f)) = e^{-8c_2(m^2+n^2)(t_f-t)} \text{cov}(z_{p,m,n}(t)) + \sigma^2 \frac{e^{-8c_2(m^2+n^2)(t_f-t)} - 1}{2\lambda_{m,n}}, \quad m^2+n^2 \neq 0 \quad (4.18)$$

$$c = W \left(1 - \frac{k_w}{W^{a_w}} e^{k_B T / E_w} \right) \quad (4.21)$$

$$c_2 = \frac{k_c}{L^2 W^{a_c}} e^{k_B T / E_c} \quad (4.22)$$

$$\sigma^2 = \frac{\pi^2}{L^2} [1 + e^{(a_t + k_t W)T - a_v - k_v W}] \quad (4.23)$$

subject to

$$c(T, W) \geq c_{\min}, \quad (4.30)$$

$$T_{\min} \leq T \leq T_{\max}, \quad W_{\min} \leq W \leq W_{\max}, \quad (4.31)$$

$$|T(t) - T(t - dt)| \leq \Delta T_{\max}, \quad |W(t) - W(t - dt)| \leq \Delta W_{\max}, \quad (4.32)$$

where t_f is the final time of the batch run, r_{set}^2 and m_{set}^2 are the respective set-points for the surface roughness square and the mean slope square, q_{r^2} and q_{m^2} are the weighting factors for the deviations of $\langle r^2 \rangle$ and $\langle m^2 \rangle$ from their respective set-points, r_{set}^2 and m_{set}^2 , at t_f , dt is the time interval between two successive sampling times and control actions, T_{\min} and T_{\max} are the lower and upper bounds on the substrate temperature respectively, ΔT_{\max} is the limit on the rate of change of the substrate temperature, W_{\min} and W_{\max} are the lower and upper bounds on the deposition rate, respectively, and ΔW_{\max} is the limit on the rate of change of the deposition rate.

The optimization problem is solved at each sampling time once a new measurement of the surface height profile becomes available. An interior point method optimizer, IPOPT [75], is used to solve the optimization problem in the MPC formulation.

Remark 4.1 *Referring to the design and implementation of estimation-based (output feedback) control systems, we note that an output feedback controller, which utilizes a Kalman–Bucy-type filter as the state estimator, was developed and used in the context of covariance control of a stochastic partial differential equation in a previous work*

of our group [26]. Furthermore, estimation-based control of a kinetic Monte Carlo model of a one-dimensional thin-film growth process was also studied in the context of roughness control [27] and porosity control [81]. In the present work, we focus on the model predictive control of surface roughness and slope of a process described by the Edwards–Wilkinson equation in two spatial dimensions. The application of the proposed controller to a kinetic Monte Carlo simulation model of a two-dimensional thin-film growth process, as well as the design of an estimation-based control scheme, will be addressed in a future work.

4.4 Closed-loop simulations

In this section, the model predictive controller of eq (4.29) is applied to the two-dimensional EW equation plant model of eq (4.1). The variation of substrate temperature is from 600–750 K and the variation of the deposition rate is from 0.1 to 1 layer/s. The initial temperature is 610 K, and the initial deposition rate is 1 layer/s. The maximum rates of change are $T_{\max} = 5$ K/s for temperature and $\Delta W_{\max} = 0.05$ layer/s for deposition rate. The sampling time is 5 s. Each closed-loop simulation lasts for 100 s. Expected values are calculated from 100 independent runs.

4.4.1 Control of Film Surface Roughness

First, the problem of regulating film surface roughness is considered. In this scenario, the cost function only contains penalty on the deviation of the expected surface roughness square from the set-point. The weighting factors are $q_{r^2} = 1$ and $q_{m^2} = 0$. The set-point is $r_{\text{set}}^2 = 15$.

Figure 4.1 shows the profile of $\langle r^2 \rangle$ under the model predictive controller of eq (4.29). It can be seen that the controller drives the expected film roughness at the end of the simulation close to the desired value. Figure 4.2 shows the expected profiles of T and W for the closed-loop simulation. The overall variations of both temperature and deposition rate are small because the initial values of these variables are close to the ones needed to accomplish the desired set-points for surface roughness and slope. As a result, the constraints on the rate of change of the manipulated variables are not reached in this case since the rates of change of the variables requested by the controller are much smaller than the imposed constraints. Figure 4.3 compares the histogram of r^2 from open-loop and closed-loop simulations. The model predictive control algorithm reduces the variance of r^2 by 47%, from 0.3179 to 0.1681.

4.4.2 Control of Film Surface rms Slope

Next, we consider the regulation of thin film surface rms slope. The cost function includes only penalty on the deviation of the expected value of rms slope square from the set point by choosing weighting factors $q_{r^2} = 0$ and $q_{m^2} = 1$. The set point is

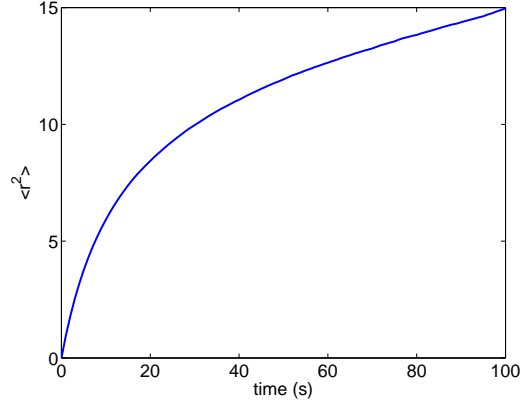


Figure 4.1: Profile of expected film surface roughness square from 100 closed-loop simulations. $q_{r^2} = 1$, $q_{m^2} = 0$ and $r_{\text{set}}^2 = 15$.

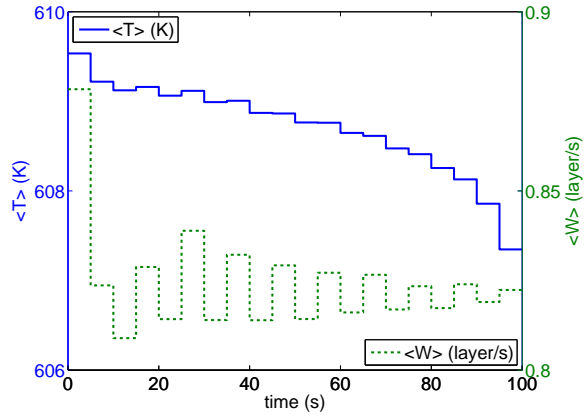


Figure 4.2: Profiles of manipulated variables. $q_{r^2} = 1$, $q_{m^2} = 0$ and $r_{\text{set}}^2 = 15$.

$$m_{\text{set}}^2 = 0.2.$$

Figure 4.4 shows the profile of expected rms slope square from 100 repeats of closed-loop simulations. The rms slope reaches its set point at $t = 100$ s. The constraint on the rate of change of the temperature takes effect in the slope-only control problem and limits the increase of the substrate temperature at the initial stage of the deposition. A peak appears in the slope profile in the first 20 seconds

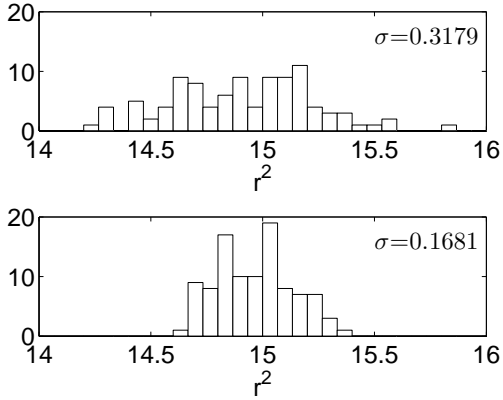


Figure 4.3: Comparison of histograms of r^2 at the end of the simulation between open-loop (top plot) and closed-loop (bottom plot) simulations. $q_{r^2} = 1$, $q_{m^2} = 0$ and $r_{\text{set}}^2 = 15$.

because the temperature can not increase fast enough from its initial value due to the rate of change constraint. Figure 4.5 shows the profile of expected temperature and deposition rate. Because the low set-point value of the mean slope square requires a relatively high substrate temperature, the controller increases the temperature at the maximum rate during the first four steps and then keeps the temperature around 716 K. The comparison of histograms of m^2 at the end of the simulation between closed-loop and open-loop is presented in figure 4.6. The MPC reduces the variance but by a smaller amount compared to the case of roughness-only control.

4.4.3 Simultaneous control of roughness and rms slope

Finally, simultaneous regulation of roughness and rms slope is carried out. The set-points of the surface roughness square and of the mean slope square are $r_{\text{set}}^2 = 15$

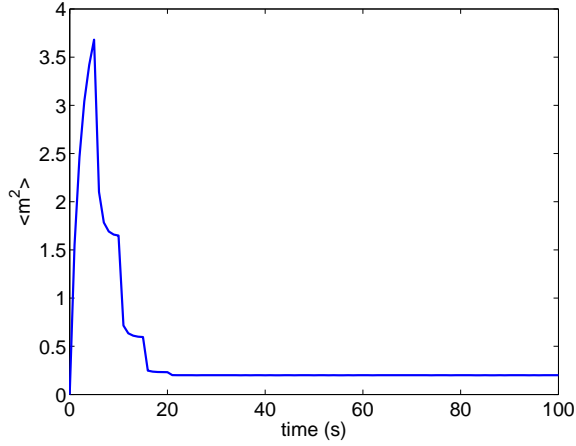


Figure 4.4: Profile of expected film surface rms slope square from 100 closed-loop simulations. $q_{r^2} = 0$, $q_{m^2} = 1$, and $m_{\text{set}}^2 = 0.2$.

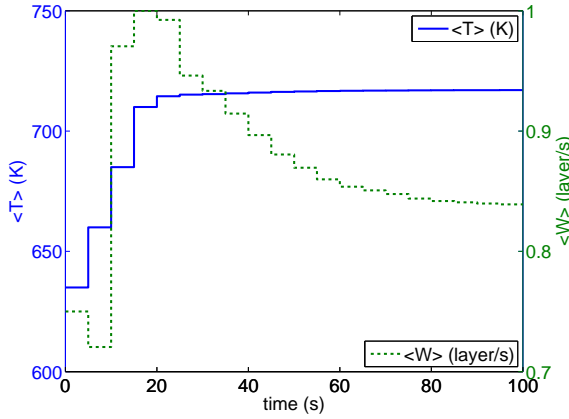


Figure 4.5: Profiles of manipulated variables. $q_{r^2} = 0$, $q_{m^2} = 1$, and $m_{\text{set}}^2 = 0.2$.

and $m_{\text{set}}^2 = 0.2$. The weighting factor of mean slope square is kept at 1, while the weighting factor of roughness square increases from 0.01 to 10^6 .

Figure 4.7 shows the change of $\langle r^2 \rangle$ and $\langle m^2 \rangle$ as a function of q_{r^2}/q_{m^2} . It can be seen that as the weighting on roughness square increases, the expected roughness square approaches more closely its set-point value at the cost of larger deviation of rms slope square from its set-point value.

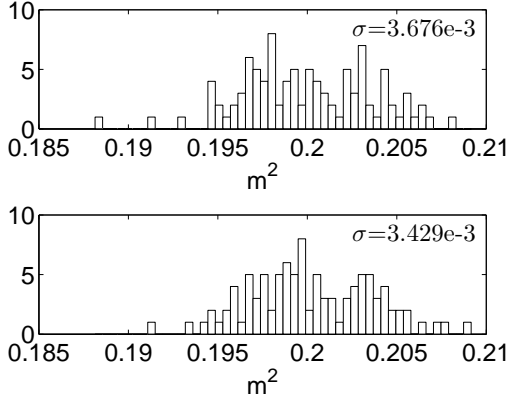


Figure 4.6: Comparison of histograms of m^2 at the end of the simulation between open-loop (top plot) and closed-loop (bottom plot) simulations. $q_{r^2} = 0$, $q_{m^2} = 1$, and $m_{\text{set}}^2 = 0.2$.

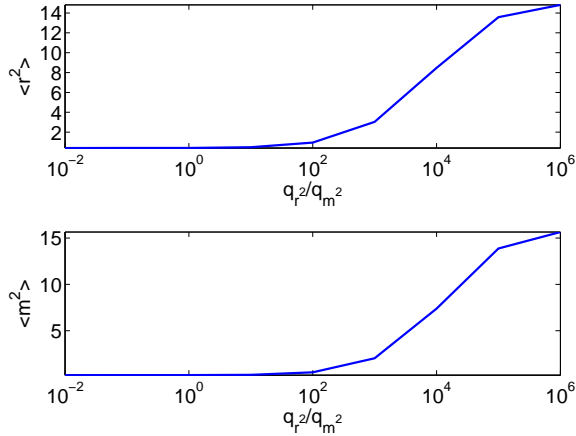


Figure 4.7: $\langle r^2 \rangle$ and $\langle m^2 \rangle$ at the end of closed-loop simulations ($t = 100$ s) for different penalty weighting factors: $q_{m^2} = 1$ and $0.01 \leq q_{r^2} \leq 10^6$.

4.4.4 Application to light trapping efficiency

For thin-film solar cells, the energy conversion efficiency is directly related to the light trapping/scattering properties of the thin film interfaces and surfaces, which can be characterized by the roughness, r , and the rms slope, m . Specifically, Rayleigh scat-

tering occurs when the incident light goes through a rough interface where it is divided into four components: specular reflection, specular transmission, diffused reflection, and diffused transmission [66, 40]. As described in chapter 1, the total reflectance, R , when a rough thin-film surface is illuminated with a beam of monochromatic light at normal incidence can be approximated by eq (1.1). The numerical integration result of eq (1.1) is shown in figure 1.2. From this plot, it can be inferred that both r and m strongly influence the intensity of light reflection (and, therefore, light transmission) by the surface/interface.

In the simultaneous control of roughness and slope in section 4.4.3, the expected surface roughness square and mean slope square can be regulated to different levels with the same set-points by choosing different weighting schemes, i.e., different ratios between the weighting factors, q_{r^2}/q_{m^2} . The corresponding light reflectance for different weighting factor ratios can be computed according to eq (1.1). In 4.8, the roughness and rms slope obtained from closed-loop simulations with different q_{r^2}/q_{m^2} are mapped to a contour of reflectance. Note that the roughness is scaled by a factor of 1.16×10^{-8} m to represent the length scales of atomic particles in thin film growth processes. We can see that by changing the ratio, q_{r^2}/q_{m^2} , we can produce films whose surface leads to different reflectance values.

Remark 4.2 *Certain set-points for both surface roughness and surface slope are desired to be attained during the manufacturing (thin-film growth) process to optimize the light trapping efficiency of thin-film solar cells. These requirements may be attained*

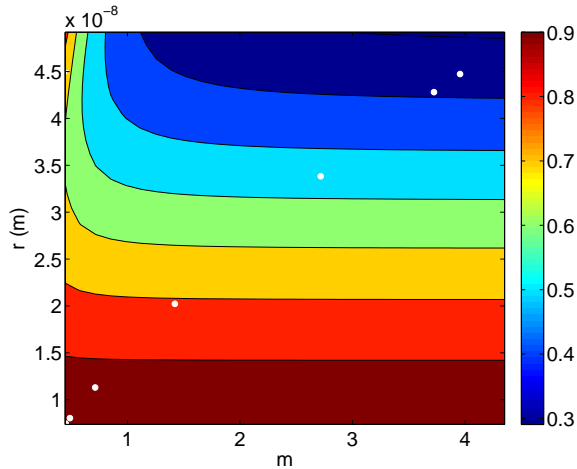


Figure 4.8: Light reflectance of thin films deposited under closed-loop operations with different weighting factor ratio.

through penalty of the deviation of surface roughness and slope in the cost functional (as done in this work) or through imposition of explicit “soft” or “hard” constraints on these variables in the model predictive control problem. The latter approach may be more suitable in applications where there is a need to achieve a roughness (slope) level that less than a maximum acceptable roughness (slope) level.

4.5 Conclusions

In this chapter, a multivariable model predictive controller was developed that simultaneously regulates both thin-film surface roughness and mean slope to optimize film light reflectance and transmittance during thin-film manufacturing. The dynamics of the evolution of the thin-film surface height profile were assumed to be described by an EW-type equation in two spatial dimensions. Analytical solutions of the expected

surface roughness and surface slope were obtained on the basis of the EW equation and were used in the design of model predictive controller that manipulates the substrate temperature and deposition rate. The model predictive controller involves constraints on the magnitude and rate of change of the control action and optimizes a cost function that involves penalty on both surface roughness and mean slope from the set-point values. The controller, which was applied to the two-dimensional Edwards–Wilkinson equation, successfully regulates both surface roughness and mean slope to set-point values at the end of the batch operation that yield desired film reflectance and transmittance.

Chapter 5

Control of Aggregate Surface

Morphology Using a Patterned

Deposition Rate Profile

5.1 Introduction

This chapter focuses on modeling and control of aggregate thin film surface morphology for improved light trapping using a patterned deposition rate profile. The dynamics of the evolution of the thin film surface height profile are modeled by an Edwards-Wilkinson-type equation (a second-order stochastic partial differential equation) in two spatial dimensions. It is first established that the use of a spatially uniform deposition rate profile cannot generate significant thin film surface roughness

and slope at large length scales (comparable to visible light wavelength), necessitating the use of a sine-wave-patterned deposition rate profile in space. The thin film surface morphology is described in terms of aggregate surface roughness and surface slope, computed with respect to appropriate visible light-relevant characteristic length scales and defined as the root-mean-squares of an aggregate surface height profile and of an aggregate surface slope profile, respectively. Using analytical solutions of the expected aggregate surface roughness and surface slope, the functional dependence of the Edwards-Wilkinson equation model parameters on the deposition rate is computed and used within a predictive control framework to predict the influence of the control action on the surface roughness and slope at the end of the growth process. The controller is applied to the two-dimensional Edwards-Wilkinson equation representing an $8,000 \text{ nm} \times 8,000 \text{ nm}$ spatial domain and using a sine-wave-patterned deposition rate profile in space, and it is shown to successfully regulate aggregate surface roughness and slope at the end of the deposition at levels that yield desired thin film reflectance and transmittance levels.

5.2 Aggregate surface morphology

5.2.1 Process description and modeling

In this work, the thin film deposition process is modeled by an on-lattice kinetic Monte Carlo model. Details of the model can be found in previous work of our group [31].

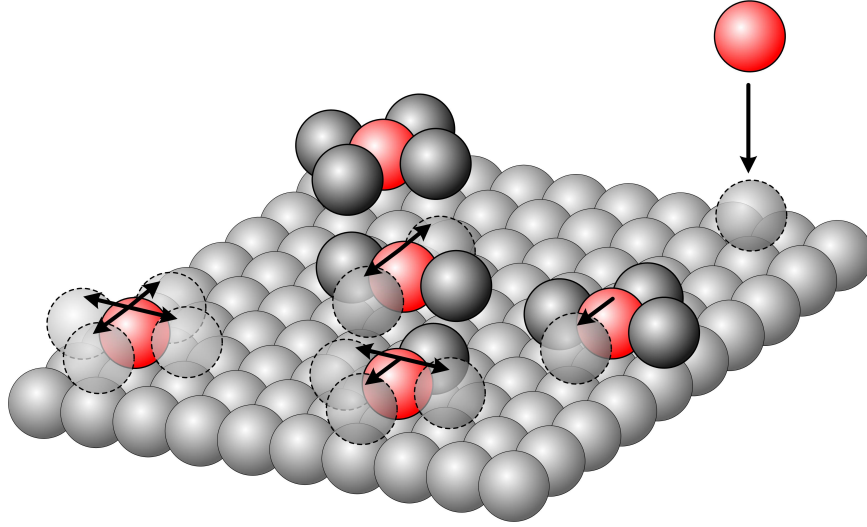


Figure 5.1: Thin film deposition process on a 2D square lattice.

The two dimensional square lattice where the deposition process takes place is shown in Figure 5.1. Periodic boundary conditions (PBCs) are applied in the directions perpendicular to the growth direction. Two different types of micro-processes are considered: an adsorption process and a migration process. In the adsorption process, incident particles are incorporated onto the thin film. The incidence direction in the adsorption process is restricted to be the vertical direction. The rate of adsorption is proportional to the average deposition rate across the simulation domain. The site in which a particle is deposited is randomly selected from all lattice sites with equal probability. During the migration process, particles on the thin film surface hop against appropriate energy barriers and move to their vacant neighboring sites. The migration rate follows an Arrhenius-type law and depends on the local particle micro-configuration (i.e., number of nearest neighboring particles). The substrate

temperature is fixed at 460 K. The lattice is initialized with a fully-packed and fixed substrate. A continuous-time Monte Carlo (CTMC)-type algorithm (e.g., [71]) is used to carry out the simulations.

5.2.2 Aggregate surface roughness and slope

Thin film surface morphology can be characterized by roughness and slope. Roughness is defined as the root-mean-square (RMS) of the surface height profile

$$\begin{aligned}
 r(t) &= \sqrt{\frac{1}{L^2} \int_0^L \int_0^L (h(x, y, t) - \bar{h}(t))^2 dx dy} \\
 &\approx \sqrt{\frac{1}{l^2} \sum_{i=0}^{l-1} \sum_{j=0}^{l-1} (h(i, j, t) - \bar{h})^2}
 \end{aligned} \tag{5.1}$$

where $h(i, j, t)$ is the surface height measurement at the (i, j) lattice site at time t , \bar{h} denotes the average surface height, L is the dimension of the simulation domain, l is the number of discrete height measurements on x or y direction. Slope is defined as the root-mean-square of the gradient of the surface height in x direction

$$\begin{aligned}
 m(t) &= \sqrt{\frac{1}{L^2} \int_0^L \int_0^L \left(\frac{\partial h}{\partial x}(x, y, t) \right)^2 dx dy} \\
 &\approx \sqrt{\frac{1}{L^2} \sum_{i=0}^{l-1} \sum_{j=0}^{l-1} \left(\frac{h(i+1, j, t) - h(i, j, t)}{\Delta x} \right)^2 \frac{L^2}{l^2}} \\
 &= \sqrt{\frac{1}{L^2} \sum_{i=0}^{l-1} \sum_{j=0}^{l-1} (h(i+1, j, t) - h(i, j, t))^2}.
 \end{aligned} \tag{5.2}$$

Roughness and slope can be defined at different length scales. The top subplot in Figure 5.2 shows a one-dimensional (1D) surface with roughness at different length scales. In order to characterize surface morphology at different length scales, an

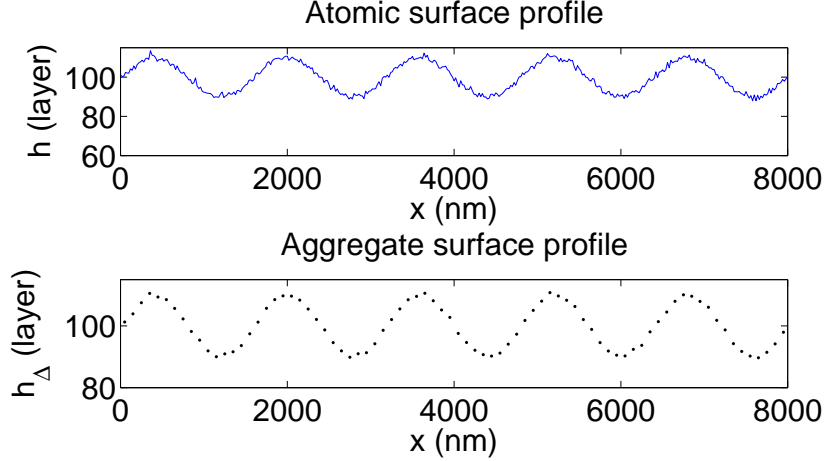


Figure 5.2: 1D surface with roughness at different length scales: atomic surface profile (top plot) and aggregate surface profile (bottom plot).

aggregate surface height profile $h_{\Delta}(i, j)$ is introduced in this work. The aggregate surface height profile is the averaged height over an interval of length Δ in 1D and a square of side Δ in 2D. In the 2D case, the aggregate surface height takes the form

$$h_{\Delta}(i, j) = \frac{\sum_{i_a=0}^{\Delta-1} \sum_{j_a=0}^{\Delta-1} h(i\Delta + i_a, j\Delta + j_a)}{\Delta^2}, \quad i, j = 0, 1, 2, \dots, l_{\Delta} - 1. \quad (5.3)$$

where l_{Δ} is the number of points on the discrete aggregate surface height profile.

Then the aggregate surface roughness, r_{Δ} , and the aggregate surface slope, m_{Δ} , can

be defined based on the aggregate surface height profile as follows

$$r_{\Delta}(t) = \sqrt{\frac{1}{l_{\Delta}^2} \sum_{i=0}^{l_{\Delta}-1} \sum_{j=0}^{l_{\Delta}-1} (h_{\Delta}(i, j, t) - \bar{h}_{\Delta}(t))^2}, \quad (5.4)$$

$$m_{\Delta}(t) = \sqrt{\frac{1}{L^2} \sum_{i=0}^{l_{\Delta}-1} \sum_{j=0}^{l_{\Delta}-1} (h_{\Delta}(i+1, j, t) - h_{\Delta}(i, j, t))^2}. \quad (5.5)$$

Remark 5.1 *Figure 5.2 shows an example of an atomic surface profile and of an aggregate surface profile. We note that in general the surface morphology, including roughness and slope, depends on lattice size and this dependence has been explored in other works of our group (the reader may refer to [25, 31, 33]).*

5.2.3 Light reflection on a rough surface

For thin-film solar cells, the energy conversion efficiency is directly related to the light trapping/scattering properties of the thin film interfaces and surfaces, that depend on the surface roughness and slope. It should be pointed out that the wavelength of visible light (380 nm-750 nm) is several orders of magnitude greater than the distance between two neighboring atoms (≈ 0.2 nm). The light reflection depends on roughness and slope defined at a length scale comparable to the light wavelength.

When incident light goes through a rough interface, it is divided into four components: specular reflection, specular transmission, diffused reflection and diffused transmission [66, 40]. If a rough thin film surface is illuminated with a beam of monochromatic light at normal incidence, the total reflectance, R , can be approxi-

mated as follows [14]

$$\begin{aligned}
 R = R_0 \exp \left[-\frac{4\pi r_{\Delta}^2}{\lambda^2} \right] \\
 + R_0 \int_0^{\pi/2} 2\pi^4 \left(\frac{a_{\Delta}}{\lambda} \right)^2 \left(\frac{r_{\Delta}}{\lambda} \right)^2 (\cos \theta + 1)^4 \sin \theta \exp \left[-\frac{(\pi a_{\Delta} \sin \theta)^2}{\lambda^2} \right] d\theta
 \end{aligned} \tag{5.6}$$

where R_0 is the reflection of a perfectly smooth surface, r_{Δ} is the aggregate surface roughness, θ is the reflectance angle, λ is the light wavelength and a_{Δ} is the autocovariance length of the surface. It can be proved that $a_{\Delta} = \sqrt{2}r_{\Delta}/m_{\Delta}$, where m_{Δ} is the slope of the aggregate profile of the surface [9]. The numerical integration result of eq (5.6) is shown in Figure 5.3 using $\lambda = 700$ nm. Both r_{Δ} and m_{Δ} strongly influence the intensity of light reflection (and therefore, light transmission) of the surface/interface. Thus, it is important to regulate r_{Δ} and m_{Δ} of the surfaces/interfaces of the thin-film solar cells to appropriate values that optimize light reflection and transmission during thin film manufacturing.

5.2.4 Patterned deposition rate profile

Figure 5.4 shows the variation of roughness and slope as a function of aggregation length for a deposition process with uniform deposition rate profile. The results are from a kinetic Monte-Carlo simulation of the two-dimensional thin film deposition process of Figure 5.1 with $l = 200$. Both aggregate roughness and slope decrease as aggregation length increases. In this case, the surface roughness is due to atomic level fluctuations and thus we conclude that atomic level fluctuations contribute mainly to

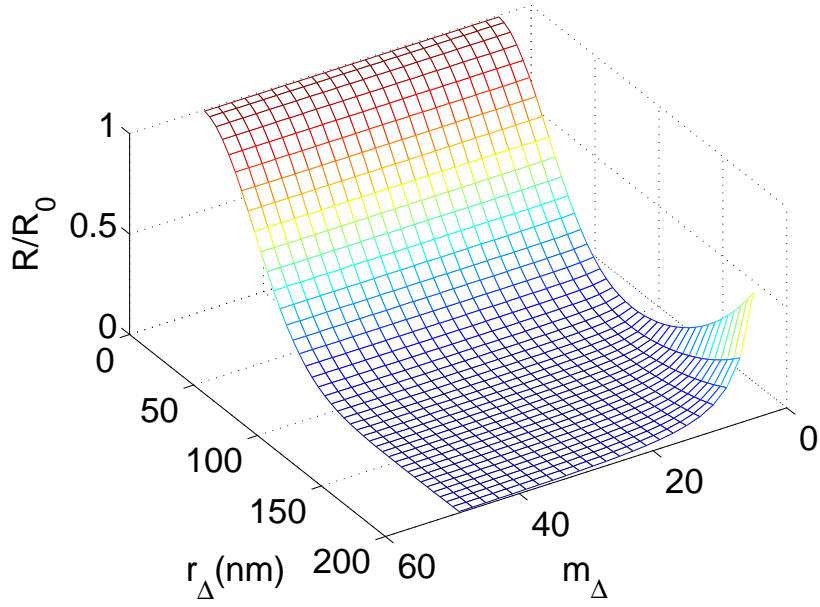


Figure 5.3: Reflection as a function of r_Δ and m_Δ of thin film surface.

roughness and slope at small length scales.

In order to generate significant roughness and slope at large length scales (i.e., comparable to the wave length of visible light), we introduce a patterned deposition rate profile of the following form

$$w(x, y, t) = w_0(t) + A(t) \sin\left(\frac{2k\pi}{L}x\right), \quad (5.7)$$

where w_0 is the mean deposition rate across the simulation domain, A is the magnitude of the sine wave, k is the number of complete periods of the sine wave within the simulation domain, and L is the length of the simulation domain.

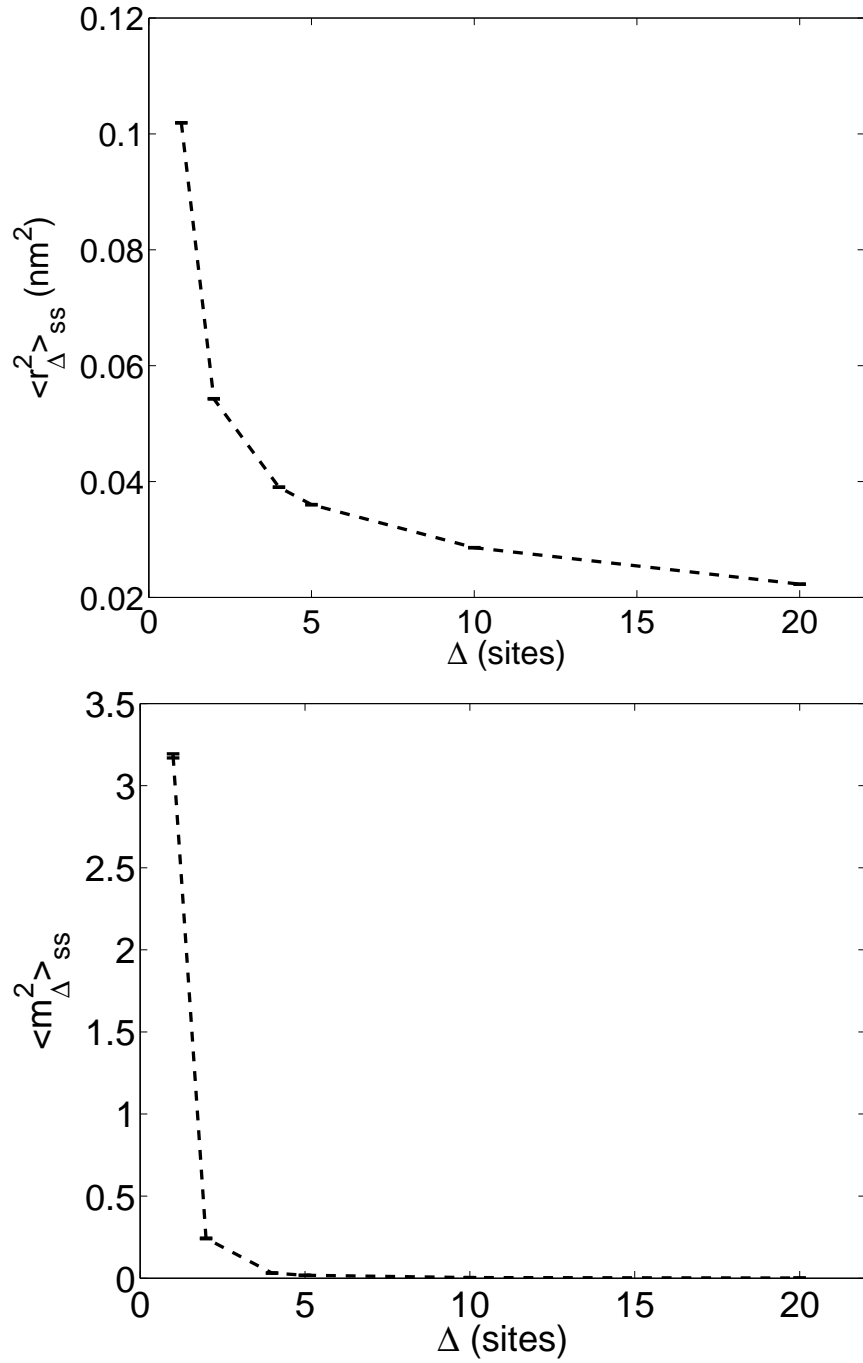


Figure 5.4: Dependence of the steady state values of aggregate roughness (top plot) and aggregate slope (bottom plot) on aggregation length.

5.2.5 Edwards-Wilkinson equation for surface height dynamics

To design a feedback controller for the thin film deposition process, a closed-form model is needed. The Edwards-Wilkinson (EW) equation, which is a second-order stochastic partial differential equation (PDE), describes adequately the dynamics of the evolution of the surface height profile in many thin film growth processes that involve a thermal balance between atom adsorption and surface migration [18, 19, 25, 33]. In this chapter, we consider a two dimensional (2D) EW type equation similar to the one used in Chapter 4 but under a patterned input profile.

$$\frac{\partial h_{\Delta}}{\partial t} = w(x, y, t) + c_2 \left(\frac{\partial^2 h_{\Delta}}{\partial x^2} + \frac{\partial^2 h_{\Delta}}{\partial y^2} \right) + \xi(x, y, t) \quad (5.8)$$

where $x \in [0, L]$, $y \in [0, L]$ are the spatial coordinates, t is the time, $h_{\Delta}(x, y, t)$ is the aggregate surface height, and $\xi(x, y, t)$ is a Gaussian white noise with zero mean and covariance

$$\langle \xi(x, y, t) \xi(x', y', t') \rangle = \sigma^2 \delta(x - x') \delta(y - y') \delta(t - t'). \quad (5.9)$$

where $\delta(\cdot)$ denotes the Dirac delta function, $w(x, y, t)$ is the patterned deposition rate profile described in eq (5.7), and c_2 and σ^2 are model parameters that depend on the mean deposition rate, w_0 . The stochastic PDE of eq (5.8) is subject to the following

periodic boundary conditions

$$h_{\Delta}(0, y, t) = h_{\Delta}(L, y, t) \quad h_{\Delta}(x, 0, t) = h_{\Delta}(x, L, t) \quad (5.10)$$

$$\frac{\partial h_{\Delta}}{\partial x}(0, y, t) = \frac{\partial h_{\Delta}}{\partial x}(L, y, t) \quad \frac{\partial h_{\Delta}}{\partial y}(x, 0, t) = \frac{\partial h_{\Delta}}{\partial y}(x, L, t) \quad (5.11)$$

and the initial condition

$$h_{\Delta}(x, y, 0) = h_{0\Delta}(x, y). \quad (5.12)$$

To analyze the dynamics and obtain a finite-dimensional approximation of the EW equation, we first consider the eigenvalue problem of the linear operator of eq (5.8) subject to the periodic boundary conditions of eqs (5.10)-(5.11)

$$\mathcal{A}\phi_{n_x, n_y}(x, y) = c_2\left(\frac{\partial^2}{\partial x^2} + \frac{\partial^2}{\partial y^2}\right)\phi_{n_x, n_y}(x, y) = \lambda_{n_x, n_y}\phi_{n_x, n_y}(x, y), \quad (5.13)$$

$$\nabla^j \phi_{n_x, n_y}(0, y) = \nabla^j \phi_{n_x, n_y}(L, y), \quad j = 0, 1 \quad (5.14)$$

$$\nabla^j \phi_{n_x, n_y}(x, 0) = \nabla^j \phi_{n_x, n_y}(x, L), \quad j = 0, 1 \quad (5.15)$$

where λ_{n_x, n_y} denotes an eigenvalue, ϕ_{n_x, n_y} denotes an eigenfunction, and ∇^j , $j = 0, 1$, denotes the value and gradient of a given function, respectively. The solution of

the eigenvalue problem is as follows

$$\lambda_{n_x, n_y} = -\frac{4c_2\pi^2}{L^2}(n_x^2 + n_y^2) \quad (5.16)$$

$$\phi_{1, n_x, n_y} = \frac{2}{L} \sin\left(\frac{2n_x\pi}{L}x\right) \sin\left(\frac{2n_y\pi}{L}y\right) \quad (5.17)$$

$$\phi_{2, n_x, n_y} = \begin{cases} \frac{1}{L} & n_x = 0 \text{ and } n_y = 0 \\ \frac{2}{L} \cos\left(\frac{2n_x\pi}{L}x\right) \cos\left(\frac{2n_y\pi}{L}y\right) & n_x \neq 0 \text{ and } n_y \neq 0 \\ \frac{\sqrt{2}}{L} \cos\left(\frac{2n_x\pi}{L}x\right) \cos\left(\frac{2n_y\pi}{L}y\right) & \text{otherwise} \end{cases} \quad (5.18)$$

$$\phi_{3, n_x, n_y} = \begin{cases} 0 & n_x = 0 \\ \frac{2}{L} \sin\left(\frac{2n_x\pi}{L}x\right) \cos\left(\frac{2n_y\pi}{L}y\right) & n_x \neq 0, n_y \neq 0 \\ \frac{\sqrt{2}}{L} \sin\left(\frac{2n_x\pi}{L}x\right) & n_x \neq 0, n_y = 0 \end{cases} \quad (5.19)$$

$$\phi_{4, n_x, n_y} = \begin{cases} 0 & n_y = 0 \\ \frac{2}{L} \cos\left(\frac{2n_x\pi}{L}x\right) \sin\left(\frac{2n_y\pi}{L}y\right) & n_y \neq 0, n_x \neq 0 \\ \frac{\sqrt{2}}{L} \sin\left(\frac{2n_y\pi}{L}y\right) & n_y \neq 0, n_x = 0. \end{cases} \quad (5.20)$$

The solution of the EW equation of eq (5.8) can be expanded in an infinite series in terms of the eigenfunctions of the operator of eq (5.13) as follows

$$h_{\Delta}(x, y, t) = \sum_{n_x=0}^{+\infty} \sum_{n_y=0}^{+\infty} \sum_{p=1}^4 \phi_{p, n_x, n_y}(x, y) z_{p, n_x, n_y}(t), \quad (5.21)$$

where $z_{p, n_x, n_y}(t)$, $p = 1, 2, 3, 4$, are time-varying coefficients.

Substituting the above expansion of $h_{\Delta}(x, y, t)$ into eq (5.8) and taking the inner product with the adjoint eigenfunctions, the following system of infinite stochastic

linear ordinary differential equations (ODEs) for the temporal evolution of the time-varying coefficients is obtained

$$\frac{dz_{2,0,0}}{dt} = w_{2,0,0} + \xi_{2,0,0}(t), \quad (5.22)$$

$$\frac{dz_{p,n_x,n_y}}{dt} = w_{p,n_x,n_y} + \lambda_{n_x,n_y} z_{p,n_x,n_y} + \xi_{p,n_x,n_y}(t) \quad (5.23)$$

$$p = 1, 2, 3, 4, \quad n_x, n_y = 0, 1, \dots, \infty, \quad n_x^2 + n_y^2 \neq 0,$$

where $\xi_{p,n_x,n_y}(t) = \int_0^L \int_0^L \xi(x, y, t) \phi_{p,n_x,n_y}(x, y) dx dy$ is the projection of the noise $\xi(x, y, t)$ on the ODE for z_{p,n_x,n_y} . The noise term, ξ_{p,n_x,n_y} , has zero mean and covariance

$$\langle \xi_{p,n_x,n_y}(t) \xi_{p,n_x,n_y}(t') \rangle = \sigma^2 \delta(t - t'). \quad (5.24)$$

Similarly, w_{p,n_x,n_y} is the projection of w on the ODE for z_{p,n_x,n_y} ,

$$w_{p,n_x,n_y} = \int_0^L \int_0^L \phi_{p,n_x,n_y}(x, y) w(x, y) dx dy \quad (5.25)$$

$$w_{1,n_x,n_y} = 0 \quad (5.26)$$

$$w_{2,n_x,n_y} = \begin{cases} w_0 L + \frac{AL}{2k\pi} [1 - \cos(2k\pi)] & n_x = 0, n_y = 0 \\ \frac{\sqrt{2}ALk}{2\pi(n_x^2 - k^2)} [\cos(2k\pi) - 1] & n_x \neq 0, n_x \neq k, n_y = 0 \\ 0 & \text{otherwise} \end{cases} \quad (5.27)$$

$$w_{3,n_x,n_y} = \begin{cases} \frac{\sqrt{2}AL}{2} & n_x = k, n_y \neq 0 \\ \frac{\sqrt{2}ALn_x}{2\pi(k^2 - n_x^2)} \sin(2k\pi) & n_x \neq 0, n_x \neq k, n_y = 0 \\ 0 & \text{otherwise} \end{cases} \quad (5.28)$$

$$w_{4,n_x,n_y} = 0. \quad (5.29)$$

The temporal evolution of the variance of mode z_{p,n_x,n_y} can be obtained from the solution of the linear ODEs of eqs (5.22) and (5.23) as follows

$$\langle z_{2,0,0}(t) \rangle = w_{2,0,0}(t - t_0) \quad (5.30)$$

$$\text{var}(z_{2,0,0}(t)) = \sigma^2(t - t_0) \quad (5.31)$$

$$\langle z(t) \rangle = e^{\lambda(t-t_0)} \langle z(t_0) \rangle + \frac{w_p}{\lambda} (e^{\lambda(t-t_0)} - 1) \quad (5.32)$$

$$\text{var}(z(t)) = e^{2\lambda(t-t_0)} \text{var}(z(t_0)) + \sigma^2 \frac{e^{2\lambda(t-t_0)} - 1}{2\lambda} \quad (5.33)$$

where $z(t) = z_{p,n_x,n_y}(t)$ and $w_p = w_{p,n_x,n_y}$ for $n_x^2 + n_y^2 \neq 0$.

For feedback control purposes (see Section 5.3 below), the modes can be calculated from a surface height measurement as follows

$$z_{p,n_x,n_y}(t) = \int_0^L \int_0^L h_{\Delta}(x, y, t) \phi_{p,n_x,n_y}(x, y) dx dy. \quad (5.34)$$

In many circumstances, only discrete height profile point measurements are available,

thus eq (5.34) can be approximated by

$$z_{p,n_x,n_y}(t) \approx \left(\frac{L}{l_\Delta}\right)^2 \sum_{i=0}^{l_\Delta-1} \sum_{j=0}^{l_\Delta-1} h_\Delta(i, j, t) \phi_{p,n_x,n_y}(i, j) \quad (5.35)$$

where l_Δ is the number of spatial height sampling (measurement) points in $[0, L]$. It is worth pointing out that, when discrete height point measurements are available, the largest number of modes that can be accurately calculated is limited by the spatial sampling points, i.e. $n_x, n_y \leq l_\Delta/2$ [82].

Substituting eq (5.21) into eq (5.4), the expected value of r_Δ^2 can be rewritten in terms of the state covariance as follows

$$\langle r_\Delta^2 \rangle = \frac{1}{L^2} \sum_{\substack{n_x, n_y=0 \\ n_x^2+n_y^2 \neq 0}}^{\infty} \sum_{p=1}^4 \langle z_{p,n_x,n_y}^2 \rangle. \quad (5.36)$$

The expected RMS slope square can also be expressed in terms of the state covariance as follows

$$\langle m_\Delta^2 \rangle = \sum_{\substack{n_x, n_y=0 \\ n_x^2+n_y^2 \neq 0}}^{\infty} \sum_{p=1}^4 K_{p,n_x,n_y} \langle z_{p,n_x,n_y}^2 \rangle, \quad (5.37)$$

where K_{p,n_x,n_y} can be computed by

$$\begin{aligned} K_{p,n_x,n_y} &= \frac{1}{L^2} \sum_{i=0}^{l_\Delta-1} \sum_{j=0}^{l_\Delta-1} (\phi_{p,n_x,n_y}(i+1, j) - \phi_{p,n_x,n_y}(i, j))^2 \\ &= \frac{4l_\Delta^2}{L^4} \sin^2 \left(\frac{\pi n_x}{l_\Delta} \right). \end{aligned} \quad (5.38)$$

5.2.6 Determination of model parameters

The EW equation has two parameters, c_2 and σ^2 , that are assumed to depend on the mean deposition rate w_0 . In our previous work [81], the dependences of EW equation parameters on operating conditions were found by fitting the analytical solution of $\langle r^2 \rangle$ to open-loop kinetic Monte-Carlo simulations. However, this approach is not applicable here because a system with a much larger physical domain is simulated. Assuming that the distance between two neighboring sites is 0.2 nm, there are 40000×40000 sites within the $8000 \text{ nm} \times 8000 \text{ nm}$ square domain that is simulated. Since it is not possible to simulate such large lattice size directly, we use the following steps to get estimates of c_2 and σ^2 as functions of w_0 .

1. For each value of w_0 , a series of open-loop kinetic Monte Carlo simulations is carried out with increasing lattice size ($l = 20, 50, 100, 150, 200, 250$). The values of c_2 and σ^2 are then determined by fitting the analytical solution of $\langle r^2(t) \rangle$ (without any aggregation) to kMC simulation data using the least square method. As a result, c_2 and σ^2 are obtained in terms of lattice size l for each value of w_0 , as shown in Figure 5.5. The following functional forms are used for the fitting of c_2 and σ^2/c_2

$$c_2(l, w_0) = a_c(w_0)l + b_c(w_0) \quad (5.39)$$

$$\frac{\sigma^2}{c_2}(l, w_0) = a_s(w_0) \log_{10}(l) + b_s(w_0) \quad (5.40)$$

where the values of the coefficients $a_c(w_0)$, $b_c(w_0)$, $a_s(w_0)$ and $b_s(w_0)$ for different w_0 values are given in Table 5.1.

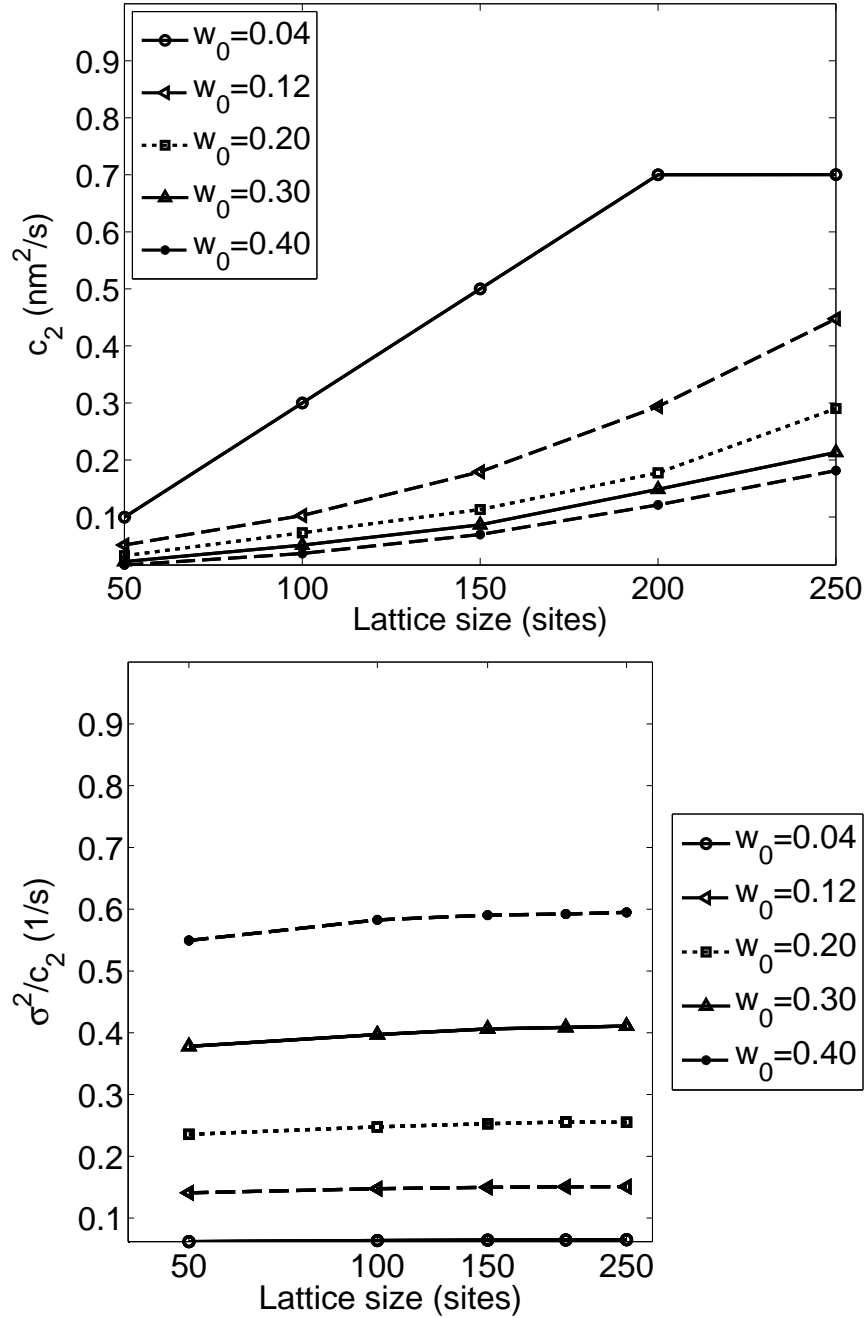


Figure 5.5: c_2 (top plot) and σ_2 (bottom plot) as functions of lattice size l

w_0	a_c	b_c	c_2	a_s	b_s	σ^2
0.04	3.20×10^{-3}	-3.04×10^{-2}	128.06	4.17×10^{-3}	5.50×10^{-2}	9.50
0.12	1.97×10^{-3}	-7.16×10^{-2}	78.67	1.43×10^{-2}	1.17×10^{-1}	14.43
0.20	1.24×10^{-3}	-4.34×10^{-2}	49.67	2.90×10^{-2}	1.87×10^{-1}	15.95
0.30	9.61×10^{-4}	-3.56×10^{-2}	38.42	4.71×10^{-2}	3.00×10^{-1}	19.84
0.40	8.33×10^{-4}	-3.63×10^{-2}	33.28	6.29×10^{-2}	4.48×10^{-1}	24.54

Table 5.1: Values of the coefficients used in eqs. (5.39), (5.40) and the extrapolated values of c_2 and σ^2 for lattice size $l = 40000$.

2. The values of c_2 and σ^2 at lattice size $l = 40000$ are determined by extrapolating the c_2 and σ^2 according to eq. (5.39) and (5.40). The extrapolated values $c_2(l = 40000, w_0)$ and $\sigma^2(l = 40000, w_0)$ are also included in Table 5.1.
3. Subsequently, we fit the extrapolated values of c_2 and σ^2 for $l = 40000$ as functions of w_0 , as shown in Figure 5.6. The following functional forms for $c_2(w_0)$ and $\sigma^2(w_0)$ are used

$$c_2(w_0) = p_{c1}w_0^3 + p_{c2}w_0^2 + p_{c3}w_0 + p_{c4} \quad (5.41)$$

$$\sigma^2(w_0) = p_{s1}w_0^4 + p_{s2}w_0^3 + p_{s3}w_0^2 + p_{s4}w_0 + p_{s5} \quad (5.42)$$

where

$$p_{c1} = -20.83 \quad p_{c2} = 110.9 \quad p_{c3} = -204.1 \quad p_{c4} = 164.9 \quad (5.43)$$

$$p_{s1} = -7.585 \quad p_{s2} = 36.65 \quad p_{s3} = -59.03 \quad (5.44)$$

$$p_{s4} = 42.91 \quad p_{s5} = 2.998.$$

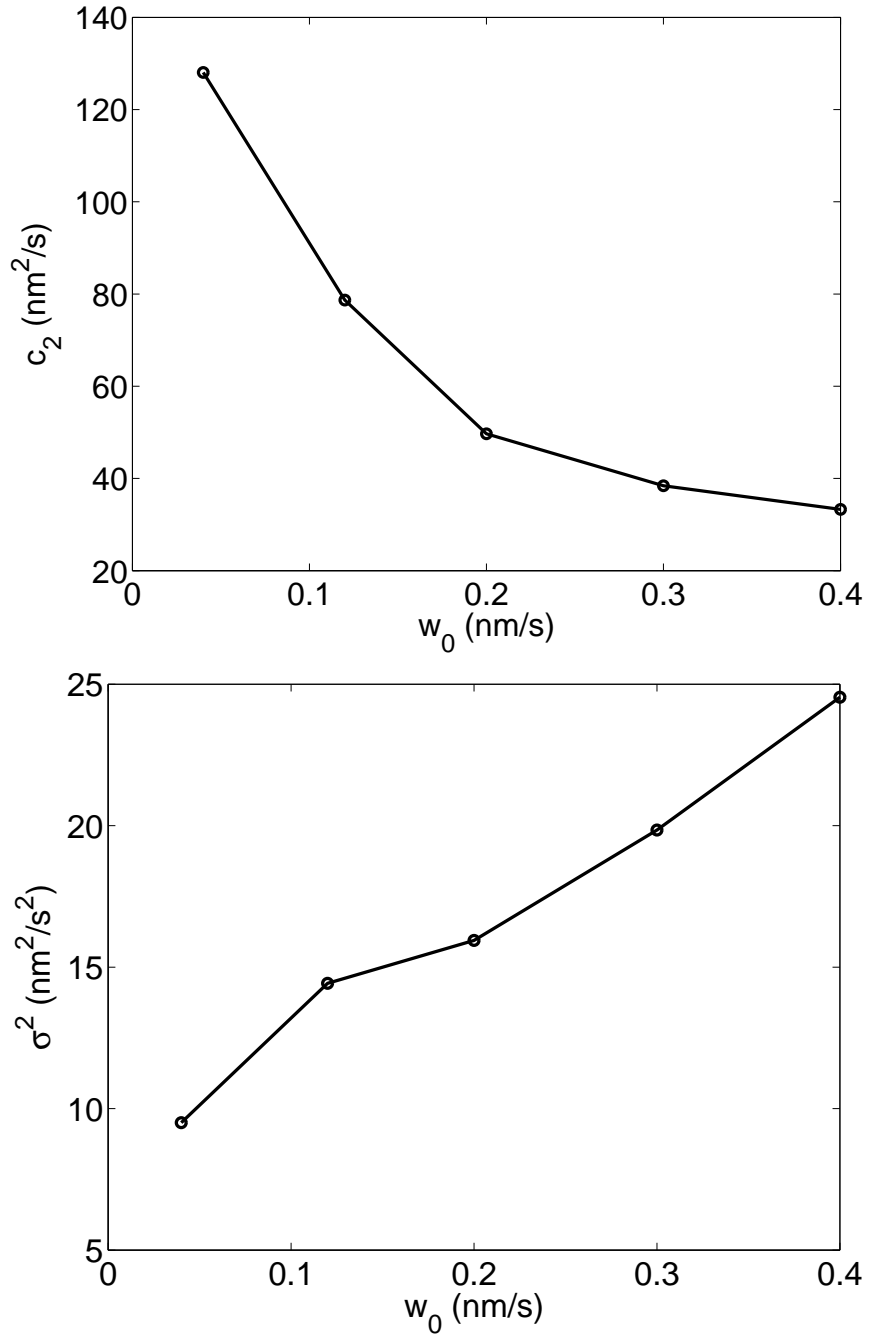


Figure 5.6: c_2 (top plot) and σ_2 (bottom plot) as functions of deposition rate w_0 .

To verify the above approach, we compare the roughness obtained from the extrapolated values of c_2 and σ^2 with that from direct extrapolation of $\langle r^2 \rangle$. First, $\langle r^2 \rangle$

is extrapolated with respect to lattice size and its value at $l = 40000$ is obtained.

Figure 5.7 shows the steady state value of $\langle r^2 \rangle$ against lattice size. According to

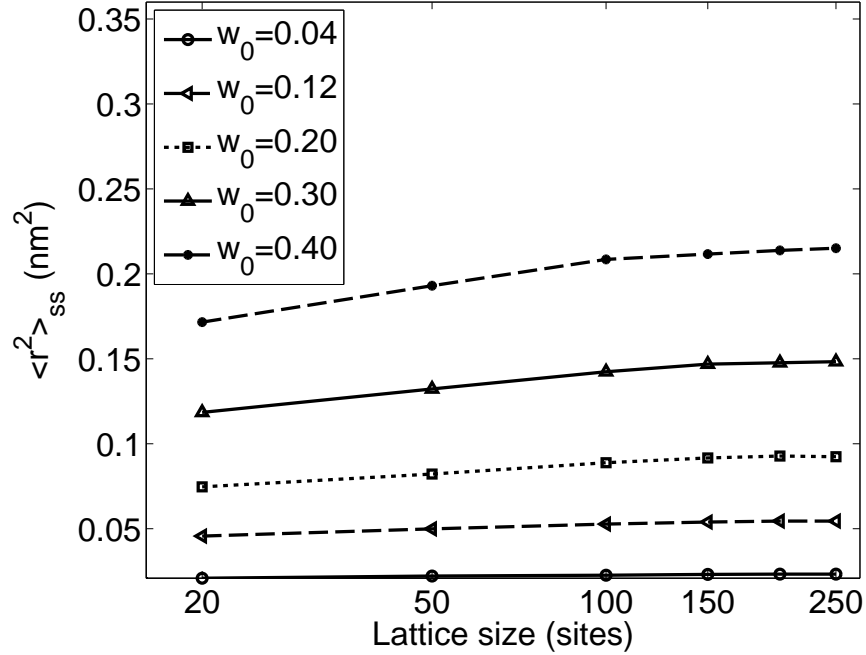


Figure 5.7: Steady state value of roughness $\langle r^2 \rangle$ as a function of lattice size l .

Figure 5.7, $\langle r^2 \rangle$ can be fitted to a linear function of $\log_{10}(l)$ of the form

$$\langle r^2 \rangle_{ss}(l) = a_r \log_{10}(l) + b_r. \quad (5.45)$$

Then the relationship between steady state roughness and aggregation length, as shown in Figure 5.8, is used to find the roughness with aggregation length $\Delta = 400$.

$\langle r^2 \rangle(\Delta)$ is fitted to a power-law function of the form

$$\langle r^2 \rangle(\Delta) = a_a \Delta^{b_a} + c_a \quad (5.46)$$

w_0	a_r	b_r	Roughness	Aggregate roughness
			$\langle r^2 \rangle_{ss} \text{ (nm}^2\text{)}$	$\langle r_{\Delta}^2 \rangle_{ss} \text{ (nm}^2\text{)}$
0.04	0.002143	0.018237	0.0281	6.25×10^{-3}
0.12	0.008171	0.035585	0.0732	1.63×10^{-2}
0.20	0.016950	0.053243	0.1313	2.92×10^{-2}
0.30	0.027590	0.084274	0.2112	4.70×10^{-2}
0.40	0.039788	0.123212	0.3063	6.81×10^{-2}

Table 5.2: Extrapolated aggregate roughness when lattice size $l = 40000$, aggregation length $\Delta = 400$, under different deposition rates.

where $a_a = 0.07883$, $b_a = -1.193$ and $c_a = 0.02247$. According to eq. (5.46),

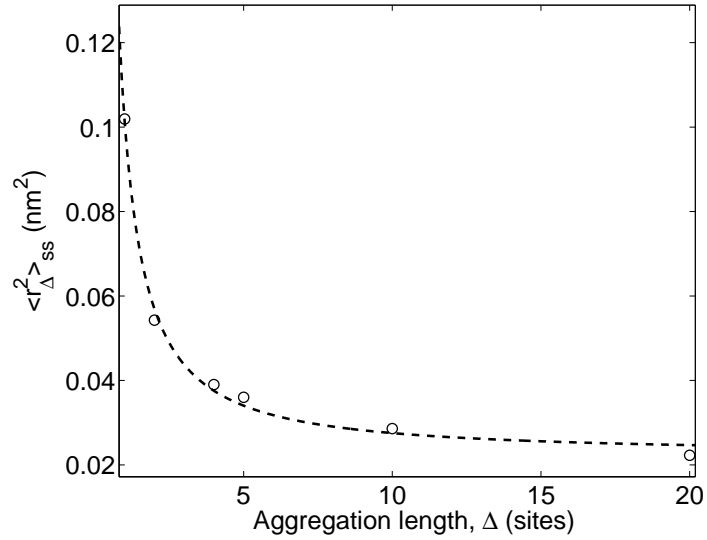


Figure 5.8: $\langle r_{\Delta}^2 \rangle$ as a function of aggregation length Δ (lattice size $l = 500$).

$\langle r_{\Delta}^2 \rangle(\Delta = 400) = 0.2224 \langle r_{\Delta}^2 \rangle(\Delta = 1)$, thus the aggregate roughness for lattice size $l = 40000$ and aggregation length $\Delta = 400$ can be calculated. The results are summarized in Table 5.2.

w_0	σ^2/c_2	$\langle r^2 \rangle_{ss}$ (nm ²)	$\langle r_{\Delta}^2 \rangle_{ss}$ (nm ²)
0.04	0.074187	0.0323	7.18×10^{-3}
0.12	0.183404	0.0800	1.78×10^{-2}
0.20	0.321012	0.1399	3.11×10^{-2}
0.30	0.516476	0.2551	5.67×10^{-2}
0.40	0.737238	0.3214	7.15×10^{-2}

Table 5.3: Calculation of atomic and aggregate steady state surface roughness at lattice size $l = 40000$ using extrapolated values of σ^2/c_2 .

Subsequently, we use the extrapolated values of σ^2/c_2 to calculate the atomic and aggregate steady state surface roughness. According to eq (5.36), the steady state roughness of a deposition process starting from a flat surface would be

$$\begin{aligned}
\langle r_{\Delta}^2 \rangle_{ss} &= \frac{1}{L^2} \sum_{\substack{n_x, n_y=0 \\ n_x^2+n_y^2 \neq 0}}^{\infty} \sum_{p=1}^4 \langle z_{p, n_x, n_y}^2 \rangle = \frac{1}{L^2} \sum_{\substack{n_x, n_y=0 \\ n_x^2+n_y^2 \neq 0}}^{\infty} \sum_{p=1}^4 \text{var}(z_{p, n_x, n_y}) \\
&= \frac{\sigma^2}{c_2 L^2} \sum_{\substack{n_x, n_y=0 \\ n_x^2+n_y^2 \neq 0}}^{\infty} \frac{L^2}{2\pi^2(n_x^2 + n_y^2)} = \frac{\sigma^2}{c_2} \sum_{\substack{n_x, n_y=0 \\ n_x^2+n_y^2 \neq 0}}^{\infty} \frac{1}{2\pi^2(n_x^2 + n_y^2)} \approx 0.4353 \frac{\sigma^2}{c_2}.
\end{aligned} \tag{5.47}$$

The results are shown in Table 5.3.

Comparing Tables 5.2 and 5.3, we can see that both approaches yield very close values for both atomic and aggregate surface roughness for $l = 40000$.

Remark 5.2 *This is the first time the above parameter identification method is proposed. This method could be used for parameter identification for other nonlinear SPDE models, e.g. Kuramoto-Sivashinsky equation (KSE), that describe surface evolution in other thin film growth models.*

5.3 Model predictive controller design

In this section, a model predictive controller is developed based on the dynamic model of the expected roughness square and slope square. The mean deposition rate, w_0 , and magnitude of sine wave, A , are used as the manipulated variables. In this work, state feedback is used. At each sampling time, the surface height profile from the stochastic PDE is fed-back to the controller and the eigenmodes are calculated. In practice, real-time surface height measurements can be obtained via atomic force microscopy (AFM) systems. The control objective is to minimize the deviation of the expected roughness square and slope square from desired set-point values. Because the thin film deposition process is a batch process, the interval between current time and the end of the batch run is used as the prediction horizon. During each predictive controller evaluation, the manipulated variable is assumed to stay fixed until the end of the batch. The constraints of the problem are: (1) the mean deposition rate has lower and upper limits; (2) the rate of change of the mean deposition rate should be less than an upper limit due to actuator limitations; (3) the magnitude of sine wave should be positive and smaller than the average deposition rate. The resulting MPC formulation is as follows

$$\min_{w_0, A} f(w_0, A) = q_{r^2} \left(\frac{r_{\text{set}}^2 - \langle r_{\Delta}^2(t_f) \rangle}{r_{\text{set}}^2} \right)^2 + q_{m^2} \left(\frac{m_{\text{set}}^2 - \langle m_{\Delta}^2(t_f) \rangle}{m_{\text{set}}^2} \right)^2 \quad (5.48)$$

where

$$\langle r_{\Delta}^2(t_f) \rangle = \frac{1}{L^2} \sum_{\substack{n_x, n_y=0 \\ n_x^2 + n_y^2 \neq 0}}^{\infty} \sum_{p=1}^4 \langle z_{p, n_x, n_y}^2(t_f) \rangle \quad (5.49)$$

$$\langle m_{\Delta}^2(t_f) \rangle = \sum_{\substack{n_x, n_y=0 \\ n_x^2 + n_y^2 \neq 0}} \sum_{p=1}^4 \left(K_{p, n_x, n_y} \langle z_{p, n_x, n_y}^2(t_f) \rangle \right) \quad (5.50)$$

$$\langle z_{p, n_x, n_y}^2(t_f) \rangle = \text{var}(z_{p, n_x, n_y}(t_f)) + \langle z_{p, n_x, n_y}(t_f) \rangle^2 \quad (5.51)$$

$$\langle z_{p, n_x, n_y}(t_f) \rangle = e^{\lambda_{n_x, n_y}(t_f - t)} \langle z_{p, n_x, n_y}(t) \rangle + \frac{w_p}{\lambda_{n_x, n_y}} (e^{\lambda_{n_x, n_y}(t_f - t)} - 1) \quad (5.52)$$

$$\text{var}(z_{p, n_x, n_y}(t_f)) = e^{2\lambda_{n_x, n_y}(t_f - t)} \text{var}(z_{p, n_x, n_y}(t)) + \sigma^2 \frac{e^{2\lambda_{n_x, n_y}(t_f - t)} - 1}{2\lambda_{n_x, n_y}} \quad (5.53)$$

$$\lambda_{n_x, n_y} = -\frac{4c_2\pi^2}{L^2} (n_x^2 + n_y^2), \quad n_x^2 + n_y^2 \neq 0 \quad (5.54)$$

Subject to

$$w_{min} \leq w_0 \leq w_{max}, \quad |w_0(t) - w_0(t - dt)| \leq \Delta w_{max}, \quad (5.55)$$

$$0 \leq A \leq w_0 \quad (5.56)$$

where t_f is the final time of the batch run, r_{set}^2 and m_{set}^2 are the respective set-points for the surface roughness square and the mean slope square, q_{r^2} and q_{m^2} are the weighting factors for the deviations of $\langle r_{\Delta}^2(t_f) \rangle$ and $\langle m_{\Delta}^2(t_f) \rangle$ from their respective set-points, r_{set}^2 and m_{set}^2 , dt is the time interval between two successive sampling times, w_{min} and w_{max} are the lower and upper bounds on the mean deposition rate,

respectively, and Δw_{max} is the limit on the rate of change of the mean deposition rate.

The optimization problem is solved at each sampling time once a new measurement of the surface height profile becomes available. An interior point method optimizer, IPOPT [75], is used to solve the optimization problem in the MPC formulation.

5.4 Closed-loop simulations

In this section, the model predictive controller of eq (5.48) is applied to the two-dimensional EW equation model of eq (5.8). The deposition rate varies from 0.02 nm/s to 0.4 nm/s, the substrate temperature is fixed at 460 K and the initial deposition rate is 0.2 nm/s. The maximum rate of change of the deposition is $\Delta W_{max} = 0.1$ nm/s and the sampling time is 1 s. Each closed-loop simulation lasts for 100 s. Expected values are calculated from 100 independent closed-loop system simulation runs.

5.4.1 Control of film surface roughness

First, the problem of regulating film surface roughness is considered. In this scenario, the cost function only contains penalty on the deviation of the expected surface roughness square from the set-point. The weighting factors are $q_{r^2} = 1$ and $q_{m^2} = 0$. The set-point is $r_{set}^2 = 0.04 \text{ nm}^2$. Because the roughness set-point is small, the surface

does not have a clear pattern.

Figure 5.9 shows the profile of $\langle r_{\Delta}^2 \rangle$ under the model predictive controller of eq (5.48). It can be seen that the controller drives the expected film roughness to the desired value at the end of the simulation. Figure 5.10 shows a surface snapshot at the end of the simulation ($t = 100$ s) from one single run.

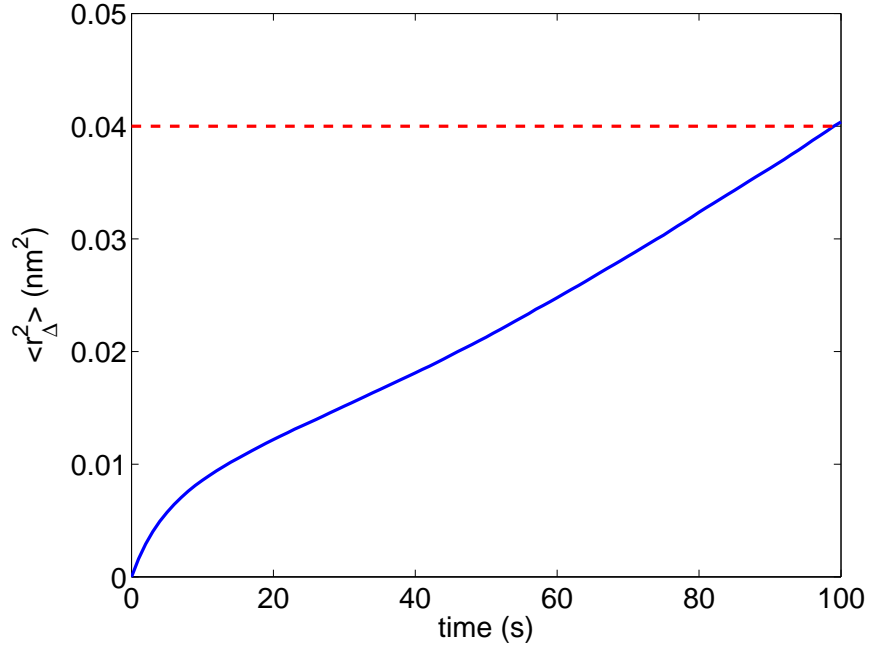


Figure 5.9: Profile of expected film surface roughness square from 100 closed-loop simulations. $q_{r^2} = 1$, $q_{m^2} = 0$ and $r_{set}^2 = 0.04 \text{ nm}^2$.

5.4.2 Control of film surface slope

Next, we consider the regulation of thin film surface slope. The cost function includes only penalty on the deviation of the expected value of slope square from the set point by choosing weighting factors $q_{r^2} = 0$ and $q_{m^2} = 1$. The set point is $m_{set}^2 = 0.025$.

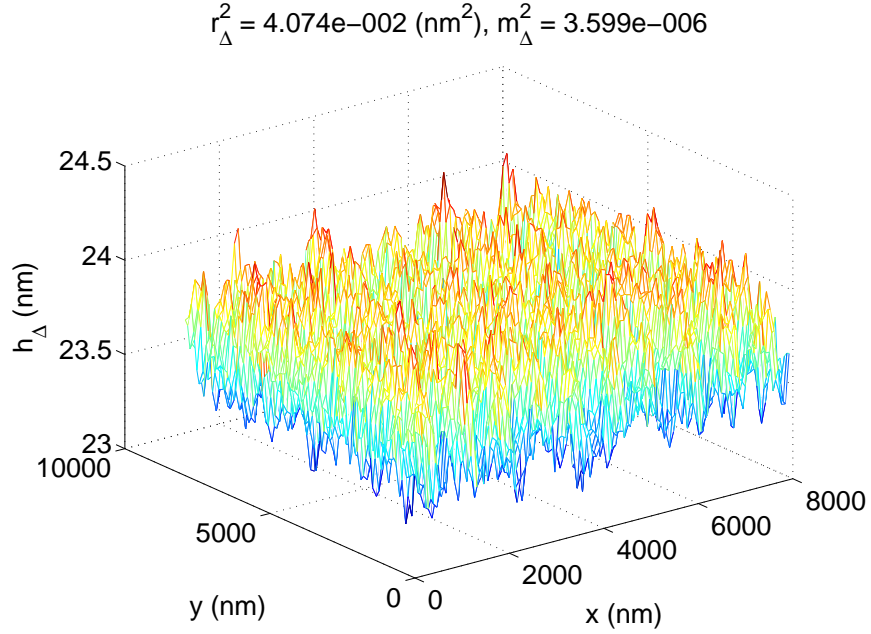


Figure 5.10: Surface profile at the end of simulation, $t = 100$ s. $q_{r^2} = 1$, $q_{m^2} = 0$ and $r_{set}^2 = 0.04 \text{ nm}^2$.

Figure 5.11 shows the profile of the expected slope square. The slope reaches its set point at $t = 100$ s. A surface snapshot at $t = 100$ s is also given in Figure 5.12. The surface in Figure 5.12 has clear sine wave pattern because the slope set-point is relatively large for this case.

5.4.3 Simultaneous control of roughness and slope

Finally, simultaneous regulation of roughness and slope is carried out. The set-points of the surface roughness square and of the mean slope square are $r_{set}^2 = 1.0 \text{ nm}^2$ and $m_{set}^2 = 0.025$. The weighting factor of mean slope square is kept at 1, while the weighting factor of roughness square increases from 10^{-8} to 1.

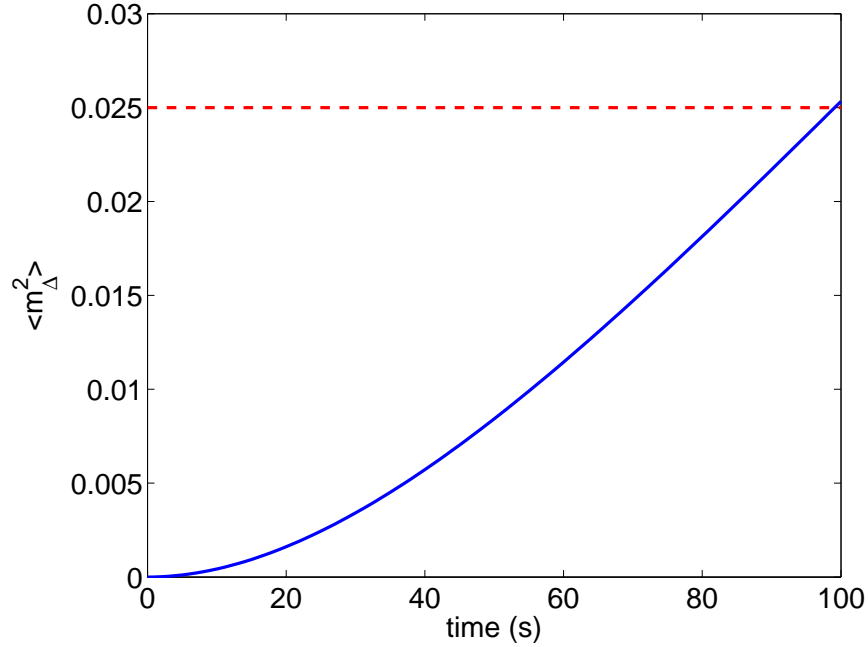


Figure 5.11: Profile of expected film surface slope square from 100 closed-loop simulations. $q_{r^2} = 0$, $q_{m^2} = 1$ and $m_{set}^2 = 0.025$.

Figure 5.13 shows the variation of $\langle r_{\Delta}^2 \rangle (t = 100 \text{ s})$ and $\langle m_{\Delta}^2 \rangle (t = 100 \text{ s})$ as a function of q_{r^2}/q_{m^2} . It can be seen that as the weighting on roughness square increases, the expected roughness square approaches more closely to its set-point value at the cost of larger deviation of slope square from its set-point value and vice versa.

5.4.4 Application to light trapping efficiency

We now demonstrate how films of different reflectance can be produced by simultaneous control of film surface roughness and slope. Specifically, the expected surface roughness square and mean slope square can be regulated to different levels by using the same set points and choosing different weighting schemes, i.e., different ratios of

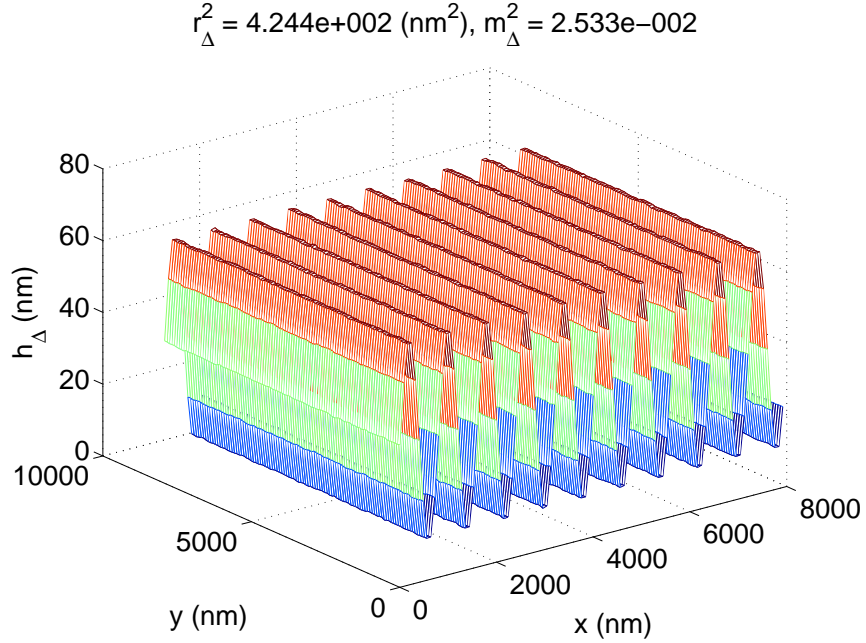


Figure 5.12: Surface profile at the end of simulation, $t = 100$ s. $q_{r^2} = 0$, $q_{m^2} = 1$ and $m_{set}^2 = 0.025$.

the weighting factors, q_{r^2}/q_{m^2} . In particular, q_{m^2} is kept at 1.0 while $q_{r^2}^2$ changes from 10^{-8} to 1. The corresponding light reflectance for different weighting factor ratios can be computed according to eq (5.6). In Figure 5.14, the roughness and slope obtained from closed-loop simulations with different q_{r^2}/q_{m^2} are mapped to a contour of reflectance. The points from upper right to lower left correspond to q_{r^2}/q_{m^2} ratios of increasing values. By changing the ratio, q_{r^2}/q_{m^2} , different films can be produced whose surface morphology is characterized by a wide range of reflectance values.

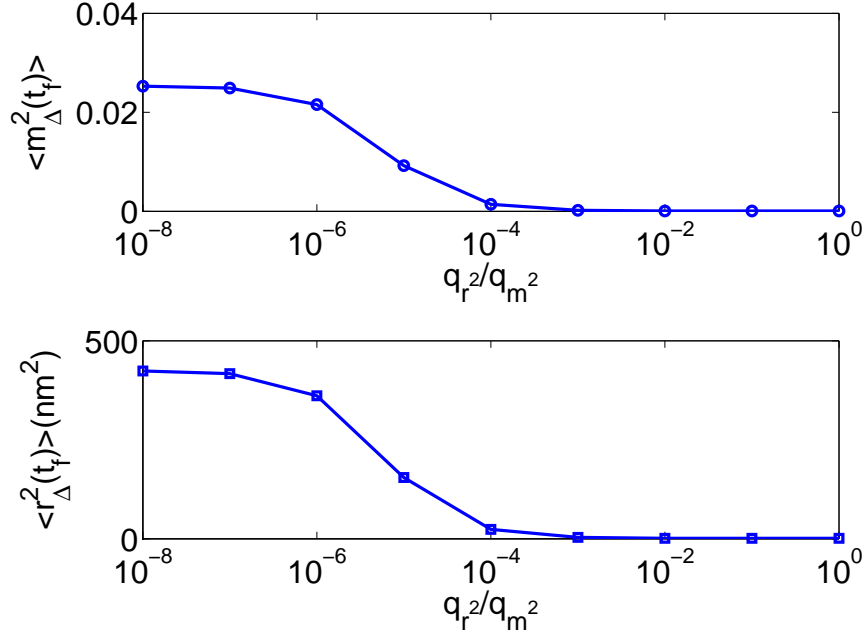


Figure 5.13: $\langle r_{\Delta}^2 \rangle$ and $\langle m_{\Delta}^2 \rangle$ at the end of closed-loop simulations ($t = 100\text{s}$) for different penalty weighting factors: $q_{m^2} = 1$, $10^{-8} \leq q_{r^2} \leq 1$, $r_{\text{set}}^2 = 1.0$, $m_{\text{set}}^2 = 0.025$.

5.5 Conclusions

In this chapter, a patterned deposition rate profile was introduced to generate significant roughness and slope at a length scale comparable to the wavelength of visible light in a thin film deposition process. Working within the framework of the two-dimensional Edwards-Wilkinson equation representing an $8,000 \text{ nm} \times 8,000 \text{ nm}$ spatial domain, a model predictive controller was developed to regulate thin film surface roughness and slope to desired levels, accounting for constraints on the magnitude and rate of change of the control actions. The mean value and magnitude of the sine wave deposition rate profile were used as manipulated variables. Simulation studies demonstrated the applicability and effectiveness of the patterned deposition rate pro-

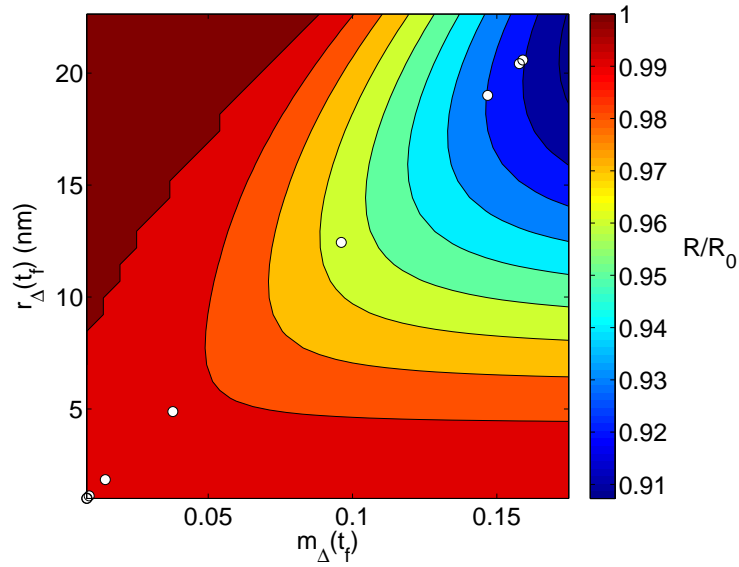


Figure 5.14: Light reflectance of thin films deposited under closed-loop operations with different weighting factor ratios: $q_{m^2} = 1$, $10^{-8} \leq q_{r^2} \leq 1$ (corresponding to points from right to left), $r_{\text{set}}^2 = 1.0$, $m_{\text{set}}^2 = 0.025$

file and of the controller in successfully regulating the final thin film surface roughness and slope to levels that yield desired thin film reflectance and transmittance.

Chapter 6

Conclusions

Motivated by the increasing importance of thin film microstructure and surface morphology in semiconductor and solar cell manufacturing, this dissertation developed a systematic methodology for stochastic modeling and control of thin film surface roughness, slope and porosity within a unified framework. Kinetic Monte Carlo (kMC) methods and stochastic/deterministic differential equation models were constructed to account for the stochastic nature of the thin film growth processes and were used as the basis for model predictive controller design.

In Chapter 2, we developed model predictive control algorithms to simultaneously control film surface roughness, porosity, and thickness in a multiscale model of a thin film growth process. On the macroscopic side, the gas phase dynamics was modeled by a continuous PDE model derived from a mass balance. On the microscopic side, the thin film deposition process was simulated via a kinetic Monte Carlo model developed

on a triangular lattice with vacancies and overhangs allowed inside the film. Dynamic models of film surface height and film porosity were developed and used in the MPC algorithms. The regulation of film thickness was addressed in two different ways. One way is to include penalty on the deviation of the film thickness into the cost function and the other one is to impose a constraint on the adsorption rate to ensure the desired film thickness at the end of the film growth process. The proposed model predictive controllers were applied to the multiscale thin film growth model to evaluate their performance. In addition, an estimation scheme of film SOR was introduced and used successfully in conjunction with the MPC schemes.

In Chapter 3, a model predictive control algorithm was developed to regulate the surface slope and roughness of a thin film growth process. The thin film deposition process was modeled on a one-dimensional triangular lattice that involves two microscopic processes: an adsorption process and a migration process. Kinetic Monte Carlo methods were used to simulate the thin film deposition process. To characterize the surface morphology and to evaluate the light trapping efficiency of the thin film, surface roughness and surface slope were introduced as the root mean squares of the surface height profile and surface slope profile. An EW-type equation was used to describe the dynamics of the surface height profile and predict the evolution of the RMS roughness and RMS slope. A model predictive control algorithm was then developed on the basis of the EW equation model to simultaneously regulate the RMS slope and the RMS roughness at desired levels by optimizing the substrate temperature at

each sampling time. The model parameters of the EW equation were estimated from simulation data through least-square methods. Closed-loop simulation results were presented to demonstrate the effectiveness of the proposed model predictive control algorithm in successfully regulating the RMS slope and the RMS roughness at desired levels that optimize thin film light reflectance and transmittance.

In Chapter 4, a multivariable model predictive controller was developed to simultaneously regulate thin-film surface roughness and mean slope to optimize film light reflectance and transmittance during thin-film manufacturing. The dynamics of the evolution of the thin-film surface height profile were assumed to be described by an EW-type equation in two spatial dimensions. Analytical solutions of the expected surface roughness and surface slope were obtained on the basis of the EW equation and were used in the design of a model predictive controller that manipulates the substrate temperature and deposition rate. The model predictive controller involves constraints on the magnitude and rate of change of the control action and optimizes a cost that involves penalty on deviation of both surface roughness and mean slope from the set-point values. The controller was applied to the two-dimensional Edwards–Wilkinson equation and was demonstrated to successfully regulate surface roughness and mean slope to set-point values at the end of the batch operation that yield desired film reflectance and transmittance.

Finally, in Chapter 5, a patterned deposition rate profile was introduced to generate significant roughness and slope at a length scale comparable to the wavelength

of visible light in a thin film deposition process. Working within the framework of the two-dimensional Edwards-Wilkinson equation representing an $8,000 \text{ nm} \times 8,000 \text{ nm}$ spatial domain, a model predictive controller was developed to regulate thin film surface roughness and slope to desired levels, accounting for constraints on the magnitude and rate of change of the control actions. The mean value and magnitude of the sine wave deposition rate profile were used as manipulated variables. Simulation studies demonstrated the applicability and effectiveness of the patterned deposition rate profile and of the controller in successfully regulating the final thin film surface roughness and slope to levels that yield desired thin film reflectance and transmittance.

Bibliography

- [1] K. J. Åström. *Introduction to Stochastic Control Theory*. Academic Press, New York, 1970.
- [2] Y. Akiyama, N. Imaishi, Y. S. Shin, and S. C. Jung. Macro- and micro-scale simulation of growth rate and composition in MOCVD of yttria-stabilized zirconia. *Journal of Crystal Growth*, 241:352–362, 2002.
- [3] H. Aling, S. Benerjee, A. K. Bangia, V. Cole, J. Ebert, A. Emani-Naeini, K. F. Jensen, I. G. Kevrekidis, and S. Shvartsman. Nonlinear model reduction for simulation and control of rapid thermal processing. In *Proceedings of American Control Conference*, pages 2233–2238, Albuquerque, NM, 1997.
- [4] F. Allgower and H. Chen. *Nonlinear model predictive control schemes with guaranteed stability*. Dordrecht, the Netherlands, 1998.
- [5] A. Armaou and P. D. Christofides. Nonlinear feedback control of parabolic PDE systems with time-dependent spatial domains. *Journal of Mathematical Analysis and Applications*, 239:124–157, 1999.

- [6] A. Armaou and I. G. Kevrekidis. Equation-free optimal switching policies for bistable reacting systems. *International Journal of Robust & Nonlinear Control*, 15:713–726, 2005.
- [7] A. Armaou, C. I. Siettos, and I. G. Kevrekidis. Time-steppers and ‘coarse’ control of distributed microscopic processes. *International Journal of Robust & Nonlinear Control*, 14:89–111, 2004.
- [8] O. Auciello and A. R. Krauss, editors. *In Situ Real-Time Characterization of Thin Film*. John Wiley & Sons, Inc, New York, NY, 2001.
- [9] H. E. Bennett and J. O. Porteus. Relation between surface roughness and specular reflectance at normal incidence. *Journal of the Optical Society of America*, 51:123–129, 1961.
- [10] A. Bindal, M. G. Ierapetritou, S. Balakrishnan, A. Armaou, A. G. Makeev, and I. G. Kevrekidis. Equation-free, coarse-grained computational optimization using timesteppers. *Chemical Engineering Science*, 61:779–793, 2006.
- [11] T. Bohlin and S. F. Graebe. Issues in nonlinear stochastic grey-box identification. *International Journal of Adaptive Control and Signal Processing*, 9:465–490, 1995.
- [12] P. D. Christofides. *Nonlinear and Robust Control of PDE Systems: Methods and Applications to Transport-Reaction Processes*. Birkhäuser, Boston, 2001.

- [13] P. D. Christofides, A. Armaou, Y. Lou, and A. Varshney. *Control and Optimization of Multiscale Process Systems*. Birkhäuser, Boston, 2008.
- [14] H. Davies. The reflection of electromagnetic waves from a rough surface. *Proceedings of the IEE-Part IV: Institution Monographs*, 101:209–214, 1954.
- [15] T. O. Drew, E. G. Webb, D. L. Ma, J. Alameda, R. D. Braatz, and R. C. Alkire. Coupled mesoscale - continuum simulations of copper electrodeposition in a trench. *AIChE Journal*, 50:226–240, 2004.
- [16] S. Dubljevic and P. D. Christofides. Predictive control of parabolic PDEs with boundary control actuation. *Chemical Engineering Science*, 61:6239–6248, 2006.
- [17] S. Dubljevic, P. Mhaskar, N. H. El-Farra, and P. D. Christofides. Predictive control of parabolic PDEs with state and control constraints. *International Journal of Robust & Nonlinear Control*, 16:749–772, 2006.
- [18] S. F. Edwards and D. R. Wilkinson. The surface statistics of a granular aggregate. *Proceedings of the Royal Society of London Series A - Mathematical Physical and Engineering Sciences*, 381:17–31, 1982.
- [19] F. Family. Scaling of rough surfaces: Effects of surface diffusion. *Journal of Physics A: Mathematical and General*, 19:L441–L446, 1986.

- [20] M. A. Gallivan and R. M. Murray. Reduction and identification methods for markovian control systems, with application to thin film deposition. *International Journal of Robust & Nonlinear Control*, 14:113–132, 2004.
- [21] C. E. Garcia, D. M. Prent, and M. Morari. Model predictive control - theory and practice - a survey. *Automatica*, 25:335–348, 1989.
- [22] D. T. Gillespie. A general method for numerically simulating the stochastic time evolution of coupled chemical reactions. *Journal of Computational Physics*, 22:403–434, 1976.
- [23] M. A. Green. Thin-film solar cells: Review of materials, technologies and commercial status. *Journal of Materials Science: Materials in Electronics*, 18:15–19, 2007.
- [24] I. P. Herman, editor. *Optical Diagnosis for Thin Film Processing*. Academic Press Inc. San Diego, 1996.
- [25] G. Hu, J. Huang, G. Orkoulas, and P. D. Christofides. Investigation of film surface roughness and porosity dependence on lattice size in a porous thin film deposition process. *Physical Review E*, 80:041122, 2009.
- [26] G. Hu, Y. Lou, and P. D. Christofides. Dynamic output feedback covariance control of stochastic dissipative partial differential equations. *Chemical Engineering Science*, 63:4531–4542, 2008.

- [27] G. Hu, Y. Lou, and P. D. Christofides. Model parameter estimation and feedback control of surface roughness in a sputtering process. *Chemical Engineering Science*, 63:1810–1816, 2008.
- [28] G. Hu, G. Orkoulas, and P. D. Christofides. Modeling and control of film porosity in thin film deposition. *Chemical Engineering Science*, 64:3668–3682, 2009.
- [29] G. Hu, G. Orkoulas, and P. D. Christofides. Regulation of film thickness, surface roughness and porosity in thin film growth using deposition rate. *Chemical Engineering Science*, 48:3903–3913, 2009.
- [30] G. Hu, G. Orkoulas, and P. D. Christofides. Stochastic modeling and simultaneous regulation of surface roughness and porosity in thin film deposition. *Industrial & Engineering Chemistry Research*, 48:6690–6700, 2009.
- [31] J. Huang, G. Hu, G. Orkoulas, and P. D. Christofides. Dependence of film surface roughness and slope on surface migration and lattice size in thin film deposition processes. *Chemical Engineering Science*, 65:6101–6111, 2010.
- [32] J. Huang, G. Hu, G. Orkoulas, and P. D. Christofides. Lattice-size dependence and dynamics of surface mean slope in a thin film deposition process. In *Proceedings of 9th IFAC Symposium on Dynamics and Control of Process Systems*, pages 803–808, Leuven, Belgium, 2010.

- [33] J. Huang, G. Hu, G. Orkoulas, and P. D. Christofides. Dynamics and lattice-size dependence of surface mean slope in thin film deposition. *Industry & Engineering Chemistry Research*, 50:1219–1230, 2011.
- [34] C. R. Kleijn, Th. H. van der Meer, and C. J. Hoogendoorn. A mathematical model for LPCVD in a single wafer reactor. *Journal of the Electrochemical Society*, 11:3423–3433, 1989.
- [35] N. R. Kristensen, H. Madsen, and S. B. Jorgensen. A method for systematic improvement of stochastic grey-box models. *Computers & Chemical Engineering*, 28:1431–1449, 2004.
- [36] J. Krč, F. Smole, and M. Topič. Analysis of light scattering in amorphous Si:H solar cells by a one-dimensional semi-coherent optical model. *Progress in Photovoltaics: Research and Applications*, 11:15–26, 2003.
- [37] J. Krč and M. Zeman. Experimental investigation and modelling of light scattering in a-si:h solar cells deposited on glass/zno:al substrates. *Material Research Society*, 715:A.13.3.1 – A.13.3.6, 2002.
- [38] J. Krč and M. Zeman. Optical modeling of thin-film silicon solar cells deposited on textured substrates. *Thin Solid Films*, 451:298–302, 2004.
- [39] K. B. Lauritsen, R. Cuerno, and H. A. Makse. Noisy Kuramoto-Sivashinsky equation for an erosion model. *Physical Review E*, 54:3577–3580, 1996.

- [40] F. Leblanc and J. Perrin. Numerical modeling of the optical properties of hydrogenated amorphous-silicon-based p-i-n solar cells deposited on rough transparent conducting oxide substrates. *Journal of Applied Physics*, 75:1074 – 1086, 1994.
- [41] Y. H. Lee, Y. S. Kim, B. K. Ju, and M. H. Oh. Roughness of $ZnS : Pr, Ce/Ta_2O_5$ interface and its effects on electrical performance of alternating current thin-film electroluminescent devices. *IEEE Transactions on Electronic Devices*, 46:892–896, 1999.
- [42] S. W. Levine and P. Clancy. A simple model for the growth of polycrystalline Si using the kinetic Monte Carlo simulation. *Modelling and Simulation in Materials Science and Engineering*, 8:751–762, 2000.
- [43] S. W. Levine, J. R. Engstrom, and P. Clancy. A kinetic Monte Carlo study of the growth of si on Si(100) at varying angles of incident deposition. *Surface Science*, 401:112–123, 1998.
- [44] Y. Lou and P. D. Christofides. Estimation and control of surface roughness in thin film growth using kinetic Monte-Carlo models. *Chemical Engineering Science*, 58:3115–3129, 2003.
- [45] Y. Lou and P. D. Christofides. Feedback control of growth rate and surface roughness in thin film growth. *AIChE Journal*, 49:2099–2113, 2003.

- [46] Y. Lou and P. D. Christofides. Feedback control of surface roughness of GaAs (001) thin films using kinetic Monte Carlo models. *Computers & Chemical Engineering*, 29:225–241, 2004.
- [47] Y. Lou and P. D. Christofides. Feedback control of surface roughness in sputtering processes using the stochastic Kuramoto-Sivashinsky equation. *Computers & Chemical Engineering*, 29:741–759, 2005.
- [48] Y. Lou and P. D. Christofides. Feedback control of surface roughness using stochastic PDEs. *AIChE Journal*, 51:345–352, 2005.
- [49] A. Lucia, P. A. DiMaggio, and P. Depa. Funneling algorithms for multiscale optimization on rugged terrains. *Industry & Engineering Chemistry Research*, 43:3770–3781, 2004.
- [50] A. Lucia, P. A. DiMaggio, and P. Depa. A geometric terrain methodology for global optimization. *Journal of Global Optimization*, 29:297–314, 2004.
- [51] J. Müller, B. Rech, J. Springer, and M. Vanecek. TCO and light trapping in silicon thin film solar cells. *Solar Energy*, 77:917–930, 2004.
- [52] D. Ni and P. D. Christofides. Dynamics and control of thin film surface microstructure in a complex deposition process. *Chemical Engineering Science*, 60:1603–1617, 2005.

- [53] D. Ni and P. D. Christofides. Multivariable predictive control of thin film deposition using a stochastic PDE model. *Industrial & Engineering Chemistry Research*, 44:2416–2427, 2005.
- [54] D. Ni, Y. Lou, P. D. Christofides, L. Sha, S. Lao, and J. P. Chang. Real-time carbon content control for PECVD ZrO_2 thin-film growth. *IEEE Transactions on Semiconductor Manufacturing*, 17:221–230, 2004.
- [55] A. Poruba, A. Fejfar, Z. Remeš, J. Špringer, M. Vaněček, and J. Kočka. Optical absorption and light scattering in microcrystalline silicon thin films and solar cells. *Journal of Applied Physics*, 88:148–160, 2000.
- [56] J. B. Rawlings. Tutorial: Model predictive control technology. In *Proceedings of the American Control Conference*, pages 662–676, San Diego, CA, 1999.
- [57] J. S. Reese, S. Raimondeau, and D. G. Vlachos. Monte Carlo algorithms for complex surface reaction mechanisms: Efficiency and accuracy. *Journal of Computational Physics*, 173:302–321, 2001.
- [58] G. Renaud, R. Lazzari, C. Revenant, A. Barbier, M. Noblet, O. Ulrich, F. Leroy, J. Jupille, Y. Borensztein, C. R. Henry, J. P. Deville, F. Scheurer, J. Mane-Mane, and O. Fruchart. Real-time monitoring of growing nanoparticles. *Science*, 300:1416–1419, 2003.

- [59] F. Roozeboom and N. Parekh. Rapid thermal processing systems: a review with emphasis on temperature control. *Journal of Vacuum Science & Technology B*, 8:1249–1259, 1990.
- [60] S. F. Rowlands, J. Livingstone, and C.P. Lund. Optical modelling of thin film solar cells with textured interface using the effective medium approximation. *Solar Energy*, 76:301–307, 2004.
- [61] E. Rusli, T. O. Drews, D. L. Ma, R. C. Alkire, and R. D. Braatz. Robust nonlinear feedback-feedforward control of a coupled kinetic monte-carlo-finite difference simulation. In *Proceedings of the American Control Conference*, pages 2548–2553, Portland, OR, 2005.
- [62] P. O. Scokaert, D. Q. Mayne, and J. B. Rawlings. Suboptimal model predictive control (feasibility implies stability). *IEEE Transaction on Automatic Control*, 44:648–654, 1999.
- [63] K. Seshan, editor. *Handbook of Thin-Film Deposition Processes and Techniques*. Norwich, 2002.
- [64] C. I. Siettos, A. Armaou, A. G. Makeev, and I. G. Kevrekidis. Microscopic/stochastic timesteppers and “coarse” control: a kMC example. *AIChE Journal*, 49:1922–1926, 2003.
- [65] J. Springer and A. Poruba. Improved three-dimensional optical model for thin-film silicon solar cells. *Journal of Applied Physics*, 96:5329–5337, 2004.

- [66] G. Tao and M. Zeman. Optical modeling of a-si:h based solar cells on textured substrates. *1994 IEEE First World Conference on Photovoltaic Energy Conversion. Conference Record of the Twenty Fourth IEEE Photovoltaic Specialists Conference-1994 (Cat.No.94CH3365-4)*, 1:666, 1994.
- [67] A. Theodoropoulou, R. A. Adomaitis, and E. Zafiriou. Inverse model based real-time control for temperature uniformity of RTCVD. *IEEE Transactions on Semiconductor Manufacturing*, 12:87–101, 1999.
- [68] W. van Sark, G. W. Brandsen, M. Fleuster, and M. P. Hekkert. Analysis of the silicon market: Will thin films profit? *Energy Policy*, 35:3221–3125, 2007.
- [69] A. Varshney and A. Armaou. Multiscale optimization using hybrid PDE/kMC process systems with application to thin film growth. *Chemical Engineering Science*, 60:6780–6794, 2005.
- [70] A. Varshney and A. Armaou. Optimization of thin film growth using multiscale process systems. In *Proceedings of the American Control Conference*, pages 2559–2565, Portland, OR, 2005.
- [71] D. G. Vlachos, L. D. Schmidt, and R. Aris. Kinetics of faceting of crystals in growth, etching, and equilibrium. *Physical Review B*, 47:4896–4909, 1993.
- [72] B. Voigtländer. Fundamental processes in Si/Si and Ge/Si studied by scanning tunneling microscopy during growth. *Surface Science Reports*, 43:127–254, 2001.

- [73] T. V. Vorburger, E. Marx, and T. R. Lettieri. Regimes of surface roughness measurable with light scattering. *Applied Optics*, 32:3401–3408, 1993.
- [74] D. D. Vvedensky, A. Zangwill, C. N. Luse, and M. R. Wilby. Stochastic equations of motion for epitaxial growth. *Physical Review E*, 48:852–862, 1993.
- [75] A. Wächter and L.T. Biegler. On The Implementation of an Interior-point Filter Line-search Algorithm for Large-scale Nonlinear Programming. *Mathematical Programming*, 106(1):25–57, 2006.
- [76] L. Wang and P. Clancy. Kinetic Monte Carlo simulation of the growth of polycrystalline Cu films. *Surface Science*, 473:25–38, 2001.
- [77] P. Wolfrum, A. Vargas, M. Gallivan, and F. Allgower. Complexity reduction of a thin film deposition model using a trajectory based nonlinear model reduction technique. In *Proceedings of the American Control Conference*, pages 2566–2571, Portland, OR, 2005.
- [78] Y. G. Yang, R. A. Johnson, and H. N. G. Wadley. A monte carlo simulation of the physical vapor deposition of nickel. *Acta Materialia*, 45:1455–1468, 1997.
- [79] M. Zeman and R. Vanswaaij. Optical modeling of a-si : H solar cells with rough interfaces: Effect of back contact and interface roughness. *Journal of Applied Physics*, 88:6436–6443, 2000.

- [80] P. Zhang, X. Zheng, S. Wu, J. Liu, and D. He. Kinetic Monte Carlo simulation of Cu thin film growth. *Vacuum*, 72:405–410, 2004.
- [81] X. Zhang, G. Hu, G. Orkoulas, and P. D. Christofides. Controller and estimator design for regulation of film thickness, surface roughness and porosity in a multiscale thin film growth process. *Industry & Engineering Chemistry Research*, 49:7795–7806, 2010.
- [82] X. Zhang, G. Hu, G. Orkoulas, and P. D. Christofides. Multivariable model predictive control of thin film surface roughness and slope for light trapping optimization. *Industry & Engineering Chemistry Research*, 49:10510–10516, 2010.